

NPS ARCHIVE  
1999.12  
REISS, A.

DUDLEY KNOX LIBRARY  
NAVAL POSTGRADUATE SCHOOL  
MONTEREY CA 93943-5101





NAVAL POSTGRADUATE SCHOOL  
Monterey, California



THESIS

EVALUATION STUDY OF THE TACTICAL  
ATMOSPHERIC MODELING SYSTEM/REAL-TIME  
(TAMS-RT) AT NPMOC SAN DIEGO

by

Arthur J. Reiss

December 1999

Thesis Advisor:

Carlyle H. Wash

Approved for public release; distribution is unlimited.



# REPORT DOCUMENTATION PAGE

Form Approved  
OMB No. 0704-0188

Public reporting burden for this collection of information is estimated to average 1 hour per response, including the time for reviewing instructions, searching existing sources, gathering and maintaining the data needed, and completing and reviewing the collection of information. Send comments regarding this burden estimate or any other aspect of this collection of information, including suggestions for reducing this burden to Washington Headquarters Services, Directorate for Information Operations and Reports, 1215 Jefferson Davis Highway Suite 1204, Arlington, VA 22202-4312, and to the Office of Management and Budget, Paperwork Reduction Project (0704-0188), Washington, DC 20503.

1. AGENCY USE ONLY (Leave blank)		2. REPORT DATE December 1999	3. REPORT TYPE AND DATES COVERED Master's Thesis
4. TITLE AND SUBTITLE <b>EVALUATION STUDY OF THE TACTICAL ATMOSPHERIC MODELING SYSTEM/REAL-TIME (TAMS-RT) AT NPMOC SAN DIEGO</b>		5. FUNDING NUMBERS	
6. AUTHOR(S) Arthur J. Reiss			
7. PERFORMING ORGANIZATION NAME(S) AND ADDRESS(ES) Naval Postgraduate School Monterey, CA 93943-5000		8. PERFORMING ORGANIZATION REPORT NUMBER	
9. SPONSORING/MONITORING AGENCY NAME(S) AND ADDRESS(ES)		10. SPONSORING/MONITORING AGENCY REPORT NUMBER	
11. SUPPLEMENTARY NOTES The views expressed in this thesis are those of the author and do not reflect the official policy or position of the Department of Defense or the U.S. Government.			
12a. DISTRIBUTION/AVAILABILITY STATEMENT Approved for public release; distribution is unlimited.		12b. DISTRIBUTION CODE	
13. ABSTRACT (Maximum 200 words) The U.S. Navy is aggressively pursuing mesoscale atmospheric modeling. The Coupled Ocean/Atmosphere Mesoscale Prediction System (COAMPS) has been developed by the Naval Research Lab in Monterey, California to meet this task. A forecast system employing COAMPS, called the Tactical Atmospheric Mesoscale System-Real Time (TAMS-RT), is currently being field tested at two of the Navy's major regional weather facilities in Manama, Bahrain and San Diego, California. Mesoscale modeling is a complex process that requires detailed knowledge of mesoscale forcing and responses, as well as a capable data display system to make the best use of this new capability. While the challenge of interpretation of forecasts on the mesoscale has increased, the time available for producing forecasts has, if anything, decreased. Optimal methods of evaluation and display are needed that enable a forecaster to rapidly, yet skillfully complete this process. This thesis illustrates analysis techniques to aid in rapidly evaluating the utility of any given mesoscale forecast and proposes optimal methods for 3-D visualization and interpretation of various weather parameters. Using these techniques and methods, TAMS-RT performance is then evaluated for critical mesoscale weather phenomena as defined by NPMOC San Diego, including the mesoscale weather effects associated with frontal passages and the Catalina Eddy.			
14. SUBJECT TERMS Mesoscale Modeling, Coupled Ocean-Atmosphere Mesoscale Prediction System (COAMPS), Tactical Atmospheric Modeling System/Real-Time (TAMS-RT), Catalina Eddies.		15. NUMBER OF PAGES 159	16. PRICE CODE
17. SECURITY CLASSIFICATION OF REPORT Unclassified	18. SECURITY CLASSIFICATION OF THIS PAGE Unclassified	19. SECURITY CLASSIFICATION OF ABSTRACT Unclassified	20. LIMITATION OF ABSTRACT UL

NSN 7540-01-280-5500

Standard Form 298 (Rev 2-89)  
Prescribed by ANSI Std. Z39-18  
298-102

THIS PAGE INTENTIONALLY LEFT BLANK

DUDLEY KNOX LIBRARY  
NAVAL POSTGRADUATE SCHOOL  
MONTEREY, CA 93943-5101

Approved for public release; distribution is unlimited

**EVALUATION STUDY OF THE TACTICAL ATMOSPHERIC MODELING  
SYSTEM/REAL-TIME (TAMS-RT) AT NPMOC SAN DIEGO**

Arthur J. Reiss  
Lieutenant Commander, United States Navy  
B.S., United States Naval Academy, 1990

Submitted in partial fulfillment of the  
requirements for the degree of

**MASTER OF SCIENCE IN METEOROLOGY AND  
PHYSICAL OCEANOGRAPHY**

from the

**NAVAL POSTGRADUATE SCHOOL  
December 1999**



## ABSTRACT

The U.S. Navy is aggressively pursuing mesoscale atmospheric modeling. The Coupled Ocean/Atmosphere Mesoscale Prediction System (COAMPS) has been developed by the Naval Research Lab in Monterey, California to meet this task. A forecast system employing COAMPS, called the Tactical Atmospheric Mesoscale System- Real Time (TAMS-RT), is currently being field tested at two of the Navy's major regional weather facilities in Manama, Bahrain and San Diego, California. Mesoscale modeling is a complex process that requires detailed knowledge of mesoscale forcing and responses, as well as a capable data display system to make the best use of this new capability. While the challenge of interpretation of forecasts on the mesoscale has increased, the time available for producing forecasts has, if anything, decreased. Optimal methods of evaluation and display are needed that enable a forecaster to rapidly, yet skillfully complete this process. This thesis illustrates analysis techniques to aid in rapidly evaluating the utility of any given mesoscale forecast and proposes optimal methods for 3-D visualization and interpretation of various weather parameters. Using these techniques and methods, TAMS-RT performance is then evaluated for critical mesoscale weather phenomena as defined by NPMOC San Diego, including the mesoscale weather effects associated with frontal passages and the Catalina Eddy.

THIS PAGE INTENTIONALLY LEFT BLANK

## TABLE OF CONTENTS

I. INTRODUCTION .....	1
A. WHY SHOULD WE DO MESOSCALE MODELING? .....	1
B. WHY A FORWARD-DEPLOYED TAMS-RT AT REGIONAL CENTERS .....	2
C. THE CHALLENGES OF SUCCESSFUL IMPLEMENTATION OF TAMS-RT AT REGIONAL CENTERS .....	2
D. THESIS OBJECTIVES .....	3
E. CHAPTER OUTLINE .....	3
II. TAMS-RT AND THE MESOSCALE MODELING INITIATIVE AT NPMOC SAN DIEGO .....	5
A. THE COUPLED OCEAN/ATMOSPHERE MESOSCALE PREDICTION SYSTEM (COAMPS) .....	5
B. TAMS-RT AS IMPLEMENTED AT NPMOC SAN DIEGO .....	6
C. UNIQUE ASPECTS OF MESOSCALE MODELING APPLICABLE TO OPERATIONAL DEPLOYMENT OF TAMS-RT AT REGIONAL CENTERS .....	9
III. TAMS-RT ANALYSIS METHODS .....	13
A. INTRODUCTION .....	13
B. DATA ASSIMILATION EVALUATION METHOD .....	13
C. FEBRUARY 9 & 10 FRONTAL PASSAGE: STATEMENT OF REALITY .....	14
D. SUMMARY OF THE EVALUATION METHOD .....	19
IV. TECHNIQUES FOR INTERPRETING COAMPS FIELDS FROM TAMS-RT USING VIS5D .....	21
A. WHAT IS VIS5D AND HOW DOES IT RELATE TO TAMS-RT? .....	21
B. WHY VIS5D? .....	21
C. MESOSCALE MODEL INTERPRETATION TECHNIQUES USING VIS5D .....	22
V. TAMS-RT PERFORMANCE AT NPMOC SAN DIEGO .....	35
A. FRONTAL PASSAGE AND THE ASSOCIATED WEATHER IN SOCAL .....	39
B. CATALINA EDDIES AND THE ASSOCIATED WEATHER IN SOCAL.....	51
VI. CONCLUSIONS AND RECOMMENDATIONS .....	63
A. WARM AND COLD STARTS .....	63
B. THE INITIAL ANALYSIS .....	63
C. VIS5D ANALYSIS TECHNIQUES .....	63
D. TOPOGRAPHY .....	64
E. LATERAL BOUNDARY CONDITIONS .....	64

F. MESOSCALE CONCEPTUAL MODELS .....	65
G. DEVELOPING AND NURTURING “MESO-SKILL” (THE MESOSCALE KNOWLEDGE BASE) .....	65
LIST OF REFERENCES .....	67
APPENDIX A. FIGURES .....	71
APPENDIX B. VIS5D SETTINGS .....	135
APPENDIX C. VIS5D AMPLIFIED PROCEDURES FOR TOPOGRAPHIC STUDIES .....	143
APPENDIX D. VIS5D COMPARISON PROCEDURES .....	145
INITIAL DISTRIBUTION LIST .....	147

## ACKNOWLEDGEMENTS

I would like to sincerely thank my advisor and coach, Dr. Chuck Wash, Chairman of the Department of Meteorology, Naval Postgraduate School, for his great patience, guidance and support throughout the development of my thesis. Additionally, I thank CAPT Chris Gunderson for providing the original motivation and vision. Also, I thank Dr. Wendell Nuss for his helpful comments as the second reader and for increasing the effectiveness of the techniques presented in this thesis by an order of magnitude.

The following Department of Meteorology, Naval Postgraduate School personnel were instrumental at various stages in my research: Mr. Bob Creasey, Mr. Dick Lind, Dr. Doug Miller, Mr. Russ Schwanz, and Mr. Bill Thompson. Also of great assistance were Mr. Kurt Nelson and LT Dave Ford of NPMOC San Diego and Dr. Cliff Mass, Department of Meteorology, University of Washington. My buddies, Oscar Monterrosa, Keith Barto, and Sean Memmen also lent a helpful hand when it was needed most. I am also thankful for the nice folks at the Thai Sweet House and Sandra at the coffee bar for keeping me well-fed and caffeinated. Heartfelt thanks to the prayer-warriors, Mike Kuypers, Dave Cook, Bob Reehm, and Chaplain Phillips.

I also want to thank my mom and dad, Kay L. Reiss and the late and great Art Reiss both of Akron, Ohio and my sister, Laura for all of their love and support over the years.

But most of all, I want to express the deepest gratitude, love, and appreciation to my dear wife, Dana, the joy and shining jewel of all my kingdom, who gives of herself endlessly and selflessly to keep me standing tall and smiling. And oh yes, thank you to my little sweethearts, Dasha, Julia, and Emma for helping me keep my sense of humor through dirty diapers, pushing all the wrong buttons on Daddy's computer, crying, laughing, tickle torture, and butterfly kisses.

Lastly, when it comes to weather, I want to thank God Almighty for keeping us guessing.

THIS PAGE INTENTIONALLY LEFT BLANK

## I. INTRODUCTION

### A. WHY SHOULD WE DO MESOSCALE MODELING?

Mesoscale atmospheric modeling represents the future of Numerical Weather Prediction (NWP). As computer power has increased, so has the ability to increase the resolutions of our NWP models. But forecast accuracy will not increase just by running the same NWP models on finer scales. Mesoscale modeling takes full advantage of available fine-scale terrain and surface property databases and efficiently incorporates numerous fine-scale observation sources to produce a more accurate forecast. Investment in mesoscale modeling means developing new ways of solving the primitive equations. It also means refining old parameterizations or developing new ones as well as making new assumptions and removing old ones that are no longer applicable on such fine resolutions. Lastly and most importantly, it involves training and equipping our forecasters with “meso-skill,” a new knowledge base of fundamental mesoscale modeling principles, weather phenomena, forcing mechanisms and responses, conceptual models to be used in conjunction with global NWP, analysis tools, and visualization techniques to leverage this new capability. Armed with both global and mesoscale NWP guidance, highly trained and skilled forecasters in the field, on ships, or back at regional data fusion sites will be able to provide an unprecedented level of high-quality and tactically relevant weather support for warfighters anywhere on the globe.

Another reason to pursue mesoscale modeling is to make ourselves better forecasters. Using a mesoscale model, forecasters learn detail about their local circulations and phenomena. Having encountered one class of mesoscale event, forecasters will possess the “local insight” to forecast similar events elsewhere. That is, he or she will immediately have local insight before gaining local knowledge (Gunderson 1999). The bottom line is that a mesoscale model can teach humans to be better forecasters.

The United States Navy is poised on the leading edge of this relatively new operational capability. The Naval Research Laboratory (NRL), under the sponsorship of the Office of Naval Research (ONR 322 AM) and the Space and Naval Warfare Systems Command (SPAWAR PMW 185), and with the support of the Commander, Naval Meteorology and Oceanography Command (CNMOC), is developing a mesoscale modeling forecast system called the On-scene Tactical Atmospheric Forecast Capability (STAFC), also known as the Tactical Atmospheric Modeling System/Real-Time (TAMS-RT) (Cook et al. 1997). The core of these systems is the Coupled Ocean/Atmosphere Mesoscale Prediction System (COAMPS). COAMPS is currently undergoing real-time operational evaluation at the Fleet Numerical Meteorology and Oceanography Center (FNMOC), Monterey, California. Meanwhile, TAMS-RT is forward-deployed for real-time

operational evaluation at the Naval Central Meteorology and Oceanography Facility, Bahrain, and the Naval Pacific Meteorology and Oceanography Center (NPMOC), San Diego, California, where it serves as an analysis (“now-cast”) and short-term forecast tool out to 36 hours. TAMS-RT is currently installed at the major forecast training command at Keesler, AFB and the Naval European Meteorology and Oceanography (METOC) Center, Rota, Spain. In the near future, TAMS-RT will be forward-deployed to all METOC Regional Centers. Chapter II provides more detail on COAMPS.

## **B. WHY A FORWARD-DEPLOYED TAMS-RT AT REGIONAL CENTERS?**

Since COAMPS runs at FNMOC, why does the Navy need a workstation version that can run at forward-deployed locations? According to Cook et. al (1997), there were four primary reasons that led to the development of TAMS-RT. They include:

- Local data—to exploit local data sources that may not be available in a timely manner at FNMOC, including water vapor and infrared cloud-tracked winds derived from the geostationary satellites and in the future, shipboard radar weather observations;
- Local control—to allow the flexibility to quickly run the model whenever and wherever it is needed, to tailor the output data products to exactly meet the customer’s needs, to access results every model time step if appropriate, and to control dissemination of the products over the network (the point is to put the regional model nearer to the decision makers);
- Timeliness—to produce a more timely product by automatically maintaining a physically consistent and updated “nowcast” and “forecast” capability on-site; and lastly,
- Local Training—to study phenomena of local interest to forecasters by using the system in research mode.

## **C. THE CHALLENGES OF SUCCESSFUL IMPLEMENTATION OF TAMS-RT AT REGIONAL CENTERS**

The decision to implement a forward-deployed mesoscale forecast system does not come without a cost, both technically and operationally. Some of these challenges include:

- overcoming the bandwidth limitations for dissemination of parent model (e.g., NOGAPS) fields for lateral boundary conditions; the requirement for rigorous on-site data management and the technical knowledge to do so;
- the ability to quality control analyses, forecasts, and the data assimilation cycle;
- the development of a basic “modeler’s mentality” among forecasters to include understanding the basic aspects of data assimilation, boundary conditions and their incorporation into the analysis and forecast, inherent errors and limitations in limited area models (LAMs) and how to effectively minimize them, and knowledge of potential error sources including the impacts of lateral boundary conditions (LBCs) on LAMs;
- the development of “meso-skill” on the mesoscale among forecasters (i.e., a mesoscale knowledge base including finding the best fit of mesoscale analysis into the current forecast process).

In essence, the greatest challenge will be the development of forecasters who can effectively combine technical modeling knowledge with operational forecasting skills to harness the mesoscale model output and add the most value to the forecast.

#### **D. THESIS OBJECTIVES**

The main objectives of this thesis are aimed at helping commands meet the above challenges with success. These objectives are:

- to develop the mesoscale knowledge base (“meso-skill”) of Navy weather forecasters by providing background information on the unique aspects and characteristics of mesoscale modeling including:
  - a description of and methods for leveraging the characteristics of “cold” and “warm starts,”
  - a description of and the associated impacts of LBCs on LAM forecasts,
  - how to configure LAMs to minimize the negative effects of LBC-generated errors on the forecast,
  - methods for evaluating the skill of the “modeled” surface boundary and minimizing the effects of significant errors in its representation,
  - a discussion of applicable conceptual models for meteorological phenomena that are considered to be “critical” by NPMOC San Diego (i.e., the forecast has significant operational impact on base operations like the mesoscale structure and weather response associated with fronts and Catalina Eddies);
- to evaluate TAMS-RT forecasts of these “critical” mesoscale features and provide feedback on its performance aimed at improving future forecasting skill;
- to recommend TAMS-RT analysis methods that bypass the requirement for a detailed understanding of the data management and assimilation process by simply evaluating the end result of the process;
- to demonstrate the impact of both good and poor analyses on the future forecast and how to apply the TAMS-RT analysis methods to evaluate the utility of the forecast beforehand; and
- to provide techniques for rapid and effective interpretation of COAMPS fields from TAMS-RT using Vis5D.

This information, along with continued use and application over time and an effective training and verification program, are the first steps towards successful implementation of mesoscale modeling at regional centers.

#### **E. CHAPTER OUTLINE**

This thesis is organized into 6 chapters. Chapter II provides background information on COAMPS in general and specifically for the TAMS-RT system as it was implemented at NPMOC San Diego for the case studies. Chapter II also provides background on the unique aspects and characteristics of mesoscale modeling and how to leverage their beneficial impact, as well as how to minimize any adverse impacts. Chapter III illustrates the importance of evaluating the TAMS-RT analysis to determine the utility of any given forecast. Chapter IV presents a method for using Vis5D visualization techniques for rapid and effective assessment of the TAMS-RT forecast.

of critical mesoscale phenomenon as defined by NPMOC San Diego, namely the mesoscale structure associated with SOCAL fronts and the Catalina Eddy, and draws conclusions from the case studies aimed at improving NPMOC San Diego's forecasting skill of these particular mesoscale features. Lastly, Chapter VI presents conclusions and recommendations.

## II. TAMS-RT AND THE MESOSCALE MODELING INITIATIVE AT NPMOC SAN DIEGO

### A. THE COUPLED OCEAN/ATMOSPHERE MESOSCALE PREDICTION SYSTEM (COAMPS)

The Marine Meteorology Division of the NRL has developed the Coupled Ocean/Atmosphere Mesoscale Prediction System (COAMPS). COAMPS is a state-of-the-art atmospheric mesoscale data assimilation system that utilizes a unique non-hydrostatic atmospheric model and sophisticated precipitation microphysics which are appropriate for numerical predictions using horizontal grid spacing of less than 10 km (Hodur 1997). Predictions on these scales imply that the hydrostatic approximation may be invalid at times, particularly for convection and smaller-scale topographic features where the vertical wavelength is a significant fraction of the horizontal wavelength and therefore the vertical acceleration term cannot be ignored (Hodur 1997).

COAMPS is comprised of an atmospheric data assimilation system including modules for data quality control, analysis, initialization, the non-hydrostatic atmospheric forecast model, a hydrostatic ocean forecast model, and a wave model. Currently under development is the revolutionary capability to "couple" the atmosphere and ocean models (i.e., integrated simultaneously) so that the surface fluxes of heat, momentum, and moisture are exchanged across the air-sea interface every time step. At the present, however, the ocean module can only perform idealized experiments and contains no provisions for data assimilation. The NRL Coastal Ocean Model (NCOM) will most likely be the ocean model for coupled ocean atmosphere implementation.

The analysis can use global fields from the Navy Operational Global Atmospheric Prediction System (NOGAPS) or the most recent COAMPS forecast as the first-guess (i.e., background fields). Lateral boundary conditions (LBCs) for the coarse mesh can be provided by NOGAPS or by a separate COAMPS model run (e.g., on-scene sites running high-resolution domains within a coarser resolution regional domain produced by a central site). In either case, the next larger COAMPS domain always provides the first-guess and LBCs for the inner meshes. In the end, aircraft, rawinsonde, ship, and satellite observations are blended with the first-guess fields and lateral boundary conditions to generate the current analysis (Hodur 1997).

Within the non-hydrostatic atmospheric forecast model, COAMPS includes predictive equations for momentum, non-dimensional pressure perturbation, potential temperature, and turbulent kinetic energy. The model also allows for the explicit prediction of water vapor, cloud droplets, ice crystals, raindrops, and snowflakes, while it parameterizes subgrid-scale mixing, cumulus convective processes, and cloud-interactive radiation (Hodur 1997). COAMPS

incorporates a globally re-locatable grid, user-defined grid resolutions and dimensions, nested grids providing multi-scale capability (synoptic to large eddy scales), and a high-resolution terrain database. The model's outer domain boundary can be rotated to align with any surface feature, such as the terrain or a coastline, or can be shaped to capture critical upstream observational points. Any number of nested grids is allowed with the only restriction being a ratio of 3:1 reduction in grid spacing between the grids. The inner grids can be specified arbitrarily within the confines of the next coarser grid, but at present, the grids are not allowed to move during the forecast (Hodur 1997).

The surface characteristics for each nest are initially read in from a global climatology database. The surface topography field is interpolated from a 20-km terrain data set; however, in certain regions around the globe, 1-km resolution terrain data is interpolated to the grid spacing resolution for meshes with grid spacing less than 20 km (Hodur 1997). With the high-resolution terrain database, COAMPS is very well suited to perform in littoral regions where there is significant mesoscale forcing from the surface. Surface irregularities such as topography and coastlines can force circulations in COAMPS even though the circulations may not be well represented in the initial data. COAMPS has been designed to be suitable for central site (FNMOC) and on-scene (METOC regional center) applications and has been applied to mesoscale phenomena including mountain waves, land-sea breezes, terrain-induced circulations, tropical cyclones, mesoscale convective systems, coastal rainbands, and frontal systems (Hodur 1997).

## **B. TAMS-RT AS IMPLEMENTED AT NPMOC SAN DIEGO**

As stated in the introduction, TAMS-RT is currently undergoing real-time operational evaluation at the NPMOC San Diego, California, where it serves as an analysis ("now-cast") and short-term forecast tool out to 36 hours. Table 1 lists the general characteristics of the operational COAMPS running in NPMOC San Diego's TAMS-RT. Characteristics of the hydrostatic ocean model are excluded since the operational COAMPS is still technically "uncoupled" (please refer to Hodur (1997) for a more complete description of COAMPS and its capabilities). The model characteristics listed in Table 1 also serve as the "baseline" configuration valid for the case study evaluations presented later in this thesis. Notes further clarify NPMOC San Diego's COAMPS settings where options exist. Figure 2-1 depicts the horizontal grid domain structure valid for the case study evaluations presented in this thesis and the distribution of the vertical levels respectively.

Table 1. General characteristics and specific configuration for NPMOC San Diego's TAMS-RT.

<b>QUALITY CONTROL</b>	
Observations	Algorithms for atmospheric observational data (Baker 1992).
<b>ANALYSIS</b>	
Levels	Analysis on 16 standard pressure levels (1000 MB to 10 MB).
Synthetic observations	Synthetic observations from NOGAPS in data sparse regions.
First-guess fields	<ul style="list-style-type: none"> <li>• NOGAPS for cold starts,</li> <li>• COAMPS for warm starts (data assimilation)</li> </ul>
<b>MVOI of winds and heights</b>	Lorenc technique (1986) for mapping obs to the model grid(s).
Volume method	Adjustable volume size for a separate analyses on each nested grid
Input	Synoptic, ship, bathymetric, ice, radiosondes, pibals, AIREPS, ACARS, SSMI, surface and cloud track winds, and synthetic observations.
D-values/Thickness	Radiosondes, DMSP, NOAA satellite.
Superobs	Aircraft and SSMI.
<b>Univariate Analysis of Temperature and Dew-point depression</b>	Cressman (1959). Radiosonde and synthetic observations only with gross-error checking.
<b>ATMOSPHERIC MODEL</b>	
<b>Dynamics, Numerics:</b>	
Equations	<ul style="list-style-type: none"> <li>• Non-hydrostatic compressible equations (Klemp and Wilhelmson 1978).</li> <li>• Equations also include map factors, terrain, lateral, lower, and upper boundary conditions and are solved using a combination of finite differencing, finite elements, and spectral methods.</li> <li>• Time-splitting method in horizontal allows large time steps for slow modes and small time steps for fast modes. Semi-implicit method in vertical.</li> </ul>
Diffusion	Horizontal diffusion (4 <sup>th</sup> order difference method) is used to control spurious, high frequency waves that are not important for the final solution.
Grid configuration	<ul style="list-style-type: none"> <li>• Staggered C grid (Arakawa and Lamb 1977)</li> <li>• Multiple nested grid options (e.g., Figure 2-1).</li> </ul>
Vertical coordinates	Terrain following coordinate (sigma z; Gal-Chen and Somerville 1975) allows flow over an irregular surface.
Vertical levels	Up to 30 <u>selectable</u> sigma levels (m). Optimal with higher density in lower troposphere (Figure 2-1).
Grid projection	Lambert conformal, mercator, or spherical.
Mesh ratio	3:1
Grid spacing	<ul style="list-style-type: none"> <li>• Synoptic to Large Eddy Scale (LES).</li> <li>• Note: NPMOC San Diego's TAMS-RT settings for thesis case studies were 45, 15, and 5 km's (coarse/medium/fine) respectively (Figure 2-1).</li> </ul>
<b>Precipitation Physics</b>	
Grid spacing $\geq 10\text{km}$	<ul style="list-style-type: none"> <li>• Stratiform: Explicit moist physics (Rutledge and Hobbs 1983).</li> <li>• Convective: Kain and Fritsch (1993) cumulus parameterization.</li> </ul>

Table 1 (continued)

Grid spacing < 10km	<ul style="list-style-type: none"> <li>Rutledge and Hobbs (1983) explicit moist physics for both stratiform and convective clouds and precipitation .</li> <li>For grid resolutions &lt; 10km, COAMPS is effectively acting as a cloud model.</li> </ul>
Options for COAMPS SP (simplified physics)	<ul style="list-style-type: none"> <li>Stratiform: Instantaneous condensation/fallout.</li> <li>Convective: Kuo (1974) cumulus parameterization.</li> <li>Note: NPMOC San Diego's TAMS-RT did not employ SP.</li> </ul>
Known characteristics	<ul style="list-style-type: none"> <li>Kain and Fritsch: under-predicts precipitation and is noisy over ocean</li> <li>Kuo: over-predicts, dependent upon grid resolution, and 3-5 times faster than KF.</li> </ul>
<b>Radiation</b>	Radiative transfer parameterization (Harshvardan et al. 1987)
<b>Boundary layer and surface parameterizations</b>	
Land-use Surface albedo Surface roughness Ground wetness Ground temperature SST	<ul style="list-style-type: none"> <li>Initially taken from a global monthly climatology database (resolution ~ 1° lat) and thereafter from the previous forecast.</li> <li>In certain regions, USGS 1-km global land-use database remapped to 0.01° resolution replaces climatology fields.</li> <li>Look up table assigns each land-use type (1-94) a value of ground wetness, albedo (open sea = 0.09, ice = 0.6), and surface roughness based primarily on Henderson-Sellers and Wilson (1986). Values are averaged at 0.01° resolution over each of the COAMPS domains to determine one value of each for every COAMPS grid point.</li> <li>Note: NPMOC San Diego's TAMS-RT now uses a 1-km global land-use database and a COAMPS Ocean Data Assimilation (CODA) SST and ice analysis updated twice daily. This value is held constant throughout each forecast cycle.</li> </ul>
Turbulence	1.5 order, level 2.5 TKE Closure (Mellor and Yamada 1982)
Surface Layer	Louis scheme (1979).
Terrain and coastal source and resolution	<ul style="list-style-type: none"> <li>Grid spacing ≥ 20km: Uses 20-km terrain database bilinearly interpolated to the grid resolution.</li> <li>Grid spacing &lt; 20km: Uses 1-km terrain database (NIMA level 1) bilinearly interpolated to the grid resolution.</li> <li>Terrain matching employed across mesh boundaries.</li> <li>Note: NPMOC San Diego's TAMS-RT uses 1-km global terrain and 400-m coastal databases.</li> </ul>
<b>Lateral Boundary Conditions</b>	
Time dependent boundary conditions	<p>Davies (1976) or optionally Perkey-Kreitzberg (1976) interpolated from NOGAPS (16 or 21 levels) available in temporal resolutions of hourly or in multiples thereof. Options for periodic, radiation, or fixed in idealized simulations. Option for sub-nesting local COAMPS domains within coarser regional domains.</p> <p>Note: NPMOC San Diego uses Davies method, 16-level, 12-h temporal resolution lateral boundary conditions (LBCs) from NOGAPS. COAMPS is typically triply nested and the LBCs of the inner meshes are updated at the model time step. Only the outer coarse mesh "sees" the NOGAPS LBCs.</p>

**C. UNIQUE ASPECTS OF MESOSCALE MODELING APPLICABLE TO OPERATIONAL DEPLOYMENT OF TAMS-RT AT REGIONAL CENTERS**

Given general initial conditions, a mesoscale forecast model is designed to provide high-resolution, physically consistent guidance as to how meteorological events may unfold, however higher resolution is not synonymous with higher accuracy. The mesoscale model is not an upgrade to the synoptic model and should be thought of as a different tool altogether, although understanding how the two work in concert is critical to interpreting the output (Gunderson 1999). As stated in the introduction, along with the mesoscale modeling initiative comes the requirement to train forecasters to intelligently and effectively implement this new capability into the forecast process to ultimately produce a more accurate and useful forecast. Thus, developing and nurturing a knowledge base of unique aspects of mesoscale modeling is essential. The purpose of the following discussion, along with the previous general discussion of COAMPS capabilities, is to help achieve that goal. Topics below include understanding the implications of both “cold” and “warm start” scenarios and understanding, minimizing and accounting for error sources unique to Limited Area Models (LAMs) like COAMPS.

**1. Cold and Warm Starts**

When a COAMPS run uses the most recent NOGAPS fields (a current analysis or a previous forecast) as the first-guess, it is referred to as a “cold start.” Cold starts are useful for calibrating COAMPS to a skillful synoptic analysis and forecast by NOGAPS; however, it may take up to 12-h into the forecast (i.e.,  $\tau_{12}$ ) for COAMPS to dampen out “noise” generated in the analysis and to develop useful mesoscale structure. This is sometimes referred to as model “spin-up” time. NPMOC San Diego forecasters have observed spin-up times as long as a complete forecast cycle. When the analysis uses the most recent COAMPS forecast as the first-guess, it is referred to as a “warm start,” or as the “data assimilation” mode. Warm starts can be advantageous in mesoscale modeling because they perpetuate previously developed mesoscale structure (inherent in the COAMPS first-guess) into the current analysis, but only if that first-guess is accurate. Otherwise, it can prove to be a detriment to the forecast.

**2. Understanding, Minimizing and Accounting for Error Sources that are Unique to Limited Area Models (LAMs) like COAMPS.**

There are a number of error sources for LAMs that limit the forecasting skill of mesoscale models. Assuming accurate model physics, the main sources of these errors originate in the boundary conditions and in the formulation of the initial conditions (Warner et al. 1997). Accurate specification of boundary conditions is very important in high-resolution LAMs. Boundary condition errors come in two forms, either lateral boundary condition (LBC) errors or errors in the

representation of the surface boundary. In general, a complex, high-resolution rendering of the surface and its interaction with the lower atmosphere will increase forecast skill over more simplistic renderings by global models. However, there are times when just the opposite happens (again, increased resolution does not always equate to increased forecast accuracy). Potential impacts of errors generated by the surface boundary and techniques to assess them are covered in more detail in Chapter IV. In the case of LBCs, small-scale errors in the initial conditions can be removed by the advection of information into the domain from the lateral boundaries in regions of inflow (Sashegyi and Madala 1992). Also, if the scale of the evolving disturbance is large compared to the domain of the limited-area model, the LBCs act to constrain the solution and further reduce error (Vukicevic and Errico 1990). On the other hand, errors obtained from such larger-scale forecast can quickly contaminate the forecast produced by a LAM, a potentially serious problem in rapidly evolving synoptic situations like fronts propagating through the domain (Sashegyi and Madala 1992). In these situations, the LAM's accuracy is directly tied to the parent model's accuracy (Vukicevic and Errico 1990). On the contrary, strong surface forcing during benign synoptic regimes can dominate the meteorological solution and result in more skillful forecasts.

Warner et al. (1997) mentions several sources of LBC-generated error and how to minimize their effects on the forecast. One source of error originates from the fact that LBCs are defined using more coarse resolution models (Warner et al. 1997). In general, LAMs have a higher resolution than the boundary information; therefore, boundary values are interpolated to the LAM grid, which introduces potential errors. Figure 2-2 depicts a “curtain” of upper-level vertical velocity noise evident in the first few hours of this particular model run. Although numerical diffusion efforts are employed to rapidly dampen these spurious structures, they may still propagate forward into the forecast as well as downscale into the inner domains. While it is suspected that these transients do not interact strongly with the meteorological solution, they can however complicate the interpretation of the forecast (Warner et al. 1997). These errors may be reduced by using successive nested grids to reach the desired target resolution and matching the outer grid resolution as close to the parent model resolution as possible (i.e., by introducing a less extreme resolution change between grid domains) (Sashegyi and Madala 1992). Another way to significantly minimize this error is to apply consistent model physics between the parent model and the LAM. If the physical process parameterizations are not consistent between the two, differences in the solution at the boundary may cause spurious gradients and feedback between the two grids, which can adversely impact the interior of the LAM domain (Warner et al. 1997). Other methods to minimize this error include avoiding the placement of boundaries within regions of complex gradients of topography or flow and creating large buffer zones between the outer

mesh boundary where the boundary conditions are ingested and the next inner mesh boundary. It appears that the errors generated in Figure 2-2 were the result of significant resolution differences between the parent model NOGAPS (~81 km) and the coarse mesh of the nested model COAMPS (45 km).

Because the LBCs generated by the parent model are usually linearly interpolated between ingestion times into the LAM, as is the case with NOGAPS and COAMPS, another method of reducing LBC error is to increase the temporal resolution of the parent model run such that the LBCs are updated more frequently (Warner et al. 1997). The TAMS-RT at NPMOC San Diego is currently constrained to 16-vertical levels of 12-h temporal resolution NOGAPS boundary conditions because of data transfer limitations between the center and FNMOC. Consider the impact of a 12-h linear interpolation process on frontal winds. In reality, the winds would shift rapidly (e.g., shift 90° in a fraction of an hour), whereas the LBCs in the model clock the winds gradually through the same 90° over a 12-h period (~5° wind shift per hour). The 9 and 10 February frontal case study is an example of a case where NOGAPS skillfully forecast the frontal location out to and beyond 24-h, however the LBCs it provided were unable to positively influence an erroneous COAMPS forecast. In the near future, TAMS-RT will be able to pull regional subsets of NOGAPS for boundary conditions using METCAST, a jointly developed METOC data exchange system developed by FNMOC and the SPAWAR. This process change will allow more of the desired data to be transferred over the existing communication lines and thereby increasing temporal resolution of the boundary conditions. Another related method is to increase the vertical resolution of the parent model LBCs. In an internal experiment, NRL noted a definite improvement in forecast skill when COAMPS ran with 21 NOGAPS levels versus 16 levels for a two-week period over an 81-km horizontal resolution domain. The improvement was most noticeable in the vertical representation of the marine boundary layer.

A second source of LBC error is introduced by erroneous forecasts by the parent model that is providing the LBCs (Warner et al. 1997). With COAMPS and other mesoscale models, LBC data is based on a global model start 12-h earlier, which must have a good handle on the forecast problems of the day. Otherwise, forecast errors in the parent model propagate into the LAM. This error is generally unavoidable and often undetectable because the LAM reflects physically consistent meteorological solutions, however they have little to no correlation to what is really happening in the atmosphere (i.e., there are no obvious “noise” patterns in the graphics like in Figure 2-2). This is a critical reason why forecasters must examine the accuracy of both the parent model and the LAM’s analysis before applying mesoscale model output to the forecast. The next chapter, “TAMS-RT Analysis Methods,” focuses on completing this process efficiently and successfully using TAMS-RT.

The overall effect of LBC-generated errors is that the error can propagate into the LAM forecast domain and impact forecast skill. Depending on the dynamics of the synoptic situation and the number of inner nests, the forecast may eventually be driven by the LBCs to the point where forecast skill is almost exclusively dependent upon the LBC errors (Warner et al. 1997). In a “cold start” scenario for example, there may only exist a narrow “window of opportunity” where a LAM like COAMPS has more skill than its global parent model, in this case NOGAPS. This occurs because during the “spin-up” time required for COAMPS to develop meaningful mesoscale structure to improve upon NOGAPS skill, the impact of LBC-generated errors is also growing and may dominate shortly after or even before COAMPS has time to “spin-up.”

Based upon the nature of LBC errors, LAMs may be most useful when the significant meteorological forcing is occurring within the innermost meshes. This occurs when strong synoptic flow interacts with the terrain or during regimes of weak synoptic flow or weak coupling of the flow field (i.e., strongly stable regimes) where mesoscale circulations like a land-sea breeze can develop and dominate. On the contrary, LAM skill may be limited by LBC errors during periods of strong flow crossing an upstream boundary or significant weather systems or forcing in the vicinity of any lateral boundary (Warner et al. 1997). Irregardless, the fact that LBC-generated errors may still be significant even when all precautionary steps have been taken makes them a critical factor in the forecast skill of models like COAMPS and a prerequisite to any forecaster’s mesoscale knowledge base. Armed with this knowledge, forecasters will understand how to intelligently configure the mesoscale models to minimize the negative effects of LBC-generated errors as well as to anticipate and interpret their unavoidable consequences on the forecast.

### III. TAMS-RT ANALYSIS METHODS

#### A. INTRODUCTION

Since their recent introduction operationally into the U.S. Navy's METOC community, mesoscale numerical weather prediction (NWP) has already earned the reputation among forecaster's as having the potential to not only produce forecasts with unprecedented accuracy, but also with unprecedented error. Because analysis errors are often a main source of error in the forecast, an evaluation of the analysis fields and its components are critical in determining whether to accept, reject, or modify the model's guidance. As mentioned in the preceding chapter, there are a number of error sources that limit the forecasting skill of mesoscale models. Assuming accurate model physics, the main sources of these errors originate in the boundary conditions and in the formulation of the initial conditions (Warner et al. 1997). Boundary condition errors come in two forms, either lateral boundary condition (LBC) errors or errors in the representation of the surface boundary. Many mesoscale modeling techniques are designed to mitigate the impact of these error sources and require changes to the initial setup of TAMS-RT. However, the following discussion illustrates the importance of evaluating the output analysis from any data assimilation process and is focused on helping the forecaster to determine the utility of a given TAMS-RT forecast. While the discussion below is directed towards TAMS-RT analysis on the coarse mesh, the general idea of the method can also be applied towards evaluating data assimilation on the *fine* mesh. Thompson et al. (1997) present a Catalina Eddy case where the mesoscale data assimilation system produced an accurate analysis and forecast by retaining much of the mesoscale structure of the low-level wind field in the previous forecast and then adjusting that structure to fit the available surface observations. Generally speaking, the fine mesh will show more mesoscale analysis error making the method a little more tenuous. The approach presented below would help the forecaster identify the accuracy of the analysis of the eddy and increase their confidence in the subsequent forecast.

#### B. DATA ASSIMILATION EVALUATION METHOD

Like using global numerical weather prediction (NWP) in an operational setting, basic methods and tools must be developed to help the forecaster make a rapid assessment of the utility of the mesoscale forecast guidance. In the case of data assimilation, accurate synoptic analysis is the key first step. For a successful forecast, TAMS-RT must accurately analyze key weather systems and synoptic forcing on the coarse mesh if it is going to successfully "funnel" them down to the fine mesh and then proceed to accurately forecast the mesoscale structure that develops in response to these systems. Otherwise, errors in the large-scale analysis directly lead

to errors of intensity, duration, and location in the mesoscale response, as many mesoscale features are critically dependent upon the nature of the synoptic scale flow (i.e., strength, direction, and stability) as it interacts with the surface (Bond et al. 1997). For example, in a cold-start scenario, the resulting mesoscale response may be inaccurately developed and located, or even an erroneous false alarm produced. In a warm-start scenario, the pre-existing mesoscale structure in the first-guess fields (assuming it is analyzed accurately to begin with) may be inaccurate.

A frontal passage case study from the 9<sup>th</sup> and 10<sup>th</sup> of February in the SOCAL bight region underscores the critical nature of being able to evaluate the data assimilation process in any given forecast. A motivating factor in this case is to show the different skill demonstrated by two successive COAMPS forecasts versus the corresponding global model forecasts from NOGAPS. A tendency is for forecasters to expect the more sophisticated and higher resolution mesoscale model to outperform the global model; however, this is not always the case. Usually, this only occurs when the mesoscale observations support a better analysis by COAMPS. As will be demonstrated, the clues to model performance were in the analysis fields.

### **C. FEBRUARY 9 & 10 FRONTAL PASSAGE: STATEMENT OF REALITY**

Satellite imagery from 0000 UTC 10 February shows the cloud signature of the actual front as it passes through the bight (Figure 3-1). A rope cloud is distinguishable on the imagery extending southwestward from Santa Catalina and San Clemente Islands southwestward through 30N-120W. A pre-frontal cloud wave pattern is also visible northeast of San Diego indicating turbulence in the presence of low-level stability. Figure 3-2 is a mesoscale analysis produced by Naval Air Warfare Center (NAWC), Pt. Mugu valid one hour earlier and clearly depicting the front over the waters between San Nicolas Island and Santa Catalina and San Clemente Islands. Also present are strong post-frontal winds on the order 10-12 m/s (20-25 kts) as well as more mild pre-frontal winds on the order of 5-7 m/s (10-14 kts). Frontal passage then occurs at the latter islands between 2300 UTC on the 9<sup>th</sup> and 0000 UTC on the 10<sup>th</sup> with the corresponding meso-analysis (not shown) valid at 0000 UTC 10 February depicting post-frontal conditions at San Clemente Island and pre-frontal conditions at San Diego.

#### **1. The Benchmark**

The utility of a mesoscale forecast model like COAMPS is demonstrated in Figure 3-3, a 12-h forecast based on an accurate analysis. This forecast was produced from a warm-start. Here, COAMPS not only propagates the position of the larger-scale front accurately down to the high-resolution nest, but also skillfully depicts the mesoscale structure of and the response to the

front. When compared against Figure 3-2, the COAMPS wind field verifies well in both location of the front (between San Clemente and San Diego) and in intensity of the pre- and post-frontal winds. The narrow rope cloud signature is even suggested in 1000-mb relative humidity fields. A less skillful forecast is made of the pre-frontal cloud conditions in the vicinity of San Diego. Figure 3-1 shows a relatively clear area ahead of the front while COAMPS depicts clouds (although this is hard to verify in view of the limited extent of the fine mesh southern boundary). The corresponding 12-h NOGAPS forecast (not shown) was also highly successful on the timing of the front, however a careful study of the more detailed mesoscale structure predicted by COAMPS (e.g., cloud droplet mixing ratio and vertical velocity) is more useful to the forecaster for gaining insight into the dynamic processes represented in the data.

## **2. A Poor Forecast**

On the other hand, the danger of unequivocally accepting the guidance provided by a mesoscale model like COAMPS is shown in Figure 3-4, a 24-h forecast verifying at the same time. This forecast was also generated from a warm-start. Depicted here are what appear to be post-frontal winds and cloud remnants over the southern bight waters and a front and its associated clouds over the coastal mountain range. In reality, however, the front is located between San Clemente Island and San Diego at 0000 UTC 10 February (Figures 3-1 and 3-2). In fact, earlier in the model run COAMPS depicted a weaker and less pronounced "modeled" front passing over San Clemente Island at 1800 UTC on the 9<sup>th</sup>, or 6-h ahead of reality. As expected, neither the medium or fine mesh forecasts improve the skill. The corresponding 24-h NOGAPS forecast (not shown) demonstrates a highly skilled forecast of the front in location, intensity, and in cloud signature. Although unable to depict a rope cloud feature, NOGAPS successfully forecasts the pre-frontal clearing in the cloud pattern that was observed at Naval Air Station, North Island. Thus, despite being seeded with highly accurate NOGAPS boundary conditions, the COAMPS 24-h forecast does not accurately predict the front and provides "detailed" but erroneous guidance to the forecaster, who in this case should have used the global model guidance from NOGAPS.

## **3. The Diagnosis**

But how can a forecaster know when the mesoscale prediction is going to be poor? Before a forecaster can tap into the valuable mesoscale structure and explicit parameter predictions available from TAMS-RT, they must first apply methods to convince themselves that COAMPS is properly reflecting the circulations of the observed atmosphere. One effective method is the study of the initial fields, particularly the analysis field with respect to the

observation fields and satellite imagery. This time-tested method of comparing the analysis against the observations and satellite imagery becomes even more paramount when using mesoscale NWP because of the added complexity of the data assimilation process and nested grids.

The initial analysis in TAMS-RT or any mesoscale model is a complex process, but a relatively easy one to evaluate in practice, provided the availability of effective display methods for the component fields that make up that analysis. In most cases, these fields are the new COAMPS analysis, the COAMPS (warm-start) or NOGAPS (cold-start) first-guess or background fields (12-h forecasts from the previous model runs), the NOGAPS boundary conditions (also a 12-h forecast from the previous model run), the observation field, and the corresponding satellite imagery to help define the actual large-scale flow (in this case the front). All of these fields are routinely available to the forecaster early in the forecast cycle. At a minimum, a fusion of the analysis and observation fields is imperative for rapid and effective evaluation; however, the ideal display system would fuse all of the above fields within the same geographic frame of reference as they are presented in this thesis. The following useful observations can be made from display combinations of these initial analysis fields.

#### 4. Document the Erroneous Analysis

An examination of the initial analysis (Figure 3-5) for the erroneous COAMPS 24-h forecast reveals an immediate problem. The COAMPS analysis appears to be disregarding most of the surface observations, especially the ship reports in the vicinity of the actual front. Again, COAMPS was running in a warm-start mode for this forecast. The analyzed front is too fast and is located approximately 120 nm to the southeast of the actual front. The observations clearly delineate the front as extending southwestward from Northern California through 35N 130W. These observations match extremely well with the corresponding satellite image (not shown). In cases where the observations are scarce, a combination of both satellite imagery and observations will have to be the primary tool for determining the location and intensity of the actual front at analysis time. Using this method of comparing the observation fields with the analysis fields, the forecaster can rapidly determine that the "mis-analysis" like the one in Figure 3-5 will lead to errors in the model forecast. Other data sources such as cloud-track satellite winds, SSMI winds and water vapor data, scatterometer wind data and other remotely sensed data over the ocean can assist as well.

A quick look at two other fields versus the analysis will help forecasters decide where to go from here. The first method involves evaluating the potential impact of LBC errors on the forecast. The NOGAPS LBCs are ingested into the COAMPS forecast through a 12-h linear

interpolation process and thus can make an impact on the forecast fields beyond the analysis, whereas first-guess/background fields can only impact the analysis. In this case, the NOGAPS 12, 24, and 36-h forecasts from the previous model run serve as the time-dependent LBCs for the current COAMPS forecast. When compared against the verifying observations and the satellite imagery, the entire NOGAPS forecast successfully depicts frontal location and intensity. From the vantage point of a post-analysis, the solid NOGAPS forecast however made little difference in the case of improving the erroneous 24-h COAMPS forecast. This contradicts the general theory that a good global model forecast will directly improve the embedded mesoscale model's performance (Warner et al. 1997).

At this point in our case study, the forecaster is armed with the knowledge that the COAMPS analysis is too fast and the previous NOGAPS forecast appears to have a handle on the front and now considers his or her options (these options are expanded below in the summary of this analysis method):

- to discard the subsequent COAMPS forecast entirely;
- to make a best-guess adjustment to COAMPS timing and use the "off-time" mesoscale structure forecast as an aid to forecasting conditions associated with the actual front;
- to use the previous NOGAPS guidance and apply conceptual models and forecast rules of thumb to forecast the mesoscale response to the front; or..
- if time permits, wait for the current NOGAPS run to come available and use it (assuming that it analyzes accurately).

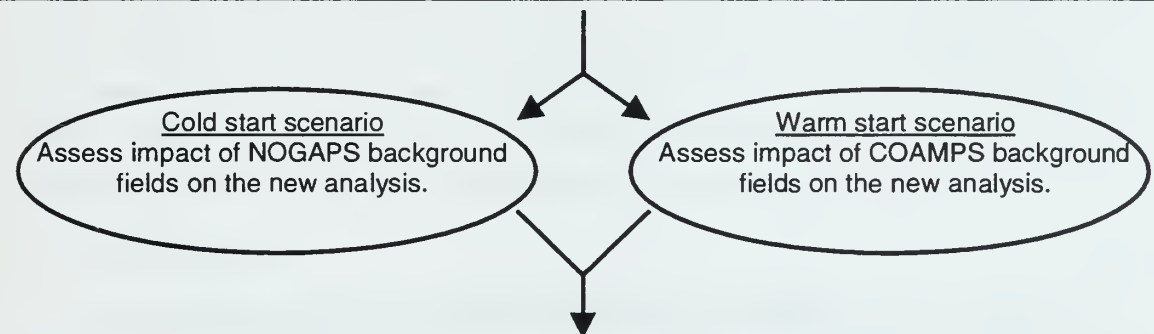
The important point in these previous steps is not for a forecaster to understand why the data assimilation process produced an erroneous analysis, but rather to provide a rapid red/yellow/or green light assessment of whether or not the mesoscale model guidance is an improvement upon the global model guidance. The last comparison method, however, is an evaluation of the first-guess/background fields, which may help to answer the question, "Why did the mis-analysis occur?" In this warm start scenario, the previous COAMPS run providing the first-guess/background fields has forecast the front too fast by 12-h and appears to be the culprit that caused the mis-analysis. The dominant effect that the COAMPS background fields had on the subsequent analysis is evidenced by the fact that the lowest level wind fields (10-m) are exact replicas of one another. The important ship and buoy data did not enter this run. This type of warm-start dominance by the background fields is not always a bad thing. In this case, the first-guess fields from the previous forecast were erroneous and dominated the analysis. Therefore, there is little reason to doubt that the new forecast will also propagate the front too fast. This is useful information if the forecaster decides to "translate" the COAMPS guidance to the suspected time of the actual frontal passage.

Surface observations and satellite imagery are not the only useful products for comparison with the COAMPS and NOGAPS fields. New web sites are being developed to help

forecasters evaluate the initial analyses as well as forecasts (e.g., first-guess fields) of both global and mesoscale models. Figure 3-6 is one such example resulting from collaborations between the University of Washington and the National Weather Service (NWS) Forecast Office, Seattle, WA, and can be found online at <http://www.atmos.washington.edu/~bnewkirk/>. This site is supported by the COMET/UCAR program and provides an evaluation of initialization fields of the ETA, AVN, MRF, and NGM models from the National Centers for Environmental Prediction (NCEP) in Washington, DC, the NOGAPS model from FNMOC, and the GEM model from the Canadian Meteorological Center in Montreal, Quebec. While Figure 3-6 consists of only ship and buoy data, comparisons between model output and observations are also available at various levels for cloud track/water vapor wind data, ACARS data, Rawinsonde data, scatterometer data, and precipitable water data from GOES. Both FNMOC (<http://www.fnmoc.navy.mil/>) and NRL Monterey ([http://www.nrlmry.navy.mil/projects/sat\\_products.html](http://www.nrlmry.navy.mil/projects/sat_products.html)) also maintain robust model initialization and comparison web sites.

#### D. SUMMARY OF THE EVALUATION METHOD

1. Evaluate the observation fields and satellite imagery to identify key synoptic patterns and mesoscale structure.
2. Evaluate the COAMPS analysis versus observation fields and satellite imagery.
3. Evaluate the NOGAPS forecast providing the LBCs for its potential impact on COAMPS.
4. Evaluate the COAMPS or NOGAPS forecast providing the first-guess/background fields for its potential impact on the COAMPS analysis.



#### 5. Suggested Courses of Action:

- NOGAPS and COAMPS both have accurate analyses and similar forecasts:
  - Use COAMPS NWP as primary guidance to take advantage of mesoscale structure prediction capability.
  - Note: if the forecasts deviate increasingly with time, use NOGAPS for the longer-range forecasts.
- NOGAPS forecast providing first-guess/background fields and LBCs verifies well and COAMPS analysis does not:
  - COAMPS missing the feature altogether:
    - Use NOGAPS NWP as guidance.
  - COAMPS has mis-analyzed the location of the feature:
    - Use NOGAPS as primary NWP guidance. The erroneous off-time COAMPS forecast can be used cautiously as secondary guidance for predicting mesoscale structure forced by the larger-scale flow pattern associated with the actual front.
- NOGAPS mis-analyzes the front: There is little improvement that COAMPS can make. Use other non-NWP methods (e.g., extrapolation, Hovmoller diagrams, and time series plot of observations).

THIS PAGE LEFT INTENTIONALLY BLANK

## IV. TECHNIQUES FOR INTERPRETING COAMPS FIELDS FROM TAMS-RT USING VIS5D

### A. WHAT IS VIS5D AND HOW DOES IT RELATE TO TAMS-RT?

Vis5D is a system for interactive visualization of large multi-variable gridded data sets such as those produced by numerical weather models. Simply stated, Vis5D is one of the COAMPS visualization tools deployed with TAMS-RT. Vis5D works on the COAMPS data in the form of a five-dimensional rectangle where the data are real numbers at each point of a "grid" which spans three space dimensions, one time dimension and a dimension for enumerating multiple physical variables. Without a doubt, Vis5D greatly facilitates real-time interpretation, product display, and the post-operational study of COAMPS output.

### B. WHY VIS5D?

Mesoscale physics go beyond many of the scaling assumptions that Navy forecasters unconsciously use while studying "conventional" 2-D weather maps (e.g., looking at 300 mb wind charts because that is where the jet stream is located). To leverage the remarkable capability provided by mesoscale modeling, Navy forecasters are going to have to learn about mesoscale systems and how to apply it efficiently and effectively. Visualization tools like Vis5D are a must in order to accomplish these goals because they are the only way to *quickly* and *effectively* capture and evaluate the complex structure and detail of the entire model run, a task that simply cannot be accomplished with 2-D plots and web pages of output. However, Vis5D alone is not the answer. An organized and systematic approach that employs 3-D pattern recognition techniques is also needed in conjunction with Vis5D to capture these benefits.

Vis5D has many features to help quantify the data being displayed in 3-D. For example, Vis5D allows a forecaster to "fly through" (probe) and vertically sound the gridded fields in four dimensions and in one-hour temporal resolution. Other standard features include the capability to make isosurfaces (a 3-D contour), contour line and color slices, and volume renderings of data in a 3-D grid, then as well as rotate, step and animate (fwd and reverse) through the images in real time. A critical feature is the capability to zoom in or out without losing resolution, a potential problem in Joint METOC Viewer (JMV). Furthermore, Vis5D allows a forecaster to create new display variables from standard model output variables, as well as provides support for comparing multiple forecasts either by overlaying them or by creating difference variables composed of data from at least two forecasts (e.g., temperature and pressure tendency displays). There's also a feature for wind trajectory tracing, a way to make text annotations for publication and also a way to save displays to graphic files for posting or later study. In essence, the maximum benefit from

mesoscale model output will be attained when forecaster skill in 3-D pattern recognition is effectively married to Vis5D's ability to display 3-D structure, quantified by color and contoured slices and probe and sounding readouts.

One of the main objectives of this thesis is to provide Navy forecasters with techniques for evaluating TAMS-RT output with Vis5D as well as recommendations for optimal settings and threshold values. The following provides general discussion concerning the techniques while Appendix B (Vis5D Settings) provides detailed procedures for making the recommended settings and thresholds and also serves as the baseline settings for the figures used throughout the remainder of this thesis. Because the procedures in Appendix B for making the recommended settings and threshold values are complex and can interrupt the flow of the following interpretation techniques, it is strongly recommended that all of the settings and threshold values be set and saved prior to application of these techniques. In many instances, the techniques are designed to work optimally with the recommended settings.

While the display capabilities of Vis5D are imperative for COAMPS evaluation, they are also ideally suited for the study of global model output. At a minimum, it makes sense to study the parent model gridded fields (i.e., NOGAPS) that are providing the lateral boundary conditions for the nested mesoscale model (COAMPS). Furthermore, visualization tools like Vis5D applied at the apex of the "forecast funnel" to fuse different data sources together would be a tremendous asset to forecasters to explore and dissect the "weather problem of the day." While not yet demonstrated, it is easy to grasp the utility of a Vis5D-based display of COAMPS grids alongside observational fields (e.g., satellite imagery, surface observations, Doppler or phased array radar data).

### **C. MESOSCALE MODEL INTERPRETATION TECHNIQUES USING VIS5D**

In harmony with the "forecast funnel" concept adopted by most Navy forecasters, the following techniques attempt to provide an incremental, sequential, and integrated approach to mesoscale model interpretation using Vis5D. In general, the techniques flow from the synoptic scale and its associated forcing on the COAMPS coarse mesh, to the mesoscale and its associated response on the fine mesh (see flow chart below).



Modeled Surface Boundary (e.g., terrain, surface albedo, land use)	Synoptic Orientation (low-level wind and upper-level pressure fields)	Mesoscale Orientation (low-level wind and mean sea level pressure fields)
Initial Analysis	Jet Stream Structure	Vertical Velocity
Successive Forecasts	Vorticity Advection	Clouds
	Thermal Advection	Precipitation
	Low-level response	High res. Low-level Winds
	Vertical Velocity	
	Clouds	
	Isentropic (dry adiabatic) Motion	

Whenever practical, conventional displays of traditionally inferred parameters (e.g., clouds from relative humidity) are presented first before introducing their corresponding explicitly derived counterparts (e.g., cloud droplet mixing ratio). Hopefully, this method will build confidence among experienced forecasters in the interpretation of COAMPS data as well as its relative performance (which may or may not be better). The techniques that follow are applicable to all forecast regimes and can provide a significant amount of insight into the guidance provided by COAMPS. However, these techniques do not address model errors that can invalidate the entire forecast (even when the analysis appears accurate). While the TAMS-RT analysis method presented in Chapter III is useful for determining whether or not to use the guidance at the outset, there is still the possibility for erroneous forecasts to follow. These errors can only be assessed through careful comparison of COAMPS analysis fields against the observations and appropriate mesoscale conceptual models.

## 1. Standard Evaluation Techniques for Using Vis5D.

### a. Techniques for Evaluating the “Modeled” Surface Boundary.

Before studying data from any particular model run, it is essential to study the “modeled” surface boundary parameters that remain fixed throughout all of the model runs. These surface boundary characteristics will provide the primary forcing mechanism for many of the observed mesoscale responses. While the critical nature of the parent model’s skill and the data assimilation process were emphasized in the previous chapter (TAMS-RT Analysis Methods), potential errors or modifications to the forecast fields resulting from poor representation or “modeling” of the surface boundary should also be evaluated. Each time a new COAMPS area

is created, it is imperative that a comparison is made between the best available products representing the surface and the “modeled” fields of those parameters in TAMS-RT (e.g., topography, coastal resolution, surface albedo, land usage and vegetation type). This comparison will yield useful information to aid in interpreting mesoscale NWP output. In some instances, the grid structure can be oriented to minimize introduction of error by the lateral and surface boundary conditions, especially the “modeled” topography. Currently, modeled topography and coastal resolution are the only surface boundary parameters that the forecaster can view in a graphical format. Future versions of COAMPS should empower forecasters with the capability to view surface albedo, land usage and vegetation type as well.

In the case of “modeled” topography (topo) and coastal resolution (also found in “topo”), forecasters should use the “probe” mode of Vis5D to explore areas of critical surface forcing and then consider the potential impacts of this evaluation on the forecast. Appendix C offers detailed procedures for this technique. Critical areas are regions known for their importance as a forcing mechanism for mesoscale features. Additionally, a forecaster should check for potential lateral boundary condition error sources identified by Warner et al. (1997) like boundaries in the vicinity of sharp gradients of the surface parameters. Some of the potential impacts of poorly resolved topography include modifications to the model’s rendering of turbulence, vorticity, or internal waves induced by flow over mountain ranges. Potential impacts of a poorly resolved coastline, surface albedo, land use and vegetation include modifications to the intensity, duration, and location of “modeled” land and sea breezes and convective processes.

Figure 4-1 is a high-resolution (20 ft in the vertical) topographic map of the SOCAL region produced by the Applied Physics Lab, Johns Hopkins University. When compared to the modeled topography in NPMOC San Diego’s TAMS-RT (Figures 4-2, 4-3, and 4-4), there are some obvious differences. The COAMPS topography is smoothed from a 1-km resolution terrain database that is bilinearly interpolated to the grid domain resolution, which is 45, 15, and 5-km in this case for the coarse, intermediate, and fine mesh domains respectively. Table 2 below highlights some of the differences apparent in the figures. Obviously, the coarse mesh will show the most disparity from the 20-ft topographic map and the fine mesh will show the least.

Table 2. A sample of elevation differences between COAMPS and actual topography.

Feature	Topographic Map	COAMPS Coarse	COAMPS Intermediate	COAMPS Fine
Mountains north of bight	5500 ft	3600 ft	3600 ft	NA
Mountains east of bight	6000 ft	3600 ft	4200 ft	4800 ft
Highest peak east of Los Angeles	11000 ft	4800 ft	4800 ft	7200 ft
Islands	~2000 ft	missing	missing	<=1200 ft

In this example, a critical area for formation of Catalina Eddies is the mountain ranges north of the bight. A closer examination of this area reveals three potential problems. First, the fine mesh does not encompass this mountain range, which takes away COAMPS best chance at a realistic depiction. Second, the northern boundary of the current inner mesh runs right through this area of steep topography and increases the potential for boundary errors to interfere with the actual solution. Third, the intermediate mesh is unaware of the top third of the mountain range. This last point may prove to be a key modifying factor in the case where an induced lee vortex (associated with formation of the Catalina Eddy) is critically dependent upon the amount of upstream blocking by the topography (Mass and Albright 1989). Displays are needed so forecasters can view and understand differences between the actual and COAMPS topography.

***b. Techniques for Evaluating the Analysis.***

In addition to evaluating the surface boundary characteristics, the current analysis and its difference from the previous forecast should also be examined before evaluating any of the subsequent forecast fields. The critical nature of evaluating the outcome of the data assimilation process was demonstrated in Chapter III. While not yet developed at NPMOC San Diego, Vis5D features a tool called “Texture Mapping” (section 6.15 of the Vis5D Readme File) that allows the display of a 2-D image over a surface in 3-D. For evaluation of the initial fields in Vis5D, these images should consist of satellite imagery and observations displayed over the topography or the bottom of the 3-D box. When evaluated against the COAMPS analysis or first-guess fields (or even Vis5D formatted NOGAPS fields), the comparison can reveal key information about the utility of a particular forecast as demonstrated in Chapter III. Although not ideal for this purpose, Figure 4-5 is an example of cloud liquid water (with a temperature/altitude color scheme) at analysis time is being displayed over the corresponding satellite imagery.

Although the data is often sparse, the forecaster should attempt to validate all aspects of the model with observations (e.g., verifying the strength and intensity of the jet stream, differential vorticity and thermal advection, vertical velocity, and cloud fields with surface and upper-air observations, satellite imagery and soundings, wind profiler and radar data, scatterometry winds and Special Sensor Microwave Imager (SSMI) wind speed and rain rate). Because this is not presently feasible in Vis5D, the use of other conventional display systems to analyze the observational fields will have to suffice. Fleet Numerical Meteorology and Oceanography Center and NRL Monterey maintain detailed maps of SSMI and scatterometry data. In these comparisons, a forecaster should look for obvious disparities between the analysis and the observation sources and then evaluate the impact on the forecast accordingly (e.g., too

fast or slow, strong or weak, or not analyzed at all) through the use of mesoscale conceptual models. Again, the advantages of developing this capability in Vis5D cannot be over-stated.

**c. Techniques for Evaluating Two Successive Forecasts Simultaneously.**

Vis5D also allows the comparison of two or more different data sets with the option of displaying the fields from the two different model runs either in a single window where difference fields can be created (as demonstrated below) or in multiple windows for a side-by-side comparison. Section 6 of the Vis5D Readme File details the various options. The following technique describes the comparison of the current COAMPS forecast with the previous one. The previous step of evaluating the analysis fields is critical for effective model-to-model comparison. The goal is to identify which run verifies more accurately with the observations then to identify any significant model trends and differences as well as the impact of new data on the current forecast. These steps should then help to “flag” areas in the new model run for closer examination by the forecaster. Appendix D (Vis5D Comparison Procedures) describes in detail the process of ingesting and displaying specific fields for comparison.

After the previous forecast is loaded and new variables are created, there are several fields that a forecaster may want to evaluate. A forecaster should look for jet stream intensity and location differences and upper-level divergence differences associated with these jet stream changes in the model. Figure 4-6 shows how the jet stream core has expanded from in the previous run (orange) to the current run (purple). The vertical slice is a wind difference comparison that subtracts the previous forecast values from the current one and it shows how the jet core has intensified. Positive values (yellow to red) are areas where the jet stream intensity in the current model run is greater than in the previous model run, whereas negative (blue) regions are of the opposite effect. Clearly, if the broader, more intense jet verifies with analysis observations and/or satellite imagery, then the most recent forecast should be an improvement upon the previous one.

A forecaster should also evaluate changes in the air temperature fields to identify temperature advection differences between two successive model runs and the corresponding impact that this has on the weather feature(s) of interest. A subsequent evaluation of pressure field differences (~500 mb and sfc) may help to identify the impact on the feature(s) (weakening or strengthening) by jet stream and temperature advection differences discovered in the previous comparisons. The pressure field comparison may reveal areas of more intense highs and deeper lows in the analysis and forecast fields as a result and thus “flag” these areas in the new model run for closer examination by the forecaster.

Every model run should show some changes from the previous one (in fact, if it doesn't this is a key indicator that something might be wrong in the data assimilation process), the question to be answered is "are these changes significant to the forecast?" An examination of the surface wind speed fields (or other sensible weather parameters) should help to quantify the impact of those changes as to whether or not they are "significant" to the specific forecast being made. The wind fields should amplify and reveal areas that may not have been obvious in the previous fields like stronger/weaker gradients and pre- or post-frontal wind intensity.

Lastly, an evaluation of the vertical velocity fields will reveal tendency changes in the mesoscale response for upward or downward motion between the two model runs. Vertical velocity is usually small at analysis time and then grows throughout the forecast as the model physics are given the time to develop it. Therefore, any significant differences should be scrutinized closely and evaluated against observations and satellite imagery. For example, large vertical velocity differences at analysis time may be indicative of potential data assimilation problems associated with "ingesting" lateral boundary conditions that are highly dissimilar from the background fields. On the other hand, large deviations occurring later in the forecast are indicative of physical differences developed in the forecasts of the two different model runs. Again, the model run that analyzes most accurately against the observations should produce the more accurate forecast. Satellite imagery at analysis time might reveal key indicators of the extent and intensity of the actual vertical velocity and help make this determination. Figure 4-7 depicts a vertical velocity difference cross-section for the current forecast minus the previous forecast. In this graphic, positive areas (red) denote areas of greater ascent (or less descent) by as much as 4 cm/s in the region just ahead of the surface front, thereby indicating the front is more active in the current forecast. This large disparity should alarm a forecaster and motivate them to closely examine the observation fields if they have not done so already to verify the current model's analysis. Dependent on their findings, they can either confidently use or discard the guidance when producing the subsequent forecast.

## **2. Techniques for Using Vis5d to Evaluate COAMPS on the Coarse Mesh.**

Once the COAMPS analysis is assessed and the forecaster has confidence that the COAMPS guidance should prove useful, they can begin to explore the COAMPS forecast fields in more depth. When working with nested grid domains, it is beneficial to study the innermost domain within the context of the encompassing domains; therefore, techniques for evaluating gridded fields on the coarse mesh will be examined first followed by techniques for the fine mesh. Words and pictures will prove inadequate to describe the utility of these techniques, so the reader is encouraged to apply a "hands-on" approach, making aggressive use of Vis5D's sounding

mode, and animation, rotation, and zoom features in conjunction with the evaluation of the techniques below.

Before continuing, it is helpful to make a few important points that apply to all of the subsequent coarse and fine mesh techniques. First, it is helpful to establish a “feature reference” that remains consistent throughout the various displays. The continuous display of the surface wind barbs is recommended as the “feature reference” for tracking its location relative to the other variables displayed in the subsequent techniques. Second, the use of low threshold settings for variables equates to a conservative display of that variable. For example, the lowest threshold setting for cloud droplet mixing ratio would equate to all possible locations of model developed cloud droplets, whereas a higher threshold setting would tend to depict only those clouds associated with a stronger forcing mechanism and hence a greater chance of actually verifying. Lastly, these techniques are hypothetically based upon the assumption that the forecast fields are highly accurate. While the overall accuracy of the actual forecast used in these examples was poor, the techniques still demonstrate how a forecaster can gain helpful insight into the dynamical aspects of COAMPS output.

**a. *Synoptic Orientation: Surface Wind Barbs (Hwind1 and Hwind2) and a Mid-level Pressure (pppp) Slice.***

A forecaster should use this graphic to achieve “synoptic orientation” (i.e., transfer the weather picture as presented by other conventional meteorological display systems like FNMOC's Joint METOC Viewer (JMV) to Vis5D). This display is ideal for identifying major synoptic weather patterns and the associated forcing for the “weather problem(s) of the day” as well as the relative orientation of related features (e.g., upper level troughs and low pressure systems relative to the surface front). Figure 4-8 is an example of a “synoptic orientation” chart depicting a mid-level pressure slice (~500 mb according to the vertical reference slice) and the surface wind barbs. A “TOP” view option is selected to give the familiar 2-D display. Note that the pressure slice is the display of all the pressure values at a constant height and is unlike the conventional display of isoheights of a constant pressure surface. Isoheights can be achieved by displaying a pressure isosurface but the vertical height differences were too difficult to effectively resolve on such a large horizontal scale (the fine mesh demonstrated the same problems as well). The purpose of the next three graphics (the jet stream structure, vorticity and thermal fields) is to give a forecaster a sense of what is forcing the vertical motion that will be viewed in a later technique.

**b. Jet Stream Structure (Wind Speed Isosurface (wspd), Streamlines (Hstream), and horizontal contour slice, and a Vertical Wind Speed (wspd) Cross-section)**

This graphic is ideal for identifying upper level long-wave troughs and ridges as well as characteristics of the jet stream including the jet core, its intensity and propagation through the long-wave pattern, and its vertical extent towards the surface. Forecasters should also look for directional diffluence in the streamlines and speed divergence in the isotach contours. Figure 4-9 depicts a 45 m/s (90 kts) jet core extending throughout the base of a long-wave trough alongside a vertical slice depicting the intensity and vertical extent of the jet stream. Both directional diffluence and speed divergence are occurring east of the trough and upper-level cyclone, whereas the vertical slice reveals that the 80-kt jet core extends down to nearly 500 mb. From these characteristics, forecasters can infer potential areas of upper-level divergence and convergence related to the jet, its vertical extent towards the surface, and infer any subsequent vertical motion that might be forced by this area of upper-level divergence.

**c. Vorticity Advection Forcing: Mid-level (~500mb) Wind Streamlines (Hstream) and Vorticity (rvor and avor) Isosurfaces and Horizontal Contour Slices.**

The purpose of this graphic is to reveal to the forecaster an indication of the strength of the quasi-geostrophic vorticity forcing causing vertical motion (one portion of the forcing in the Petterssen development equation). A forecaster should identify regions of both positive and negative vorticity advection (PVA and NVA respectively), noting its vertical extent, and apply the reasoning that upward/downward vertical velocities are inferred in regions where PVA is increasing/decreasing with height (Petterssen 1956). In Figure 4-10 (left side), PVA is occurring east of the upper-level trough.

**d. Thermal Advection Forcing: Lower Level (~850mb) Wind Streamlines (Hstream) and Air Temperature (ttt) Horizontal Color and Contour Slices.**

The purpose of this graphic is to reveal to the forecaster an indication of the strength of the quasi-geostrophic thermal forcing causing vertical motion (the other portion of the forcing in the Petterssen development equation). A forecaster should identify regions of both warm and cold air advection (WAA and CAA respectively) and apply the reasoning that upward vertical velocities are inferred in regions of localized WAA, whereas downward velocities occur in regions of localized CAA (Petterssen 1956) and that strong confluent regions also correspond to

frontogenesis regions. As expected, Figure 4-10 (right hand side) shows CAA occurring into the base of the long-wave trough while WAA is occurring out ahead of the surface front. Both PVA and WAA regions coincide with the upper-level divergence associated with the jet stream. These three factors considered together give a pretty clear indication of where to expect the model to develop strong ascent regions from quasi-geostrophic considerations. It should be kept in mind, however, that such quasi-geostrophic considerations may not hold for mesoscale features.

**e. *Low-level Response: Low-level Wind Barbs (Hwind1 and Hwind2) and a Mean Sea Level Pressure (slp4) Horizontal Slice.***

In this technique (not shown) a forecaster should look for the surface reflection of the upper level forcing identified in the previous steps (e.g., surface low-pressure regions, fronts, troughs, convergent areas). Locating these primary features in time and space now will help the forecaster to later associate the applicable portion of the often-noisy displays of other mesoscale parameters.

**f. *Vertical Velocity (W) Isosurface and vertical slice.***

The study of the previous forcing inferences (upper-level divergence associated with the jet, vorticity and thermal forcing) culminates in the actual display of the vertical velocity fields. Although vertical velocity could have been viewed at any time, it is suggested that going through the process of becoming acquainted with the forcing fields first will allow a forecaster to better interpret this field. This graphic is best evaluated when displayed in the sounding mode and with the vertical velocity plotted alongside the temperature traces (as in Figure 4-11).

Figure 4-11 is a zoomed-in view of the vertical velocity associated with a front passing through the SOCAL bight. In this graphic, a forecaster should first identify the vertical motion associated with the feature of interest based upon forcing inferences made thus far. In this case, the surface front is associated with the “finger-like” structure extending from northeast to southwest. Vertical ascent associated with the upper-level front is shown arching back up and over the inferred frontal surface. Note the frontal signature in the vertical velocity profile in the Skew-T as indicated by the positive “bump” in the profile. Coarse mesh familiarization with the actual signal relating to the weather feature of interest will serve as a “hook” for locating and identifying that signal again on the fine mesh where the signal to noise ratio is often less than on the coarse mesh.

After a careful study of this aspect of vertical motion, the forecaster should then evaluate vertical motion resulting from other forcing mechanisms. The following techniques are designed to help the forecaster correlate vertical motion to its forcing mechanism. For example,

vertical motion associated with advective processes will propagate through the domain whereas vertical motion caused by topography will generally remain anchored over the corresponding topographic feature. In Figure 4-12, the vertical ascent associated with the front (i.e., the yellow to red region in the center of the figure) is located where expected based upon the quasi-geostrophic forcing inferences made in the previous steps. The vertical velocity has a maximum value of +8 cm/s in the vicinity of the upper-level front and -6 cm/s in the broad descent (blue) region of in the cold air behind the front. Apart from these areas, note the upper-level ascent region to the southeast in the upper levels. This region is geographically separated from the primary quasi-geostrophic forcing regions noted previously, but is coincident with a mountainous terrain (~6000 ft) at the surface. Additionally, this region remains stationary when the fields are looped and must therefore be associated with terrain induced vertical motion.

**g. Isentropic (Dry Adiabatic) Motion: Potential Temperature (pott)  
Isosurface and Vertical Color and Contour Slices.**

This technique is an effective educational tool in that it ties the response (vertical motion) to the forcing mechanism (flow on an isentropic (i.e., potential temperature) surface). Used with the sounding mode, it also helps a forecaster to separate quasi-geostrophic forcing from other forcing mechanisms like terrain. Figure 4-12 also shows a 286° K potential temperature isosurface. Again, note how the ascent region (yellow to red) arches back over the frontal surface as inferred from the orientation of the potential temperature surface.

In isentropic analysis, the goal is to identify regions of “slantwise ascent or descent” (see Carlson 1991 for a concise description of the method). In isentropic (dry adiabatic) motion, parcels conserve energy and either ride up or down an isentropic surface when ascending or descending dry adiabatically (and a little bit of a steeper moist adiabatic trajectory when saturated). In an ideal isentropic analysis, the relative winds are used (actual winds minus the translation of the system) to identify places where parcel trajectories are either riding up or down a constant isentropic surface. However, animating a potential temperature isosurface in Vis5D allows an adequate inference as to parcel trajectory and can be used to identify broad regions of ascent or descent. Just like vertical velocity, it is especially useful to use the sounding mode with vertical velocity plotted alongside the temperature traces for this evaluation. In this way, broad areas of ascent and descent can also be associated with tropopause height changes. The tropopause is identified in the upper levels (~10 km) where either tight packing of the potential temperature surfaces occurs or at the base of the stratospheric inversion (upper-level stable layer) in the temperature trace. This technique is also conceptually related to the earliest

Norwegian cyclone models. Observing a potential temperature surface propagate through a region provides a visualization of a cold wedge of air undercutting a warmer air mass.

*h. Clouds: Relative Humidity ( $relh$ ) Isosurfaces.*

The first application of this technique (not shown) involves using the relative humidity fields to identify “tongues” of dry air and their potential impact on the cloud fields to be viewed subsequently. This is accomplished by displaying a relative humidity isosurface at a low threshold (e.g., 50%) and looking for “voids” or “holes” in the isosurface, which indicate the presence and intrusion of dry air. This can be compared to dry regions on water vapor satellite animations.

*i. Clouds and Vertical Motion: Vertical Velocity ( $W$ ) Isosurface and Cloud Isosurfaces (Ice Crystal and Cloud Droplet Mixing Ratios ( $q_{iii}$  and  $q_{ccc}$  Respectively)).*

This technique ties the signature and magnitude of the cloud prediction to the vertical motion fields evaluated in all of the preceding techniques. A forecaster should use this graphic to examine the correlation between the location and intensity of ascent and descent regions and the corresponding cloud formation or lack thereof, noting that not all ascent regions will form clouds. Included in this task is an effort to identify different cloud origins (stratus or cumulus). In general, cumulus clouds will be associated with strong, deep convection (i.e., vertical motion) whereas the stratus clouds will be associated with weak convection or even broad descent regions. Small values of cloud droplet and ice crystal mixing ratios ( $q_{ccc}$  and  $q_{iii}$  = 0.01 g/kg) are used to display *all* of the forecast clouds.

*j. Cloud Comparisons: Relative Humidity ( $relh$ ) and Cloud Droplet and Ice Crystal Mixing Ratios ( $q_{ccc}$  and  $q_{iii}$ ).*

This technique is primarily an educational tool to help the forecaster compare clouds indicated by relative humidity thresholds to clouds explicitly defined by the mesoscale model. Figure 4-13 is an example of a comparison of the two types of cloud renditions. Forecasters will be comforted to see general agreement between the two and thus increase their confidence in cloud depictions as defined by cloud droplet and ice crystal mixing ratios.

In most global models (NOGAPS and older), clouds are parameterized by relative humidity thresholds and are usually indicative of large-scale ascent and stratoform type clouds. A common cumulus parameterization scheme and the one used in NOGAPS (Arakawa-Shubert) is a function of stability (temperature) and moisture in the vertical. The scheme is

activated when relative humidity exceeds a pre-determined threshold (often referred to as a “knob” by modelers because you can adjust it). Upon activation, the scheme invokes vertical motion to stabilize lapse rates. Just as in the real atmosphere, the modeled cumulus clouds are “vertical mixers.” On the contrary, mesoscale models have an additional set of equations that explicitly compute cloud droplet or ice crystal mixing ratios and their dispersion in space and time (variables include size, distribution, fall velocity, evaporation rate, etc.). A characteristic of these equations is that once a cloud is formed, it tends to remain until it dries out by other processes (i.e., modeled clouds will hang on even as the relative humidity drops off). In general, this should equate to a more “realistic” rendering of the forecast clouds.

Forecasters should try to validate this assumption by looking for time lags between the two (i.e., cloud droplet mixing ratio fields persisting after relative humidity fields) and verifying their observations against actual cloud conditions. At a minimum, forecasters should try to identify differences and/or similarities between the two cloud field renditions, noting the relative humidity thresholds that equate to the model derived clouds, and finally verifying them against the actual cloud fields. By continuously comparing the two, forecasters will develop a keen sense of how to interpret the model derived cloud fields and the knowledge to adjust them according to their strengths and weaknesses in various forecast scenarios. In general, forecasters will find that the explicitly derived clouds in COAMPS are more conservative than common rules of thumb for clouds defined by relative humidity thresholds (usually +80%). In COAMPS, the lowest possible cloud droplet and ice crystal mixing ratios usually correspond to high relative humidity thresholds (~+95%). On a final note, familiarization with the cloud pattern on the coarse mesh will provide a guide for interpretation on the fine mesh.

### **3. Techniques for Evaluating COAMPS on the Fine Mesh.**

Many of the graphics in this section are the same as those presented for the coarse mesh evaluation. To apply these techniques, forecasters should follow the same procedures as those outlined above for the coarse mesh analysis with the added focus of identifying mesoscale structure that so often only develops on the fine mesh because of the closer grid-point spacing and the interaction of the flow with the high-resolution surface boundary. In order to capture that resolution graphically, forecasters are strongly encouraged to use the modeled topography as the background instead of the Vis5D default topography because of the latter’s coarse resolution.

a. ***Mesoscale Orientation: Low-level Wind Barbs (Hwind1 and Hwind2) and a Mean Sea-level Pressure (slp4) Horizontal Slice.***

As in the corresponding coarse mesh technique, the forecaster should look for location of the “weather problem(s) of the day” in both space and time. A natural consequence of evaluating frontal or synoptic-scale features in nested models is that the feature may appear within the coarse mesh and still be outside the domain of the fine mesh. Often, features will propagate rapidly through the fine mesh domain in only a fraction of the total time steps. Therefore, locating the surface reflection of the feature in these fields will help the forecaster to more readily identify the corresponding vertical motion in the vertical velocity fields to be evaluated next. On the other hand, many mesoscale features (e.g., sea breeze circulations, the Catalina Eddy, terrain-induced clouds or mountain waves) are geographically anchored and will not propagate between domains.

b. ***Vertical Velocity (W) Isosurface and Vertical Color and Contour Slices.***

A characteristic of the fine mesh is that the vertical velocity fields are generally “noisier” (i.e., both signal and noise values are higher). In fact, a higher vertical velocity threshold for the Vis5D isosurface is recommended for fine mesh than on the coarse mesh in order to increase the signal to noise ratio associated with the feature of interest. Even with the higher threshold setting, the vertical velocity fields will continue to exhibit considerably more mesoscale structure. Both the previous surface wind and pressure field evaluation and the prior coarse mesh vertical velocity evaluation will help to distinguish the signal of interest in the fine-mesh vertical velocity fields. Again, this graphic is best evaluated when displayed in the sounding mode and with the vertical velocity plotted alongside the temperature traces in order to quantify positive ascent regions with the 3-D isosurface.

c. ***Clouds and Vertical Velocity: Vertical Velocity (W) Isosurface and Cloud Isosurfaces (Ice Crystal and Cloud Droplet Mixing Ratios ( $q_{ii}$  and  $q_{ccc}$  Respectively)).***

The same coarse mesh techniques apply here, except that the vertical velocities are usually amplified and the corresponding cloud fields altered on the fine mesh as a result (both signal and noise). As such, forecasters should try to correlate the mesoscale structure observed in the cloud fields to the mesoscale structure in the vertical velocity fields. Areas with high correlation should provide more accurate guidance than areas of low correlation. Figure 4-14

depicts detailed mesoscale structure in the fine mesh cloud bands associated with a front passing through the SOCAL bight.

- d. Precipitation and Vertical Velocity: Vertical Velocity (W) Isosurface and Precipitation Fields (Rain Drop and Snow Flake Mixing Ratio Isosurfaces (qrrr and qsss Respectively), and 12-h Total Accumulated Precipitation (prcp) Horizontal Color and Contour Slices).**

In this graphic, the precipitation thresholds are first set low ( $q_{rrr} = 0.01$  and  $q_{sss} = 0.1 \text{ g/kg}$ ) to show the forecaster *all* locations in the domain where the model is developing precipitation. The threshold can then be increased to highlight only those areas of the most intense “modeled” precipitation. Potential areas of heavy precipitation can be inferred by correlating the precipitation fields to the strength and extent of vertical motion fields. These areas also show up in the 12-h total precipitation fields as areas of the heaviest accumulated rainfall. Forecasters might be surprised to observe that the greatest “weather” is not actually associated with the previously identified “weather problem(s) of the day.” Often, the highest accumulations of precipitation might be orographically induced rather than as the result of the most intense convection. One last item a forecaster may be interested in is identifying areas where the precipitation is reaching the ground as snow instead of rain.

Figure 4-15 depicts rain droplet mixing ratio (large transparent green cloud) over the 12-h total accumulated precipitation fields. While there is a significant region experiencing rainfall, the heaviest 12-h accumulation regions (orange to red areas) are associated with pre-frontal flow ascending the mountains north of the SOCAL bight as well as the interaction of the flow with the islands.

#### **4. Techniques for Using Vis5D in Specific Forecasting Scenarios.**

The purpose of this section is to demonstrate Vis5D’s utility in actual forecast scenarios. The “sensible weather” forecast parameters featured in this section are all elements of routine forecast products currently provided by NPMOC San Diego, California and NPMOC Pearl Harbor, Hawaii including operating area of responsibility (OPAREA), aviation/ship weather (AVWX), and flight planning (OPARS) forecasts. While only a few of these parameters are demonstrated graphically in this section, forecasters are encouraged to view the Naval Postgraduate School’s (NPS) Mesoscale NWP web site at (<http://www.met.nps.navy.mil/~ldm/wash/meso/ajreiss/>) for a more complete demonstration.

Because of the higher resolution surface databases (assuming they are accurate) and to minimize the effect of LBC errors associated with LAMs, forecasters should use the highest resolution domain available for their forecast area; however, the following recommendations are applicable for any of the domains. An obvious word of caution is for forecasters to be aware that the same variables will differ spatially and in intensity (sometimes significantly) between various domains. The previous discussion concerning the different vertical velocity thresholds for the coarse and fine mesh illustrates this point. As with the coarse and fine mesh analysis techniques, the aggressive use of the sounding mode, contour slices, animation, rotation, and zoom features in Vis5D is highly recommended to quantify the model output to gain maximum benefit from the following techniques.

**a. Recommended Graphics and Techniques.**

The techniques in this section are summarized at the end of the chapter in Table 3 which consists of the sensible weather parameters, followed by the recommended Vis5D variables to use as forecast guidance for that parameter. Again, these techniques assume a hypothetically “perfect” forecast and do not address model errors that can invalidate the entire forecast. These errors can only be assessed through careful comparison of COAMPS analysis fields against the observations and appropriate mesoscale conceptual models.

Figure 4-16 depicts one way to illustrate turbulence in a Vis5D graphic. This graphic is a fusion of the vertical velocity isosurface pertaining to upward vertical motion and the cloud fields (both cloud droplet mixing ratio and ice crystal mixing ratio). Identifying turbulent regions is accomplished by comparing the vertical velocity and cloud fields. Turbulence can be inferred everywhere within the vertical velocity and/or cloud isosurfaces. Turbulence intensity can be inferred by varying the vertical velocity threshold. Remembering that the magnitude of vertical velocity will be greater on finer meshes, forecasters must choose thresholds carefully to tune into values of “significant” vertical motion and hence turbulence. In-cloud versus clear-air (CAT) turbulence can be distinguished by whether or not the vertical motion is occurring within a cloud field isosurface. Another way to illustrate turbulence in a Vis5D graphic is to slide a contoured horizontal wind speed (wspd) slice vertically through the domain (not shown). Forecasters should look for areas of strong horizontal wind shear (i.e., where the contour spacing is relatively tight). Additionally, turbulent kinetic energy (tkee) was not studied in this thesis but could also provide turbulence forecast guidance.

Figure 4-17 depicts forecast guidance for icing in a Vis5D graphic. This graphic is a fusion of a cloud droplet mixing ratio isosurface and a 0° C air temperature isosurface. Icing is inferred wherever cloud droplets (i.e., the same as cloud liquid water and indicated by the cloud

droplet mixing ratio isosurface) are located within sub-freezing air (demarcated and indicated by the 0° C air temperature isosurface). Forecasters should remember that low thresholds for clouds equate to low thresholds for icing forecasts (i.e., *all* possible regions will be indicated where icing can occur according to the model). Thresholds can be set higher to attain higher confidence levels (assuming the model is accurately depicting clouds and the freezing level to begin with).

Figure 4-18 depicts forecast guidance for producing high wind warnings in a Vis5D graphic. Displays of horizontal color and contoured wind speed are used to highlight a gale area just off the northern California coast. Wind speed isosurfaces can also be used on COAMPS fine mesh to capture high wind events in valleys and mountain passes.

##### **5. Other Forecasting or Education Possibilities Available with Vis5D.**

Using some of the aforementioned procedures as well as displaying new variables available in Vis5D also allows forecasters to evaluate other pertinent fields such as boundary layer height (blht) and fluxes, refractivity parameters (M-units (mref) and refractivity gradient (dm/dz)), and turbulent kinetic energy (tkee). As a final note, study of certain variables like coarse mesh vertical velocity at the analysis time, presents a rare and useful educational opportunity to “graphically” depict potential error sources associated with the boundary conditions of limited area models like COAMPS. The upper-level “curtain” of upward vertical velocity in Figure 2-2 is a graphical depiction of spurious “noise” most likely generated because of the large resolution differences between NOGAPS and the COAMPS coarse mesh (~81 km versus 45 km). Forecasters are encouraged to refer to the NPS mesoscale meteorology homepage for additional graphics.

Table 3. Techniques for Using Vis5D in Specific Forecasting Scenarios.

Sensible Wx Parameters	Vis5D Variable
Winds:	
LL winds/warnings (Figure 4-18)	Horizontal wind barbs (Hwind1, Hwind2) + wind speed (wspd) color and contour horizontal slices
UL winds	Same as above
Clouds: (Figure 4-14)	
Coverage	Relative humidity (relh) + Cloud droplet (qccc) and Ice crystal (qiii) mixing ratio Isosurfaces <sup>1</sup>
Min ceiling	Same as above + Boundary layer height (blht) horizontal slice <sup>2</sup>
Max ceiling	Same as above + Boundary layer height (blht) horizontal slice <sup>2</sup>
Visibility	Same as above + Boundary layer height (blht) horizontal slice <sup>2</sup>
Precipitation	Rain drop (qrrr) + Snow flake (qsss) mixing ratio Isosurfaces
Temperature extremes	Air (ttt) and ground temperature (ttgg) horizontal slices <sup>3</sup>
Turbulence	<ul style="list-style-type: none"> <li>Vertical velocity (W) Isosurface and vertical slices + Cloud droplet (qccc) and Ice crystal (qiii) mixing ratio Isosurfaces. (Figure 4-16)</li> <li>Contoured horizontal wind speed slice (wspd).</li> <li>Turbulent kinetic energy (tkee) isosurface and horizontal contours.</li> </ul>
Freezing level	Air temperature (ttt) 0° isosurface
Icing (Figure 4-17)	Cloud droplet mixing ratio (qccc) Isosurface + Air temperature (ttt) 0° isosurface
SST	Ground temperature (ttgg) horizontal slice (note: static throughout forecast cycle)

Table 3 notes:

<sup>1</sup>The temperature and dew point temperature traces in the SKEW-T display of the sounding mode should also be used to infer “modeled” cloud layers.

<sup>2</sup>Boundary layer height gives an indication of the extent of vertical mixing and therefore the tops of a low stratus cloud deck.

<sup>3</sup>Air and ground temperature differences set up (or are the cause of) fluxes that are accounted for in the boundary layer physics, however a forecaster may want to create and view a temperature difference variable between the two. Refer to the NPS Mesoscale NWP web page for a sample graphic and Appendix B (Vis5D Settings) for procedures on creating an air-ground (or sea) temperature difference variable called “C\_AIR.”

## V. TAMS-RT CASE STUDIES AT NPMOC SAN DIEGO

### A. FRONTAL PASSAGE AND THE ASSOCIATED WEATHER IN SOCAL

#### 1. Introduction

Of the several frontal passage events archived, the case studies below were specifically selected to highlight the critical nature of the data assimilation process and how a basic understanding of this process, along with a verification of the initial analysis against available observations and satellite imagery, can help forecaster's significantly improve their ability to interpret COAMPS forecasts. In addition to the case study for a frontal passage on the 9<sup>th</sup> and 10<sup>th</sup> of February that was presented in Chapter III, two more detailed verification studies are presented for frontal passage events on the 15<sup>th</sup> of March and the 12<sup>th</sup> of April. Both of the February and March cases are examples of warm-start scenarios whereas the April case serves as an example of a cold-start scenario. Additionally, a qualitative verification of COAMPS performance is provided for wind, precipitation, cloud and vertical structure forecasting. Studies have evaluated COAMPS performance from a statistical approach, however the reader is especially encouraged to review the results obtained by Monterrosa (1999) in his master's thesis, which utilized the same data set and covers roughly the same time period as the case studies presented below.

#### 2. General Climatology of Fronts in the SOCAL Region

The frontal cases presented in this chapter are fairly typical of the climatological record for fronts associated with extra-tropical cyclones in the Northeast Pacific Ocean. A condensed summary of their origin and propagation climatology taken from NPMOC San Diego's Forecaster's Handbook (1995) is presented to set the stage for presentation of the cases. In general, the vast majority of extra-tropical cyclones forming in the Northeast Pacific Ocean develop over the seas surrounding Japan. This region is one of the world's principal cyclogenesis regions due to the unique continental topography of East Asia and the strong low-level instability introduced by the interaction of the warm Kurushio ocean current with the overlying atmosphere. After an initial period of rapid growth, these cyclones and their associated fronts usually begin dissipating as they move into the Bering Sea, Gulf of Alaska, or move over North America. As the winter progresses and the polar jet stream migrates toward the equator, the storm track also migrates south. By mid to late winter, mature cyclones move through the Eastern Pacific Ocean and continue eastward into the southern Gulf of Alaska and into the west coast of North America. Upper level conditions are usually favorable for secondary development of cyclones along the frontal bands of the mature storms and these secondary cyclones often

provide the dynamical forcing to push well-defined fronts southward along the coast of California and into the SOCAL bight.

Frontal passage in SOCAL is generally a late fall through early spring phenomenon occurring from the end of October through April. The majority of the rain falls during the months of November through March. Heaviest rains are associated with storms and fronts approaching California from the west, which frequently tap into a moisture supply from the subtropics. Lightning and thunder, as well as heavy downpours, often accompany the more significant frontal passage events. Precipitation rarely falls as snow except at higher elevations in the mountains. Wind and precipitation effects can be greatly modified by the diverse topography of the region (Figure 4-1). Channels between islands, valleys, and topographic steering can greatly intensify wind speeds, while precipitation is greatly enhanced by upslope flow over the mountain ranges. Elevation and proximity to the ocean are also major modifiers of the sensible weather parameters associated with fronts, especially temperatures and relative humidity.

### 3. CASE STUDY for Frontal Passage on 15 March 1999

#### a. *Statement of Reality (A Synopsis of the Actual Front)*

Figure 5-1 depicts a well-defined surface cyclone in the vicinity of 35N 125W at 1200 UTC on 15 March 1999. This cyclone and its associated frontal band developed in the base of a long wave trough that was situated over the western U.S. Surface measurements and wind profiler/radio acoustic sounding system (WP/RASS) data at San Clemente show frontal passage occurring at approximately 1330 UTC as indicated by the rapid wind shift, sharp drop in temperature, minimum pressure, the onset of precipitation, and the corresponding wind shift and drop in low-level temperature in the surface data (Figure 5-2). Note also the strong low-level pre-frontal winds in the WP data.

While the number of observations are scarce, wind profiler and buoy data in the northern bight region recorded pre-/during/and post-frontal surface wind speeds of 10-15 / 5-10 / and 10-15 kts respectively with slightly stronger winds recorded by the two buoys to the north (Figure 5-3). A dense band of multi-level clouds is evident along the California coast from San Francisco Bay southward past Point Conception. A low to mid-level cloud band extending further south and then southwestward defines the surface front. The observations from Los Angeles and Santa Barbara and the Santa Catalina and Santa Barbara channel buoys clearly delineate the location of the front in the northern bight. Satellite imagery and a ship observation in the vicinity of 27N 125W give a good indication of the front's location seaward. The post-frontal Vandenberg AFB (VBG) upper-air sounding correlated with the infrared satellite imagery (Figure 5-3) shows cloud top temperatures of -40 to -50 °C with corresponding tops in the 400 mb

range. Composite reflectivity data from the San Diego (Miramar MCAS) WSR-88D radar site shows pre-frontal returns of 15-20 dB increasing to 20-25 dB (Figure 5-4) west of Santa Catalina Island and south of the Channel Islands. By 1400 UTC (not shown), 40-50 dB returns were observed in this same radar band as deep convection grew and as the front advanced southeastward through the bight.

***b. COAMPS 24-h Forecast Verification***

The following discussion verifies frontal location, wind, cloud, and precipitation fields from the 24-h COAMPS forecast valid at 1200 UTC on 15 March with the actual conditions described above.

(1) Winds. The first item to point out in the wind field is that COAMPS is too fast on the front's location. Figure 5-5 shows the front passing over San Clemente and Santa Catalina Islands at 0900 UTC on the 15<sup>th</sup>, approximately 4½-h earlier than recorded by the observations. Taking into account this erroneous phase shift and adjusting the location of the front accordingly, COAMPS forecasts the pre-/during/ and post-frontal winds skillfully. While there are no observations to verify the strong post-frontal winds within the bight and south and west of the islands, it is a reasonable depiction based upon the cold air and post-frontal cloud signature (Figure 5-1).

(2) Clouds and precipitation. As in the wind field, the rendition of the frontal clouds is also out of phase with the actual front (i.e., fast) (Figure 5-6). However, if adjusted in time to account for this phase lag, the general frontal pattern is in agreement with the actual conditions. In order to facilitate comparison with the available infrared satellite imagery, only the coarse mesh cloud fields are displayed. Differences existed between the coarse and fine mesh renditions of the clouds, however because of the broad nature of the actual frontal band, the fine mesh cloud fields were difficult to verify even when compared to 1-km resolution satellite imagery.

Significant differences occur in the post-frontal clouds, which are in reality typical post-frontal cumulus clouds becoming strato-cumulus further back into the cold air. COAMPS depicts these clouds as a single low-level stratus cloud (even on the 5-km fine mesh) most likely because the grid spacing is too coarse to resolve the open cell nature of the actual post-frontal clouds. The pre-frontal clouds undergo a similar smoothing tendency, however not as severe as in the post-frontal case. In essence, low "stratus-like" layers depicted by COAMPS will most likely verify as open and or closed cell cumulus or stratocumulus. COAMPS does not forecast the upper-level cirrus streak evident in the satellite imagery, nor the extent of the vertical development of the frontal clouds (400 mb actual in Figure 5-3 versus 750 mb modeled in Figure

5-7). Another significant error appears to be in the under-development of the convective clouds stretching along the coast from Point Conception to the north of San Francisco Bay (Figure 5-6), which may also impact (i.e., under-forecast) precipitation, turbulence, and icing forecasts, although unverified by observations.

There is also considerable breaking apart of the frontal cloud band in the modeled cloud fields as compared to reality since COAMPS has already propagated the front through the mountains north of the bight in its fast forecast. Previous to making landfall, COAMPS did depict a coherent frontal band structure with a high degree of similarity to actual conditions. Lastly, the damping found around the boundary zone occurs for all variables and is an inherent part of all limited area models (LAMs) like COAMPS and it is not reasonable to verify parameters within these zones.

Since rainfall data was only recorded for San Diego, verification is difficult. However, because the front was the only major precipitating feature in the model run as well as in reality, the total precipitation for the event can be qualitatively verified by comparing the 12-h precipitation total at the end of the model run (Figure 5-8) versus the 24-h precipitation total recorded by NWS, which is 0.01". By this method, COAMPS total precipitation for San Diego was over-forecast at 6-12 mm (0.25 - 0.5"). COAMPS also shows a "realistic" precipitation pattern along the immediate coastal mountain range west of San Diego. It would be interesting to see if this pattern and the quantities of accumulated rainfall verify because COAMPS shows a significant onshore component in the wind field versus what the coastal buoy and land stations are reporting (Figure 5-1). This might be due to COAMPS "smoother than reality" topography (discussed earlier) is not blocking the flow and is allowing more onshore flow than indicated by the verifying alongshore winds. In reality perhaps, the flow has already reached a steady-state response to the blocking and is being deflected to the north as the observations in Figure 5-1 show. Lastly, note the problem with the southern boundary where COAMPS seems to be "precipitating out" all of the moisture content in flow crossing that boundary. It is almost as if COAMPS sees the boundary as a topographic barrier.

### **c. COAMPS 12-h Forecast Verification**

The COAMPS 12-h forecast valid at 1200 UTC on 15 March (not shown) reduces the phasing error to approximately 2 ½-h (still fast). While there are some distinct improvements, the general forecast tendencies for winds (skillful), clouds (smoothing the low-level stratus field and under-developed frontal convection), and precipitation (under-forecast) remain unchanged when adjusted to account for the phasing error.

***d. NOGAPS 24 and 12-h Forecast Verification***

Both the 24 and 12-h NOGAPS forecasts (only the 24-h forecast shown in Figure 5-9) were successful forecasts verifying the position of the front accurately compared to the observations and satellite imagery. The cloud rendering in NOGAPS (chosen as a relative humidity threshold of 70% at 850 mb) shows skill in the pattern and extent of the well-developed multi-layer clouds associated with the front, however there is little to no indication of the low-level stratus. Neither the NOGAPS nor COAMPS forecasts depicted a closed cyclonic circulation that verifies in the low-level stratus field in the vicinity of 35N 125W at 1200 UTC (Figure 5-1). This is most likely due to neither model resolving a short wave trough that intensified and coupled to the surface as it moved rapidly into the base of the long-wave trough. In a warm-start mode, this feature will be missed unless resolved by new observations, analyzed and retained in the first-guess from the previous forecast, or imported via NOGAPS boundary conditions (meaning NOGAPS has to have observed and assimilated it). In regards to NOGAPS inadequate depiction of the cloud fields, it should be pointed out that NOGAPS is not expected to provide that kind of detail in its guidance (like COAMPS). Therefore, a forecaster can apply local rules of thumb to produce a skillful forecast of actual frontal conditions having been armed solely with NOGAPS' knowledge of the front's location and timing. On the other hand, a forecaster might espouse the detailed guidance provided by COAMPS and produce an erroneous forecast unless a method existed for determining the phase error in the COAMPS guidance.

***e. Verification of the Initial Analysis for the 24-h Forecast***

The COAMPS analysis for the 24-h forecast is compared against the observations in Figure 5-10. Initially, the 30-kt southerly wind observation seems to be in error. However, the observation gains credibility when fused with infrared satellite imagery (Figure 5-11). In fact, this observation is critical for correctly locating the position of the surface front and stresses the importance of verifying the analysis against all available data at analysis time as in the method described in Chapter III. Based on this and the other ship, buoy and land observations in the vicinity, the front can be placed with reasonable confidence as extending south then southwestward from Cape Mendocino to 31N 126W and then further southwestward. Based on this position, COAMPS has analyzed the front as extending south then southwestward from the San Francisco Bay region to a point southeast of the 30-kt ship observation, clearly an analysis that is too fast. As evidenced above, the fast analysis translates into a fast forecast and hence COAMPS provides erroneous forecast guidance to the forecaster. Like the warm-start February case discussed in Chapter III-C, the NOGAPS analysis of the front is highly accurate but the analysis and forecast boundary conditions do not have any noticeable impact on

improving the forecast. An examination of the COAMPS first-guess field (not shown) reveals its forecast to be even faster than the analysis. Repeating the problem in the February case, the erroneous first-guess has essentially pulled the analysis away from the correct solution and the subsequent forecast is too fast as depicted in Figure 5-5.

#### 4. CASE STUDY for Frontal Passage on 12 April 1999

##### a. *Statement of Reality (A synopsis of the Actual Front)*

Figure 5-12 depicts a frontal system passing through the SOCAL bight at 0000 UTC on 12 April 1999 with a pronounced trough located just off of Point Conception and trailing behind the actual front. This cyclone and its associated frontal band developed from a short-wave trough that intensified as it moved into the base of a long wave trough that was situated over the western U.S. Surface data from the San Clemente wind profiler site shows ambiguity in the actual time of frontal passage at that station and even suggests the possibility of two frontal passages between 2300 and 0300 UTC (Figure 5-13). The cloud pattern at 130 W in Figure 5-1 certainly supports this possibility. Visible satellite imagery valid at 0130 UTC and Doppler radar data valid at 0243 UTC (Figure 5-14) suggest a considerable amount of pre-frontal clouds and precipitation associated with this front. Based on this information (albeit ambiguous) and for the purpose of comparison with COAMPS, a single frontal passage will be assumed to have occurred no later than 0200 UTC at San Clemente Island (note that only Santa Catalina Island appears in the radar graphic).

Since surface ship observations are missing, only the wind profiler and buoy data in the northern bight region were used for wind forecast verification. They recorded pre-/during/and post-frontal surface wind speeds of approximately 10 / 5 / and 8 kts respectively. The available satellite imagery (Figures 5-12 and 5-14) reveals a dense band of multi-level clouds over most of central and southern California with a slight clearing of the upper level clouds from Monterey Bay south to Point Conception. The imagery also suggests that there are multiple bands of clouds with "frontal-like" characteristics and this leads to the ambiguity in the actual time of frontal passage. Although very difficult to prove, the combination of satellite, radar, and surface data suggest that a primary frontal band is located towards the trailing end of the cloud band in the northern bight. This would support frontal passage occurring at San Clemente in the 0200 UTC hour timeframe. Further seaward in the vicinity of 30N 120W, a rope signature along the leading edge of the cloud band (Figure 5-12) is evident. Again, a "dual" frontal signature is evident in the cloud signature at 130W.

The post-frontal Vandenberg AFB upper-air sounding (not shown) shows considerable low-level instability and cloud top heights to about 850 mb which corresponds with the satellite imagery (note that these values are for post-frontal conditions and that the actual frontal clouds extend to greater heights). Composite reflectivity data from the Los Angeles WSR-88D radar site shows returns of up to 40-50 dB by 0300 UTC as the front continues its southeastward advance through the bight (Figure 5-14). Precipitation totals recorded by the NWS show 0.44" of accumulated rainfall throughout the event at San Diego, while automated rain gauges throughout the region varied widely.

*b. COAMPS 24 to 30-h Forecast Verification*

The following discussion verifies frontal location, wind, cloud, and precipitation fields from the 24 to 30-h forecast fields from COAMPS valid between 0000 and 0600 UTC on 12 April with the actual conditions described above. To demonstrate their utility, forecast soundings are also verified against upper-air observations from selected sites.

(1) Winds. Even assuming the worst case for frontal ambiguity in the recorded data, this COAMPS cold-start forecast is demonstrating much more skill than the warm-start forecasts on the 9<sup>th</sup> of February and the 15<sup>th</sup> of March. In fact, Figure 5-15 depicts a clearly defined front passing through San Clemente and Santa Catalina Islands at 0400 UTC, or within 1-h of the actual frontal passage as determined above. COAMPS has over-forecast by approximately 5 and 10 kts respectively the pre- and post-frontal winds, but verifies well on the winds in the vicinity of the front.

(2) Clouds, forecast soundings, and precipitation. As in the wind field, the rendition of the frontal clouds is also in phase with the actual front and the general pattern is in very good agreement with the actual conditions. Figure 5-16 compares the COAMPS generated clouds to satellite imagery. The different valid time of the two (0000 UTC imagery versus 0400 UTC COAMPS) is not a critical factor in this "general pattern" comparison. The major differences include COAMPS under-forecasting low-level clouds over the Central Valley, pre-frontal convergence bands ("A"), filling-in of low-level clouds further behind the short-wave trough ("B"), and depiction of an erroneous gap ("C") in the front seaward. COAMPS accurately forecasts the immediate post-frontal clearing and even indicates vertically developed clouds up to 600 mb (~4 km) in the general vicinity of the short-wave trough ("D") that trails behind the front. However, infrared imagery (not shown) reveals that these clouds are extremely well developed (even more than the actual front) with cloud top temps of -40° C and heights up to 300 mb (~9 km).

The actual imagery also indicates some mountain wave activity in the vicinity of the Baja and Southern California border and belies the underlying calm surface reports in that region (Figure 5-12). In this region, COAMPS depicts a single orographically induced cloud instead of the striations of the wave pattern. This is most likely because the grid spacing is too coarse to resolve the feature. The fine mesh did not extend far enough eastward to cover this region, however, COAMPS has demonstrated an ability to forecast mountain waves and can be expected to pick up on this feature in higher resolution (< 5-km) domains. A comparison of the sounding profiles embedded in Figure 5-17 shows that COAMPS verifies fairly well on the vertical extent of the pre-frontal cloud shield (~600 mb).

Direct comparison of the NWS precipitation totals with the COAMPS 24 to 30-h total accumulated precipitation fields is not a valid comparison. However, because the front was the only major precipitating feature in the model run as well as in reality, the total precipitation for the event can be compared (i.e., the 12-h precipitation totals at the end of the model run versus the 24-h precipitation totals recorded by NWS (Figure 5-18). Generally speaking, COAMPS demonstrated skill in the relative distribution of the rainfall, but showed less precipitation than was recorded by rainfall gauges for most stations. This might be attributed to the fact that COAMPS did not forecast most of the pre-frontal clouds and precipitation as well as under-developed the convection associated with the post-frontal short-wave trough. The large disparities at higher elevations (e.g., Palomar Mountain's 3.8" versus COAMPS 6 mm (~0.25")) are most likely attributable to terrain differences. Some specific areas for comparison in the figures include Huntington Beach (1.30" versus COAMPS 24 mm (~1.0")) and Poway (0.51 " versus COAMPS 6-12 mm (0.25-0.5")). Additionally, official climatological data for San Diego recorded by NWS showed 0.44" for the event versus COAMPS 12-18 mm (~0.5-0.75").

(3) Forecast soundings. Figure 5-19 further demonstrates the utility of forecast soundings. They are a plot of the COAMPS 24-h forecast sounding against the verifying upper-air soundings at pre-frontal and post-frontal sites, Montgomery Field (MYF) and Vandenberg AFB (VBG) respectively. It is important to point out that in this plotting routine, the COAMPS sounding is smoothed to only points at mandatory levels instead of the original 30 vertical levels that are visible in the embedded plots. Nevertheless, the depiction provides a good qualitative display for comparison to the actual soundings. One observation is that the COAMPS lapse rate near the surface remains stable while the VBG sounding captures weak instability in the profile immediately above the surface.

Looking at the middle to upper levels, it is likely that there is stronger cold air advection on the backside of this front than COAMPS was able to resolve. In the cold-start mode, this knowledge would have had to come from either upper-air observations or the

NOGAPS first-guess or background fields. Without this critical information from upstream data sources, neither NOGAPS nor COAMPS could resolve this characteristic of the post-frontal air mass. Though rarely observed over the data sparse ocean, this would also be a good COAMPS analysis field to verify as part of the methods presented in Chapter III. The RASS on the San Clemente Island wind profiler depicts a low-level lapse rate of about  $8^{\circ}$  C/km, which is more in line with the COAMPS forecast (Figure 5-20). Compared to the actual soundings in Figure 5-19, COAMPS handles the thermodynamic structure well. At MYF, the only major disparity is in the height of the tropopause and only minor disparities occur in the middle to upper-level stability profiles with COAMPS generally running a little cooler than reality. At post-frontal VBG, the opposite effect is observed (i.e., COAMPS is running a little warmer than reality). While the vertical structure is satisfactory, the mid to upper-level wind forecast is significantly in error. This might be due to the critical position of VBG relative to the front and trailing surface trough and the difference between the models true vertical sounding versus the actual flight path of the radiosonde. The time that the balloon was released might also be a factor. Another contributing factor is COAMPS under-development of the strength of the trailing surface trough. In reality, the effects of the trough on the wind field is much stronger than COAMPS is forecasting. Instead, COAMPS is forecasting the main front as the dominant player in the wind field forecast.

Overall, this 24-h cold-start COAMPS forecast demonstrated more skill in forecasting the timing of frontal passage in the SOCAL bight than did the two previous warm-start cases examined thus far (i.e., within 2-h of frontal passage versus 6 and  $4\frac{1}{2}$ -h). Clouds and precipitation remain difficult parameters to forecast and verify accurately, but keeping in mind that these are 24-h forecasts, it is fair to say that COAMPS provided useful guidance concerning these effects. COAMPS also demonstrated moderate skill at forecasting the vertical, or thermodynamic structure associated with this front. On a critical note, even on the fine mesh, COAMPS definitely smoothed the complex, multi-frontal band structure observed in the observations and imagery into a single “modeled” front. According to the data, the effects of the first significant frontal band to pass through San Clemente Island would have been felt at 2300 UTC. COAMPS did not bring the modeled front through until almost 0400 UTC. However, COAMPS did show considerable pre-frontal “weather” associated with its modeled front and the human forecast may not have been adversely impacted in any significant way.

### **c. COAMPS 12 to 18-h Forecast Verification**

The COAMPS 12 to 18-h forecast valid between 0000 and 0600 UTC on 12 April (not shown) also demonstrates the same high skill level as the 24 to 30-h forecast in timing the front, however some of the sensible weather elements were forecast less accurately. For

example, the strength of the modeled winds increased to roughly 30, 15, and 15 kts respectively for pre-, during, and post-frontal conditions. This is over-forecast by approximately 20, 10, and 7 kts respectively. The modeled cloud pattern continued to under-forecast low cloud cover in the Central Valley and maintains the erroneous “break” in the seaward extent of the cold front. However, COAMPS does retain accuracy in post-frontal clearing. The only disturbing result is the lack of low-level convection associated with the short-wave trough trailing behind the cold front. In fact, there are hardly any peripheral clouds and only the clouds associated with the front are well defined. However, there is much more isolated convective activity and clouds on the fine mesh, a natural result of the high-resolution surface and subsequent vertical forcing of the flow. In this regard, the wind pattern also displays much more mesoscale response characteristics.

Where the modeled cloud pattern lacked accuracy, both an instantaneous rain pattern and the overall precipitation coverage and totals continued to verify well with a slight under-forecast in the accumulation of rainfall for the event. Compare COAMPS depiction of instantaneous rainfall to the verifying radar image (Figure 5-21).

Figure 5-22 is a plot of the COAMPS 12-h forecast sounding and the verifying upper-air soundings at pre-frontal and post-frontal sites, Montgomery Field (MYF) and Vandenberg AFB (VBG) respectively. The same tendencies (stable immediately above the surface and generally warmer up to 400 mb) are observed in the COAMPS profile at VBG as in the 24-h forecast. At MYF, COAMPS is in good agreement with the actual pre-frontal conditions and has slightly improved its rendition of the tropopause. However, the cool bias in the middle to upper levels remains. In summary, COAMPS continues to demonstrate skill at forecasting the vertical structure associated with this front. In this light, forecast soundings should prove to be a viable item in the forecaster’s tool kit.

#### ***d. NOGAPS 24 and 12-h Forecast Verification***

Both the 24 and 12-h NOGAPS forecasts (only the 24-h forecast shown in Figure 5-23 were successful forecasts verifying accurately the position of the front against the observations and satellite imagery. Unlike the 15 March case, NOGAPS (and therefore COAMPS) was able to resolve the short-wave trough trailing behind the front. In this cold-start case, the NOGAPS analysis of the short-wave trough was the critical factor in the first-guess fields that enabled the transfer of this knowledge into the COAMPS analysis and forecast.

#### ***e. Verification of the Initial Analysis for the 24-h Forecast***

The COAMPS analysis valid at 0000 UTC on the 11<sup>th</sup> of April is compared against the verifying observations and satellite imagery in Figure 5-24. This is the analysis

corresponding to the 24-h forecast. At analysis time, this case is less clearly defined as the previous ones. However, when the two coastal buoys in the vicinity of Cape Mendocino and San Francisco Bay and the three surface ship observations west of 130W are considered together with the distinct cloud edge along 38 N, a good estimate is obtained for the location of a surface trough. Note that the mature frontal system has not yet evolved by the analysis time. Based on this estimate, COAMPS depicts the feature as a relatively more pronounced area of troughing in the wind field. Although there is a large disparity between COAMPS and the Cape Mendocino buoy wind fields, COAMPS fits the other observations well.

When the skill of the COAMPS analysis is not clear, it is useful to observe the NOGAPS background/first-guess fields in relation to current observations and satellite imagery in a cold-start scenario since it will provide the most influence (in the absence of accepted observations) on the COAMPS analysis through the first-guess field. Since there are no upper level observations upstream to verify against, only the surface wind field will be considered. Figure 5-25 shows that NOGAPS also has analyzed the trough skillfully. Therefore, the COAMPS analysis can be trusted to produce a skillful forecast and, as observed earlier, this is the case (Figure 5-15).

## 5. Summary and Conclusions for SOCAL Fronts

### a. *Cold and Warm Start Effects on Forecast Accuracy*

In this evaluation, a natural consequence is to group performance trends according to whether COAMPS was either running in a cold or warm-start mode. Both the February and March frontal cases are examples of warm-start scenarios. In both cases, COAMPS showed increasing skill going from the 24 to 12-h forecasts, however the March frontal case still had significant timing errors in the 12-h forecast. However, an additional consideration must not be overlooked that is unique to model domains with coasts downstream from major bodies of water. As fronts approach the coast, they are resolved by more and more heavily weighted (i.e., reliable) land and upper-air observations for each successive data assimilation cycle. Thus, the increased data leads to a more skillful analysis, which in turn leads to a more skillful forecast. This is particularly true for that portion of the front propagating down the California coast and the primary forecast problem for land stations. However, the trailing ends of fronts approaching the SOCAL operating areas often remain unresolved and usually show small timing errors. This is an important factor to consider when forecasting the onset and duration of frontal weather for ships operating in the SOCAL operating areas.

Generally speaking, in a warm start scenario, the background or first-guess field dominates and is only adjusted slightly by the observations—the more observations or the more

reliable the existing observations, the more adjustment and the better the analysis. Thus, a trade-off of warm starts is that on the one hand it is invaluable for maintaining mesoscale structure, once developed, in the analysis and there is essentially no spin-up time required to develop that structure for each successive forecast. On the other hand, if the first-guess fields are in error, they tend to dominate the subsequent analysis by causing the quality control scheme to reject accurate observations because they deviate significantly from the first-guess. This is an important consideration in the case of fronts where a rapid wind shift occurs and phase errors of only a couple of hours could cause accurate observations to be rejected. It is also a consideration with small-scale mesoscale features like coastal eddies where a relatively small positional error can equal or exceed the diameter of the eddy itself and potentially cause any observations in the vicinity to be 180° off in direction.

In this evaluation, both the 24 and 12-h COAMPS forecasts originating from cold-starts demonstrated more skill than did their warm-start counterparts. This result is most likely a consequence of NOGAPS demonstrated short-range forecast skill. Further studies need to be performed to quantify COAMPS skill in both cold and warm start scenarios for frontal regimes (or any active synoptic regime) and in both data rich and data sparse regions.

Regardless of their outcome, a comparison of the analysis with the observations, satellite imagery and any other available data must be performed (like the method presented in Chapter III) in order to effectively interpret the probable skill of the subsequent COAMPS forecast. Additionally, TAMS-RT should alert the forecaster as to which observations were rejected by the quality control routine and were not assimilated. Ideally, this would occur in the same graphic context as the analysis and forecast fields (e.g., blinking observations on a map of the domain).

## B. CATALINA EDDIES AND THE ASSOCIATED WEATHER IN SOCAL

### 1. Introduction

During the spring and summer months, Southern California (SOCAL) coastal areas and valleys experience many days with low clouds and fog in the early mornings and late evening, with accompanying burn-off during the peak daytime hours. At times, usually on the coast and less often in the valleys, there are days when the low clouds and fog persist into the afternoon and occasionally all day. A coastal eddy called the Catalina Eddy is often the cause for low clouds and fog to last into the afternoon (Evans and Halvorson 1998). The Catalina Eddy is a quasi-stationary mesoscale vortex with a horizontal scale of roughly 100-km and extends through a layer from the surface to between 1 and 2-km above mean sea level (MSL) (Mass and Albright 1989). Most studies agree that the Catalina Eddy is produced by the interaction between the synoptic-scale flow and the formidable topography of the region, which results in the formation of a cyclonically circulating low-pressure area within the SOCAL bight. Catalina Eddies occur predominantly during the “stratus season,” which is between April and September with a peak occurrence in June, and vary in size, intensity, and may last from a few hours to several days (Evans and Halvorson 1998). In order to develop the mesoscale knowledge base for NPMOC San Diego forecasters, the following discussion describes the current theory for the initiation and evolution of Catalina Eddy events and state-of-the-art and future outlook for observing and forecasting this mesoscale phenomenon.

### 2. Effects and Manifestation of the Catalina Eddy

The effects of the Catalina Eddy on the weather over SOCAL can be quite dramatic from one day to the next. In general, Catalina Eddy formation is accompanied by a southerly shift in coastal winds, a rapid increase in the depth of the marine layer, a corresponding rise in the base of the inversion, and a resultant thickening of the coastal stratus (Figure 5-26). The cloud ceilings at San Diego will often rise as much as 1,000 to 1,500 ft (NPMOC San Diego 1995). The cloud height, inland extent, and duration of the stratus layer also increases. Usually, the increased thickness of the stratus clouds inhibits the typical morning/early afternoon dissipation. When the Catalina Eddy is at its strongest, the depth of the low clouds may extend to 6000 ft and these clouds will move through the inland valleys and reach into the high deserts (Figure 5-27) (NPMOC San Diego 1995). Paradoxically, eddy-related lifting of the marine inversion may occasionally result in the marine layer lacking sufficient moisture to produce clouds and the skies may become mostly clear (Mass and Albright 1989). In the case of fog, the rise of the inversion associated with an eddy event often results in the dissipation and lifting of fog for the duration of the event and improved visibility at low-elevation airports and adjacent fleet operating areas.

Coastal temperatures will be several degrees cooler than the day before eddy formation, since cloud cover reduces the amount of surface heating from the sun. Air quality may be improved since the Catalina Eddy weakens and lifts the typically strong inversion over the coast and allows pollutants to be mixed through a greater depth (Mass and Albright 1989).

Typically, Catalina Eddies are manifest as a cyclonic circulation in the surface wind field and occasionally as a trough in the surface pressure field centered within the SOCAL bight near Santa Catalina Island. In satellite imagery, Catalina Eddies may create a spiral pattern in the stratus cloud signature (Mass and Albright 1989). When the skies are relatively clear at initiation, a narrow tongue of coastal stratus develops and spreads northward from the Baja Peninsula as the southerlies and the associated marine layer deepen, which allows coastal stratus to develop and thicken (Mass and Albright 1989). In time, the stratus tongue moves along the coast and westward past Point Conception, where it meets the synoptic-scale northerlies. The combination of coastal southerlies and synoptic-scale northerlies often produces the classic spiral pattern in the stratus. At other times, the pre-existing stratus deck associated with large-scale subsidence in the region obscures the spiral pattern (Mass and Albright 1989).

Strong mesoscale diurnal effects such as the sea breeze may significantly weaken the intensity and satellite signature of the Catalina Eddy by deflecting the flow onshore during the day (Mass and Albright 1989). Davis et al. (1999) downplay the effect of the sea breeze and point to the stratification changes upstream from the northern mountain barrier (composed of the San Rafael, Santa Ynez, and San Gabriel Mountains) as the dominant mesoscale diurnal effect on the Catalina.

### **3. Climatology and Current Theory of Development**

Previous studies have included wide-ranging speculations about the eddy's origin and synoptic setting, although most agree that this phenomenon results from some kind of interaction between the synoptic-scale flow and the topography of the region. By far the most exhaustive study of the Catalina Eddy was that of Mass and Albright (1989). They focussed on a June 1988 case, as well as a composite of 50 eddy events from 1968 through 1982. Their climatology demonstrates the importance of changes on the synoptic-scale that trigger an eddy event. In this view, a Catalina Eddy results from the interaction between the synoptic-scale flow and the complex topography surrounding the SOCAL bight. When this interaction creates an alongshore pressure gradient in the bight such that pressure is lower to the north, mesoscale topographically trapped southerly flow is established in the coastal zone, while northerlies remain offshore (Mass and Albright 1989). The result is the initiation of a Catalina Eddy event. Mass and Albright (1989) define four stages through which a Catalina Eddy event progresses.

**a. Pre-Eddy Stage**

Diffluent flow over the West Coast at 500 mb usually exists during this period. The major surface features are the East Pacific high and the inland heat trough extending from northwestern Mexico into the southwestern United States. As a result, westerly and northwesterly surface flow is the standard in the SOCAL bight except for large diurnal wind variations at the coastal stations. Marine stratus is generally thin and burns off within the coastal zone each day (Mass and Albright 1989).

**b. Eddy Initiation Stage**

Initiation of a typical Catalina Eddy event begins when a short-wave trough moves onshore over the Pacific Northwest. The substantially cooler air associated with the trough causes pressure increases in the Pacific Northwest and pressure falls in the lower troposphere over the remainder of the western United States and northern Mexico. As a result, the pre-existing 850-mb synoptic-scale trough over the western United States extends southwestward towards the SOCAL bight, while the interior heat trough spreads northwestward into central California at the surface. These synoptic-scale changes dramatically intensify the east-west pressure gradient between the Pacific high and lower pressure inland. As a result, northerly flow along the California coast is greatly enhanced (Figure 5-28) (Mass and Albright 1989).

With a strengthening of the northerly flow approaching the mountain barrier to the north of the bight, mesoscale lee troughing is enhanced at low levels in the vicinity of Santa Barbara (Mass and Albright 1989). As a result of synoptic-scale and mesoscale lee troughing in the SOCAL bight, an alongshore pressure gradient with lower pressure to the north becomes established along the coast (Mass and Albright 1989). It is important that the pressure gradient created by the mesoscale lee troughing is only on the order of 1 to 2 mb. In essence, the role of the synoptic-scale troughing is critical in that it not only strengthens the northerly flow impinging the northern mountain barrier, but also weakens the gradient sufficiently over SOCAL to allow the induced mesoscale pressure gradient to dominate. Mass and Albright (1989) have shown that in a coastal zone with an adjacent topographic barrier, such a gradient accelerates flow to the north within a Rossby radius (~100 km) of the coastal mountain barrier. With nearly geostrophic northerlies remaining offshore, considerable cyclonic vorticity is generated in the coastal zone.

### *c. The Mature Eddy*

The strengthening southerly flow causes an associated increase in the depth of the moist marine layer in the coastal zone (Mass and Albright 1989). Mass and Albright (1989) point to the Coriolis turning of the southerly flow that causes marine layer damming on the coastal mountain barrier, and to the erosion of the capping marine inversion as the southerlies replace the inversion-sustaining warm subsiding northerly flow associated with the East Pacific high as the causes for this occurrence. The deeper cool marine air in the coastal zone creates a narrow mesoscale pressure ridge. For stronger and more mature eddies, an actual low-pressure center can develop offshore as the coastal pressure ridge intensifies and extends northward. With or without the development of a low-pressure center, all Catalina Eddies possess large cyclonic vorticity in the bight as a result of the coastal southerlies and strong offshore northerlies (Mass and Albright 1989).

### *d. Dissipation Stage*

The eddies continue as long as synoptic pattern enables southerly flow to remain in the SOCAL coastal zone. When the synoptic-scale troughing over the western United States weakens, the strong northerly flow subsides and reduces the mesoscale lee troughing effect in the northern bight (Mass and Albright 1989). Moreover, a moderate to strong gradient of higher pressure to the north replaces the previously weak synoptic-scale gradient in the bight and masks any remaining influence of the now weak mesoscale lee troughing. When this occurs, the normal westerly and northwesterly wind regime returns to the SOCAL bight (Mass and Albright 1989).

## **4. Observing the Catalina Eddy**

As mentioned earlier, the pre-existing stratus cloud deck that is so prevalent in the region often obscures the satellite signature of a Catalina Eddy. In these cases, sampling theory calls for an observation network of approximately 25-50 km grid spacing to observe the Catalina Eddy. Fortunately, few coastal zones possess a denser array of operational observing sites on land and in the nearby offshore waters than in SOCAL. There are numerous surface reporting locations over land, several island stations, and three stationary buoys in the offshore waters. Efforts are routinely made to synthesize the routine surface observations into a meso-analysis (Figure 5-29). Several ship reports are also generally available each synoptic hour. Upper-air soundings are available at San Diego, Vandenberg Air Force Base, and occasionally from Point Mugu and San Nicholas Island (Mass and Albright 1989). The Vandenberg surface observation and upper-air sounding are particularly critical because of its strategic location just north of Point Conception. Observations from this site are useful for correcting a synoptic-scale model that otherwise would

not accurately resolve the large-scale forcing. Recent installations of the wind profiler/radio acoustic sounding system (WP/RASS) also further populate the network (Figure 5-30). Although not at 25-km density, the overall observation network is sufficient for observing almost all Catalina Eddy events. Thompson et al. (1997) further clarify that while the density is sufficient for “detecting” the presence of a Catalina Eddy, the conventional network has insufficient resolution to represent detailed atmospheric structure for mesoscale modeling purposes. They argue that it is necessary for the model physics to generate realistic horizontal and vertical mesoscale features and to retain this structure through the analysis and initialization process in order for the model to display skill in forecasting mesoscale features. In other words, they emphasize the importance of running COAMPS in the warm-start, data assimilation mode for the most accurate analysis and forecast of the Catalina Eddy.

## 5. Forecasting the Catalina Eddy

### a. *Pre-mesoscale Modeling Era*

Prior to the operational employment of skillful numerical weather prediction (NWP) on the mesoscale, forecasting the eddy event was essentially an exercise in predicting when the appropriate alongshore pressure gradient would exist within the SOCAL bight (Mass and Albright 1989). In this case, forecasters must infer the alongshore pressure gradient in the coastal zone from the synoptic-scale model charts. Mass and Albright (1989) demonstrated that the required alongshore pressure gradient is associated with a specific synoptic evolution: the movement of an upper level trough across the Pacific Northwest; pressure and height falls in the lower troposphere of the western third of the United States; the extension of the interior heat trough of southeastern California and northwestern Mexico northwestward; and the creation of a large height gradient (and associated strong northerly winds) along the central coast of California. Most operational global models skillfully predict the above synoptic-scale changes a day or more in advance and provide the possibility of accurately forecasting eddy initiation and development (Mass and Albright 1989).

### b. *Forecast Rules of Thumb*

In essence, use of local rules of thumb for forecasting weather is an early form of mesoscale modeling. Many rules of thumb point either to synoptic-scale indicators or their mesoscale responses to help the forecaster determine the local weather. In fact, one of the best uses of mesoscale modeling to date in the U.S. Navy has been to teach forecasters the mesoscale responses that lead to forecast rules of thumb (Angove 1998). Forecasters at

NPMOC San Diego have developed several rules of thumb over the years to assist in forecasting the development of the Catalina Eddy. It is important to note that these rules were formulated over past years based on lower-density surface observation networks and prior to the operational deployment of mesoscale NWP systems. The following discussion will quote several of these locally developed thumb rules from NPMOC San Diego (1995) and offer explanations for their utilization.

- **Rule:** “A widely used parameter in recognizing the existence of a Catalina Eddy is southerly surface winds at San Diego with a speed of 5 to 10 kts and persisting for three hours or more.”
  - Explanation: The southerly winds are associated with the alongshore pressure gradient that develops (lower pressure to the north) in the vicinity of the mesoscale lee troughing south of the northern mountain barrier. The 3-h duration of the winds is required because it takes time after the alongshore pressure gradient develops for the mesoscale induced southerly coastal flow to interact with the synoptic-scale northerly flow and create sufficient cyclonic vorticity to spin up an eddy. This rule is primarily used for detecting the “existence” of an eddy. However, it is interesting to note that the onset of southerly winds at San Diego is a good indicator of subsequent eddy development and is thus a good forecasting tool when used in conjunction with other synoptic-scale developments of eddy climatology.
- **Rule:** “A surface pressure gradient of 5 to 10 mb between 35N 125W (just east of Point Conception) and Los Angeles, along with positive vorticity advection ahead of an upper level trough moving through the southwestern United States resulting in vorticity values of 7 to 10 units (10e-5/sec) at Los Angeles, will generate a Catalina Eddy.”
  - Explanation: The alongshore pressure gradient from Point Conception to Los Angeles (higher pressure at L.A.) is certainly relevant to eddy generation since it is associated with lower pressure forming in the northern bight. The vorticity advection is most likely linked to the rapid deepening of the marine layer associated with eddy development. However, Mass and Albright (1989) show that most eddies are not associated with upper-level short waves moving through the southwestern United States, but rather with upper-level troughs and associated fronts that are predominantly directed towards the coasts of the Pacific Northwest.
- **Rule:** “During a Catalina Eddy, winds at Point Conception will be north or north-northwest 20 to 30 kts, and at San Nicholas Island northwest 15 to 30 kts. Winds from San Diego to Long Beach and Los Angeles will be more southerly than normal; southeasterly during night and early morning hours, and south-southwest to southwest in the afternoons.”
  - Explanation: The consistently moderate to strong winds at Point Conception and San Nicholas Island are associated with a well-developed offshore (higher pressure seaward) pressure gradient and are relevant to eddy generation and strong synoptic-scale northerly flow. The diurnal variation is associated with sea breeze effects. Stronger onshore flow is present in the afternoons and gives the winds a large southwest component, while offshore winds at night are weak and allow the coastally trapped southerly flow to proceed on course towards the mesoscale lee trough created in the northern bight.

- **Rule:** “Pressure will usually be lower at Santa Barbara and Los Angeles than at Point Conception, and slightly lower at Los Angeles than at San Nicholas Island and San Diego, with difference on the order of 1 or 2 mb.”
  - **Explanation:** The lower pressure at Santa Barbara than at Point Conception is associated with the mesoscale lee troughing induced by strong northerly flow over the mountainous terrain. With the northerly flow increasing to the west and the height of the topography decreasing to the west of Santa Barbara, the strongest mesoscale lee troughing occurs in the northwestern portion of the bight near that city (Mass and Albright 1989). Again, the well-developed offshore (higher pressure seaward) gradient between Los Angeles and San Nicolas Island is relevant to eddy generation since it is associated with strong northerly flow. The lower pressure at Los Angeles is associated with the alongshore pressure gradient that develops during eddy generation. However, Mass and Albright (1989) note that the pressure at Los Angeles is often slightly lower than at San Diego during non-eddy events, especially during the daytime. They suggest that the differing coastal topography of the two locations is the cause. At San Diego, the coastal plane is relatively narrow (~20 km) and is bordered to the east by mountains reaching heights of ~1800 m. In contrast, the highly urbanized Los Angeles Basin is far wider (~60 km) and is surrounded by substantially higher topography (reaching ~3000 m). Therefore, the Los Angeles basin experiences greater heating, both at low levels and aloft, and more substantial daytime pressure falls than at San Diego (Mass and Albright 1989).
- **Rule:** “Development of an eddy brings an increase and deepening of pre-existing fog or low clouds. If no fog is present, there will be a tendency toward its formation. If fog has already formed, the change will be toward increasing fog that tends to lift to form a low cloud layer; and if a general low cloud layer has formed, there will be a tendency toward lifting to higher elevations with improving visibility beneath.”
  - **Explanation:** The increase and deepening is associated with the lifting of the marine layer that develops. The increase in fog may be associated with advection fog from seaward, but usually the fog lifts as stated later in the rule in view of greater mixing depth of a lifted marine layer (Mass and Albright 1989). The case of fog developing where none existed before is unusual and seems to go against the reasoning outlined in Mass and Albright (1989). However, one possible explanation is that the synoptic situation prior to eddy development was not conducive for fog formation (e.g., the East Pacific High and its associated subsidence and strong marine layer inversion were weak or absent). The synoptic situation then changed so that conditions were favorable for eddy development. The synoptic conditions favorable for eddy development as outlined in this paper are also favorable for the formation of low-level stratus and fog.
- **Rule:** “As a general rule, when San Nicholas Islands’ wind drops below 10 kts from the northwest, or blows from another direction, there is no Catalina Eddy present.”
  - **Explanation:** Again this points to the importance of a well-established offshore pressure gradient and strong northerly flow that are relevant to eddy generation.

### c. Mesoscale Modeling Era

In the operational mesoscale modeling era, it is now possible to predict eddy formation explicitly. One task in this effort has been to better define a coherent physical model of the origin, structure, and evolution of Catalina Eddy events. Mass and Albright (1989) conceded that their composite model was based on modest amounts of upper-air information and

recommended the use of additional observed or synthetic upper-air soundings generated by mesoscale models. Even though the current density of surface observations is sufficient for observing the Catalina Eddy, the relative sparseness of observations, especially the lack of upper-air soundings on the mesoscale, precludes detailed analysis of an eddy's structure (Davis et al. 1999). Therefore, much of the current research includes diagnosis of eddy evolution as produced by numerical simulations.

Davis et al. (1999) used numerical simulation of the June 1988 eddy event to study the source of cyclonic vorticity that comprises the eddy and how this source depends on the diurnal cycle. Their numerical simulations revealed two time scales governing eddy formation, that of the synoptic-scale flow and the diurnal cycle. Enhanced synoptic-scale, northerly flow traversed the high mountains north of the bight and strongly depressed the marine layer over the bight, and resulted in a warm-core vortex. A decrease in the synoptic-scale northerlies, which resulted from the movement of the anticyclone to the northeast of the region, reduced the mean advecting velocity and allowed vorticity, once formed, to remain nearly in the bight. The main diurnal effect modulating the Catalina Eddy's intensity was not from the sea breeze, but rather from the modulation of the strength and stratification of the flow impinging on the mountains, and hence the downstream response. The diurnal cycle caused a regime transition from blocked flow (morning) to flow over the mountains (evening). The flow over the mountains in the evening resulted in a pronounced depression of the marine layer in the lee and in an eddy forming preferentially at night. The blocked flow in the morning produced a wake during the daytime with numerous elongated filaments of vorticity, but no coherent eddy (Davis et al. 1999). "Model depicts an eddy over Santa Catalina Island 03Z (8 p.m. local) through 21Z (2 p.m. local), then reforming after sunset again." Comments like this are frequent in NPMOC San Diego's forecast discussions in Catalina Eddy regimes and seem to support this hypothesis.

Based on these findings, they recommend more theoretical work to examine idealized flows of varying complexity past three-dimensional mesoscale topography. It would be interesting to determine if their numerical simulation produced an overly active diurnal modulation of the topographic flow compared to reality. In any case, our understanding of coastal phenomena could be greatly increased with an ability to more strongly link the results of observational and modeling studies with results from these more idealized calculations (Davis et al. 1999).

## 6. CASE STUDIES for Catalina Eddy Events

### a. **Summary of Over-development Cases**

The critical nature of the “modeled” topography was also noted throughout the period of this evaluation (March through August 1999). Daily reviews of NPMOC San Diego’s COAMPS fields quickly revealed an over-developmental tendency in the model (i.e., COAMPS spins up more eddies than verify). This fact is also well documented by NPMOC San Diego forecasters. Coastal eddies, ranging in size from small channel eddies in the Santa Barbara Channel to full-scale Catalina Eddies, would often become manifest in the fields without corresponding verification from satellite imagery of observation fields. To understand the reason for this tendency, the domain structure and the “modeled” topography was examined. The original domain structure of NPMOC San Diego’s TAMS-RT had the medium resolution (15-km) nest encompassing the northern mountain barrier, while the inner mesh (5-km resolution) was located in the southeastern region of the bight (Figures 4-3 and 4-4). The terrain resolution of the intermediate mesh is 1-km data bilinearly interpolated to the 15-km grid, whereas the topographic resolution of COAMPS’ inner mesh is 1-km data bilinearly interpolated to the 5-km inner grid. Assuming COAMPS accurately analyzed the wind field, the effect of the “smoother than reality” terrain as resolved in the intermediate mesh (a 1900 ft difference as shown in Chapter IV) was to let too much flow over the mountains, which led to model-enhanced mesoscale lee troughing and over-development of the eddies.

Forecasters at NPMOC San Diego recently increased the geographic coverage of the inner domain to encompass the full extent of the mountains north of the bight. It is suspected that fewer eddies will develop as a result of more realistic topographic blocking of the upstream flow. In either case, the surface roughness parameterization might be a critical factor for fine-tuning the model to respond correctly to various terrain resolutions. According to the Davis et al. (1999) findings, COAMPS’ resolution of the stratification upstream from the range is also a critical factor in determining how much flow goes over the range and develops subsequent mesoscale lee troughing in the northern bight. According to this theory, it may be even more prudent to extend the inner domain further north to capture routine upper-air stations, however there is a trade-off between increased geographic coverage and horizontal resolution. Another option is to increase the vertical resolution, or to change the vertical coordinate system of the current domain structure. Again there will be a trade-off, this time with computer processing time. Obviously, further study using controlled simulations is needed to test these hypotheses and if necessary, to determine the most effective set-up for COAMPS.

**b. CASE STUDY for an 8 June 1999 Catalina Eddy**

During the period of this evaluation, there were no events observed where a Catalina Eddy formed in reality, but COAMPS did not forecast it. Apart from the over-development tendency mentioned above, COAMPS demonstrated great success in forecasting the onset, location, diurnal fluctuation, and duration of Catalina Eddy events. A Catalina Eddy that formed on the 8<sup>th</sup> of June 1999 is chosen to represent these cases of successful forecasts. In line with the Mass and Albright (1989) theory of development, this eddy developed after a short-wave trough moved onshore in the Pacific Northwest and in a synoptic regime that was dominated by a strong offshore (higher pressure seaward) pressure gradient between the Eastern Pacific High and inland troughing. During this event, TAMS-RT was operating in a warm-start mode and was able to benefit from retained mesoscale structure in the data assimilation routine.

Figure 5-31 shows a 24-h forecast from COAMPS that verifies very well in location with the available satellite imagery and observations. The intermediate mesh of COAMPS over-forecasts the strong northwesterly winds over San Nicolas Island by ~20 kts, however the turbulent low-level cloud pattern just seaward (Figure 5-32) and scatterometry data valid just 6-h later (Figure 5-33) supports the stronger winds that COAMPS is showing in the outer bight. A loop of the modeled wind fields also demonstrates a strong diurnal fluctuation with onshore flow from about local noon into the late evening. Whether the fluctuation is caused by the increasing strength and eventual domination by the sea breeze, or by the relaxation of the lee troughing (Davis et al. 1999) is a subject for further study.

The COAMPS cloud forecast is shown in Figure 5-34 and is suggestive of the actual cloud conditions as shown in Figure 5-32, especially in the depiction of the thicker cloud layer along the coast that spreads inland into the valleys and onto the western slopes of the coastal mountain range. Also, COAMPS skillfully depicts the sheared-off edge in the outer bight in the presence of the strong northwesterly winds. The thicker cloud layer along the coast fits the Mass and Albright (1989) description that at initiation, a narrow tongue of coastal stratus develops and spreads northward as the southerlies and the associated marine layer deepen, which allows coastal stratus to develop and thicken. Figure 5-35 displays a low-level potential temperature surface, which also clearly indicates the presence of this cold tongue along the coast and is in line with the Mass and Albright (1989) theory of development. Looping these fields clearly shows a northward advance along the coast that eventually curves back around the northern bight to form the classic cyclonic pattern in the stratus and wind fields. COAMPS apparent skill at resolving the effects of the Catalina Eddy on lifting the coastal marine layer inversion (up ~50 mb

to a base of 2500 ft) is supported by comments from NWS forecasters in their forecast discussions.

Figure 5-36 is a comparison of the modeled forecast sounding and the actual sounding for Montgomery Field (MYF) valid at 1200 UTC on the 8<sup>th</sup>. COAMPS demonstrates skill in depicting the inversion base height, but lacks the resolution to capture both the inversion temperature and dew point temperature gradients (as should be expected). Note that the marine boundary layer compares favorably even though COAMPS has errors in the flow and temperature profile aloft.

## 7. Summary and Conclusions for Catalina Eddies

The Catalina Eddy is a quasi-stationary mesoscale vortex with a horizontal scale of roughly 100-km that extends from the surface to 1-2 km above mean sea level (MSL) (Mass and Albright 1989). Eddies occur during the late spring through early fall and may last from one to several days. Most studies agree that the Catalina Eddy is produced by the interaction between the synoptic-scale flow and the formidable topography of the region, which results in the formation of a cyclonically circulating low-pressure area within the SOCAL bight. The climatology of Mass and Albright (1989) suggests the importance of mesoscale lee troughing in the northern bight induced by strong northerly synoptic flow over the topographic mountain barrier to the north. The effects of the Catalina Eddy on the weather over SOCAL can be quite dramatic from one day to the next. However, the Catalina Eddy generally results in southerly winds along the SOCAL coast, an increase in the duration and extent of the stratus cloud deck, lifting of fog, more moderate temperatures, and improved air quality. The most notable manifestation of the eddy occurs as a spiral pattern in the stratus cloud signature. Although observing the eddy is currently within reach, the data is still too sparse for the most effective operational analysis and forecast, as well as detailed scientific research. Numerical simulations are currently the best methods for detailed study of the Catalina Eddy's causes and effects.

COAMPS displays an over-development tendency that is most likely the result of inadequate blocking of the actual upstream flow because of its "smoother than reality" topography. Apart from this over-development tendency, COAMPS not only demonstrates significant skill in forecasting many of the qualitative indicators of Catalina Eddy development and its effects, but also shows signs of significant forecast accuracy even out to 24-h for most Catalina Eddy events.

THIS PAGE LEFT INTENTIONALLY BLANK

## VI. CONCLUSIONS AND RECOMMENDATIONS

### A. WARM AND COLD STARTS

The preliminary results of this evaluation suggest that it is possible to use warm and cold starts as a tactic to produce the most accurate forecast dependent upon the synoptic regime, especially in regions where upstream data is sparse within the COAMPS domain. In active synoptic regimes (i.e., synoptic-scale systems are moving rapidly through the COAMPS domain), cold-starts capitalize on NOGAPS analysis and short-range forecast skill to force a more accurate COAMPS coarse-mesh analysis and subsequent fine-mesh forecast as systems propagate downscale. In a parallel study covering the same time periods and domain structures, Monterossa (1999) demonstrated that COAMPS had more skill in its 24-h forecast when run in a cold-start mode without new observations versus when run in the same mode with new observations. In more benign synoptic regimes, warm-starts capitalize on the previously developed mesoscale structure in the COAMPS first-guess field to produce a more accurate fine-mesh analysis and subsequent forecast. More studies should be performed to study this possibility.

### B. THE INITIAL ANALYSIS

Regardless of which mode COAMPS is in, the utility of any given forecast can be inferred from a quick verification of the COAMPS analysis versus observational data. Naturally, when the analysis was accurate, accurate forecasts were observed and vice versa. Displays are needed that effectively fuse this information together in the same geographical frame of reference. It is strongly recommended that the “texture mapping” capability of Vis5D be developed and implemented to fuse both observational data (e.g., satellite imagery, observations, radar data) and the COAMPS analysis at a minimum.

### C. Vis5D ANALYSIS TECHNIQUES

Visualization tools like Vis5D are a must in order to *quickly* and *effectively* capture and evaluate the complex structure and detail of the entire model run, a task that simply cannot be accomplished with 2-D plots and web pages of output. However, operating Vis5D can be a complex process. Threshold limits, color schemes, and the order and display combinations of various parameters need to be purposeful and thoughtful. The techniques presented in this thesis for exploring COAMPS model output with Vis5D are intended to remove that complexity and provide the best way for forecasters to incorporate COAMPS guidance into the forecast process. However, Vis5D alone is not the answer. An organized and systematic approach that

employs 3-D pattern recognition techniques is also needed in conjunction with Vis5D to capture these benefits.

#### D. TOPOGRAPHY

Many mesoscale events are low-level features that are strongly driven by interaction between the flow and the topography. Forecasters must have a comprehensive knowledge of the “modeled” topography and how it compares with the real topography within their forecast domain (e.g., topography, coastal resolution, surface albedo, land use and vegetation type). Currently, COAMPS offers the ability to view some of these modeled fields, like the terrain and coastlines. In the case of “modeled” terrain and coastal resolution, forecasters should use the “probe” mode of Vis5D to explore areas of critical surface forcing and then consider the potential impacts of this evaluation on the forecast. Appendix C offers detailed procedures for this technique. Future versions of COAMPS should empower forecasters with the capability to view surface albedo, land usage and vegetation type as well. After all, these fields are already present in the TAMS-RT resident database. Ideally, displays are needed so forecasters can view and understand differences between the actual and COAMPS topography. Since both the high-resolution topographic data base and the COAMPS modeled topography values are present, an automated scheme could be developed to alert forecasters to poor model fits to the actual topography. It is only with this knowledge that forecasters can fully understand the mesoscale weather development in their area and more effectively employ mesoscale NWP.

#### E. LATERAL BOUNDARY CONDITIONS

Errors generated in the LBCs will propagate into the inner domains and adversely impact the accuracy of the forecast. Warner et al. (1997) suggests several methods for minimizing the impacts of LBC-generated errors. For some of these methods a forecaster has control, like ensuring the physics between the parent model and COAMPS are consistent, and increasing the temporal and vertical resolution of the LBCs. However, there are also several methods that forecasters can control. These include minimizing the differences in grid resolution between the parent model and the outer mesh of COAMPS, defining a large buffer zone within the coarse mesh that extends upstream from the nested grids, and not placing the edges of grid domains in regions of steep gradients (e.g., mountain ranges and coastlines). In conjunction with the automated topography check routine, TAMS-RT could be modified to alert forecasters of poor placement of lateral boundaries.

## **F. MESOSCALE CONCEPTUAL MODELS**

Forecasters must be equipped with mesoscale conceptual models that are *specifically* applicable to certain mesoscale features and *generally* adaptable to any location on the globe. The advance of high-resolution (1 km/1-10 min) data has led to the identification and documentation of a wide variety of conceptual models of mesoscale circulation systems (Davis et al. 1999). Forecasters equipped with conceptual models of convective mesoscale systems such as the Mesoscale Convective Complex (MCC), coastal mesoscale systems such as the Catalina Eddy, and other mesoscale circulation systems such as mesoscale convergence zones are more likely to be able to identify and interpret model performance of these features within their area of responsibility (AOR). After observing the variations from the conceptual model over time and as experienced-based knowledge grows, forecasters will be able to identify which modeling factors dominate in their AOR and then anticipate model trends when forecasting the development and intensity of specific mesoscale circulation systems.

## **G. DEVELOPING AND NURTURING “MESO-SKILL” (THE MESOSCALE KNOWLEDGE BASE)**

Forecasting fronts and eddies and their associated weather is best approached by a marriage between mesoscale modeling capability and forecaster knowledge of local rules of thumb, conceptual models, and modeling factors, including the effects of warm and cold-starts on data assimilation, the effects of disparities between the “modeled” topography or other surface characteristics and reality, and the effects of lateral boundary condition (LBC) errors on the forecast. On top of this, forecasters must understand the importance of the analysis and how to verify its accuracy versus observational data, as well as the operation and application of 3-D visualization tools and techniques. This requires a robust forecaster training program for understanding model principles and known model limitations, as well as a robust command training program. In this manner, forecasters will know when and how to take preventative model setup steps to reduce known error sources and to maximize forecast effectiveness. Without this applied knowledge, the model output cannot be used with any level of confidence or degree of accuracy. In summary, the best results in our mesoscale forecast capability will be attained with a continuous and balanced effort to improve both the mesoscale model and the forecaster’s knowledge and application of mesoscale model output. It is hoped that this review will assist in the latter half of this worthwhile endeavor.

THIS PAGE INTENTIONALLY LEFT BLANK

## LIST OF REFERENCES

Angove, M.D., 1998: A one-year retrospective analysis of the mesoscale modeling initiative at the Naval Pacific Meteorology and Oceanography Detachment, Whidbey Island Washington. NPMOD Whidbey Island, WA, 10 pp. [Available from Department of Meteorology, Naval Postgraduate School, 589 Dyer Road, Room 254, Monterey, CA 93943-5114, Tel. (831) 656-2516.]

Arakawa, A. and V. Lamb, 1977: Computational design of the basic dynamical processes in the UCLA general circulation model. *Methods. in Computational Physics.*, **17**, J. Chang, Ed., Academic Press, 174-264.

Baker, N.L., 1992: Quality control for the U.S. Navy operational database. *Wea. Forecasting*, **7**, 250-261.

Bond, N.A., C.F. Mass, B.F. Smull, R.A. Houze, M. Yang, B.A. Colle, S.A. Braun, M. A. Shapiro, B.R. Colman, P.J. Neiman, J.E. Overland, W.D. Neff, and J.D. Doyle, 1997: The Coastal Observation and Simulation with Topography (COAST) Experiment. *Bull. Amer. Meteor. Soc.*, **78**, 1941-1955.

Carlson, T.N., 1991: *Mid-Latitude Weather Systems*. Routledge, 507pp.

Cook, J., J. Schmidt, R. Hodur, P. Tsai, S. Chen, and L. Phegley, 1997: The On-Scene Tactical Atmospheric Forecast Capability (STAFC). *Proc. 1997 Battlespace Atmospherics Conf.*, San Diego, CA, 7 pp.

Cressman, G. P., 1959: An operational objective analysis system. *Mon. Wea. Rev.*, **87**, 367-374.

Davies, H.C., 1976: A lateral boundary formulation for multi-level prediction models. *J. Royal. Met. Soc.*, **102**, 405-418.

Davis, C.A., C.F. Mass, and S. Low-Nam, 1999: Dynamics of a Catalina Eddy revealed by numerical simulation. (submitted to *Mon. Wea. Rev.*).

Doyle, J.D., M. Shapiro, R. Gall, and D. Bartels, 1997: Research aircraft observations and the numerical simulation of a breaking gravity wave event over Greenland observed during FASTEX. *Editor Map Newsletter*, Zurich, Switzerland.

Evans, T. E., and D. A. Halvorson, 1998: Climate of San Diego, California. NOAA Tech. Memo. NWS/WR-256, 89 pp.

Gal-Chen, T., and R. Somerville, 1975: On the use of a coordinate transformation for the solution of the Navier-Stokes equations. *J. Comp. Phys.*, **17**(2), 209-228.

Gunderson, C., 1999. Early returns on the San Diego local mesoscale modeling initiative. NPMOC San Diego, CA, 11 pp. [Available from Commanding Officer, NPMOC San Diego, PO BOX 357076, San Diego, CA, 92135-7076, Tel. (619) 545-6027.]

Harshvardan, R Davies, D. Randall, and T. Corsetti, 1987: A fast radiation parameterization for atmospheric circulation models. *J. Geophys. Res.*, **92**, 1009-1015.

Henderson-Sellers, A., and M.F. Wilson, 1986: Current global land-surface data sets for use in climate-related studies. NCAR Research Tech. Note, NCAR/TN-272+STR, 102 pp.

Hodur, R., 1997: The Naval Research Laboratory Coupled Ocean/Atmosphere Mesoscale Prediction System (COAMPS). *Mon. Wea. Rev.*, **125**, 1414-1430.

Kain, J.S., and J.M. Fritsch, 1993: Convective parameterization for mesoscale models: The Fritsch-Chappell scheme. *The Representation of cumulus in numerical models. Meteor. Monogr.*, K.A. Emanuel and D.J. Raymond, Eds., Amer. Meteor. Soc., 159-164.

Klemp, J. B., and R. B. Wilhelmson, 1978: The simulation of three-dimensional convective storm dynamics. *J. Atmos. Sci.*, **35**, 1070-1096.

Kuo, J. L., 1974: Further studies of the parameterization of the influence of cumulus convection on large-scale flow. *J. Atmos. Sci.*, **31**, 1232-1240.

Lorenc, 1986: Analysis methods for NWP. *J. Royal Met. Soc.*, **112**, 1177-1194.

Louis, J.F., 1979: A parametric model of vertical eddy fluxes in the atmosphere. *Bound Lay. Meteor.*, **17**, 187-202.

Mass, C.F., and M.D. Albright, 1989: Origin of the Catalina Eddy. *Mon. Wea. Rev.*, **117**, 2406-2436.

Mellor, G.L., and T. Yamada, 1982: Development of a turbulence closure for geophysical fluid problems. *Rev. Geophys and Space Phys.*, **20**, 851-875.

Monterrosa, O., 1999: Comparison of COAMPS surface wind and temperature fields with surface observations in the SOCAL area. M.S thesis, Dept. of Meteorology, The Naval Postgraduate School, 90 PP. (submitted to NTIS). [Available from Department of Meteorology, Naval Postgraduate School, 589 Dyer Road, Room 254, Monterey, CA 93943-5114, Tel. (831) 656-2516.]

Naval Pacific Meteorology and Oceanography Center (NPMOC) San Diego, CA, 1995: *Forecaster's Handbook for NAS North Island*. NPMOC San Diego, CA, 124 pp. [Available from Commanding Officer, NPMOC San Diego, PO BOX 357076, San Diego, CA, 92135-7076, Tel. (619) 545-6027.]

Perkey, D.J., and C. Kreitzberg, 1976: A time dependent lateral boundary scheme for limited area primitive equations models. *Mon. Wea. Rev.*, **104**, 744-755.

Petterssen, S., 1956: *Weather Analysis and Forecasting*, Vol. I. McGraw-Hill Book Company.

Rutledge, S.A., and P.V. Hobbs, 1983: The mesoscale and microscale structure of organization of clouds and precipitation in mid-latitude cyclones. VIII: A model for the "seeder-feeder" process in warm-frontal rainbands. *J. Atmos. Sci.*, **40**, 1185-1206.

Sashegyi, K.D., and R.V. Madala, 1992: Initial conditions and boundary conditions. *Mesoscale Modeling of the Atmosphere*, R.A. Pielke and R.P. Pearce, Eds., Amer. Metero. Soc., 1-12.

Thompson, W.T., S.D. Burk, and J. Rosenthal: 1997: An investigation of the Catalina eddy. *Mon. Wea. Rev.*, **125**, 1135-1146.

Vukicevic, T., and R.M. Errico, 1990: The influence of artificial and physical factors upon predictability estimates using a complex limited-area model. *Mon. Wea. Rev.*, **118**, 1460-1482.

Warner, T.T., R.A. Petersen, and R.E. Treadon, 1997: A tutorial on lateral boundary conditions as a basic and potentially serious limitation to regional numerical weather prediction.  
*Bull. Amer. Meteor. Soc.*, **78**, 2599-2617.

THIS PAGE INTENTIONALLY LEFT BLANK

## APPENDIX A. FIGURES

The following pages of figures are grouped together in this appendix to help make reading them easier. Additional examples of graphics are available online at the Naval Postgraduate School's Mesoscale Numerical Weather Prediction home page at <http://www.met.nps.navy.mil/~ldm/wash/meso/ajreiss/> and are referred to periodically throughout this thesis.



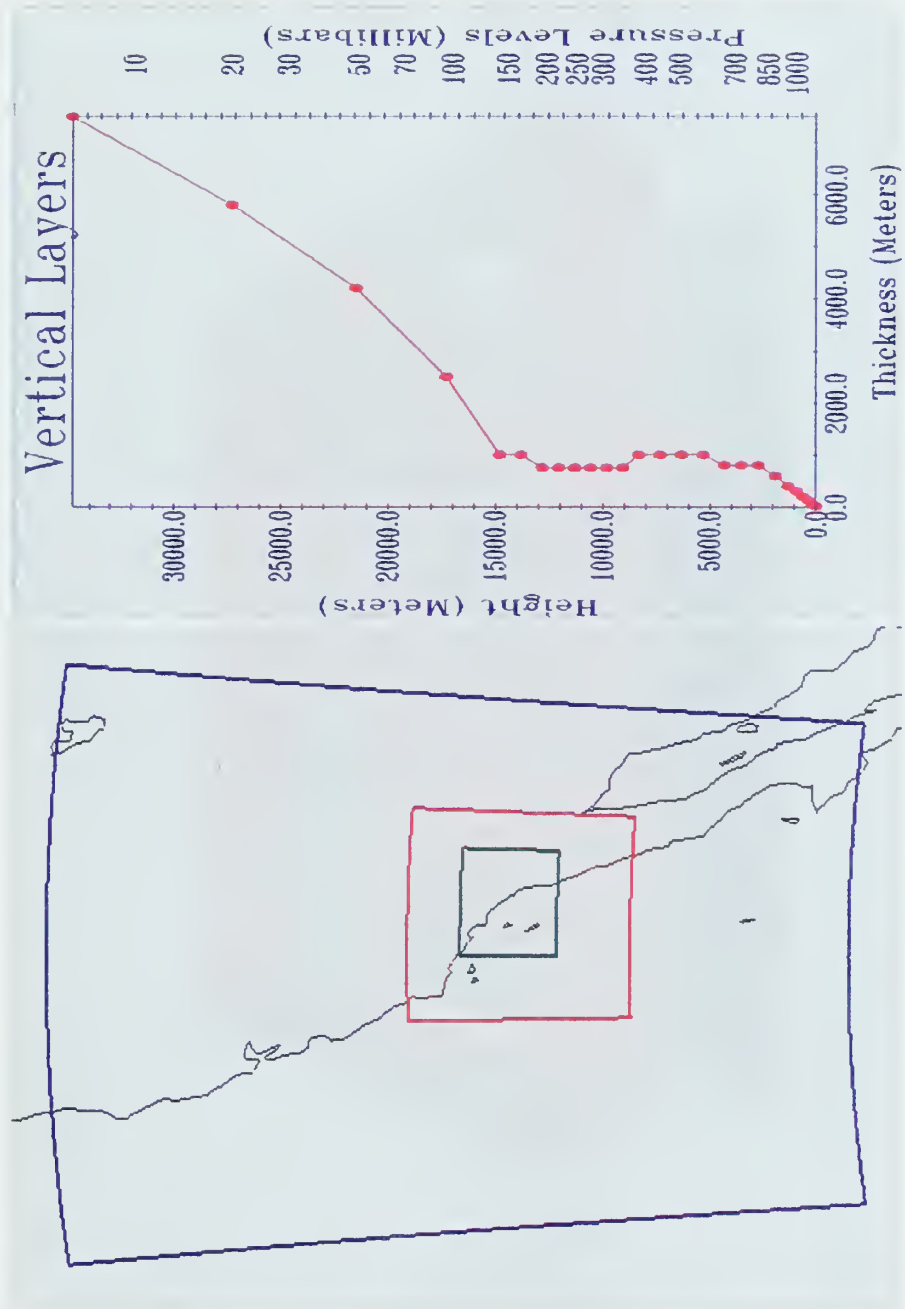


Figure 2-1. Left: COAMPS horizontal grid domain in NPMOC San Diego's TAMS-RT valid for the case studies presented in this thesis. Right: COAMPS 30 vertical  $\sigma$ -levels with increased resolution depicted in the lower troposphere.



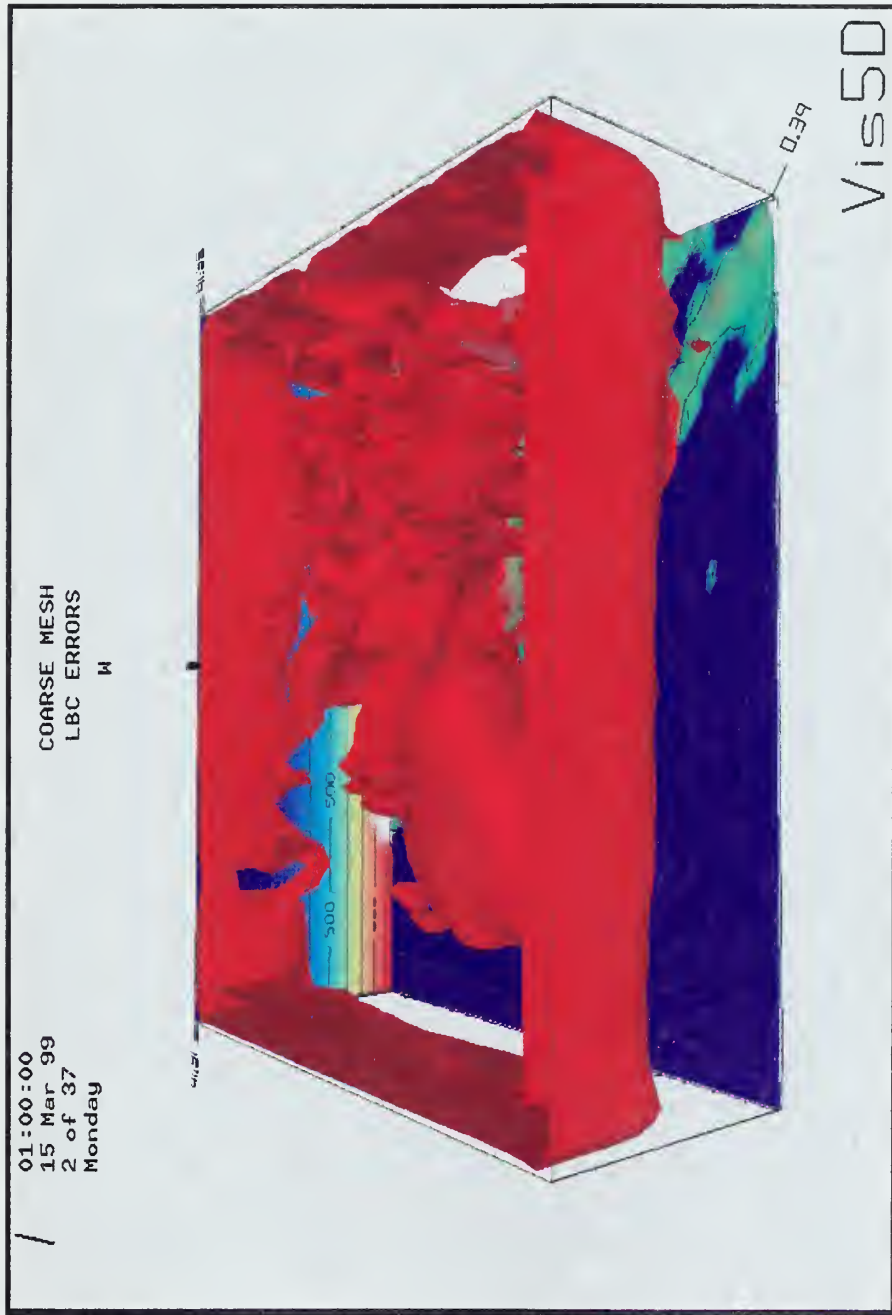


Figure 2-2. Example of LBC-generated error evident as a "curtain" of upper level vertical velocity noise in the first few hours of this particular model run. The errors are the result of the western lateral boundary intersecting a particularly strong flow gradient associated with the jet stream in the parent model, NOGAPS.



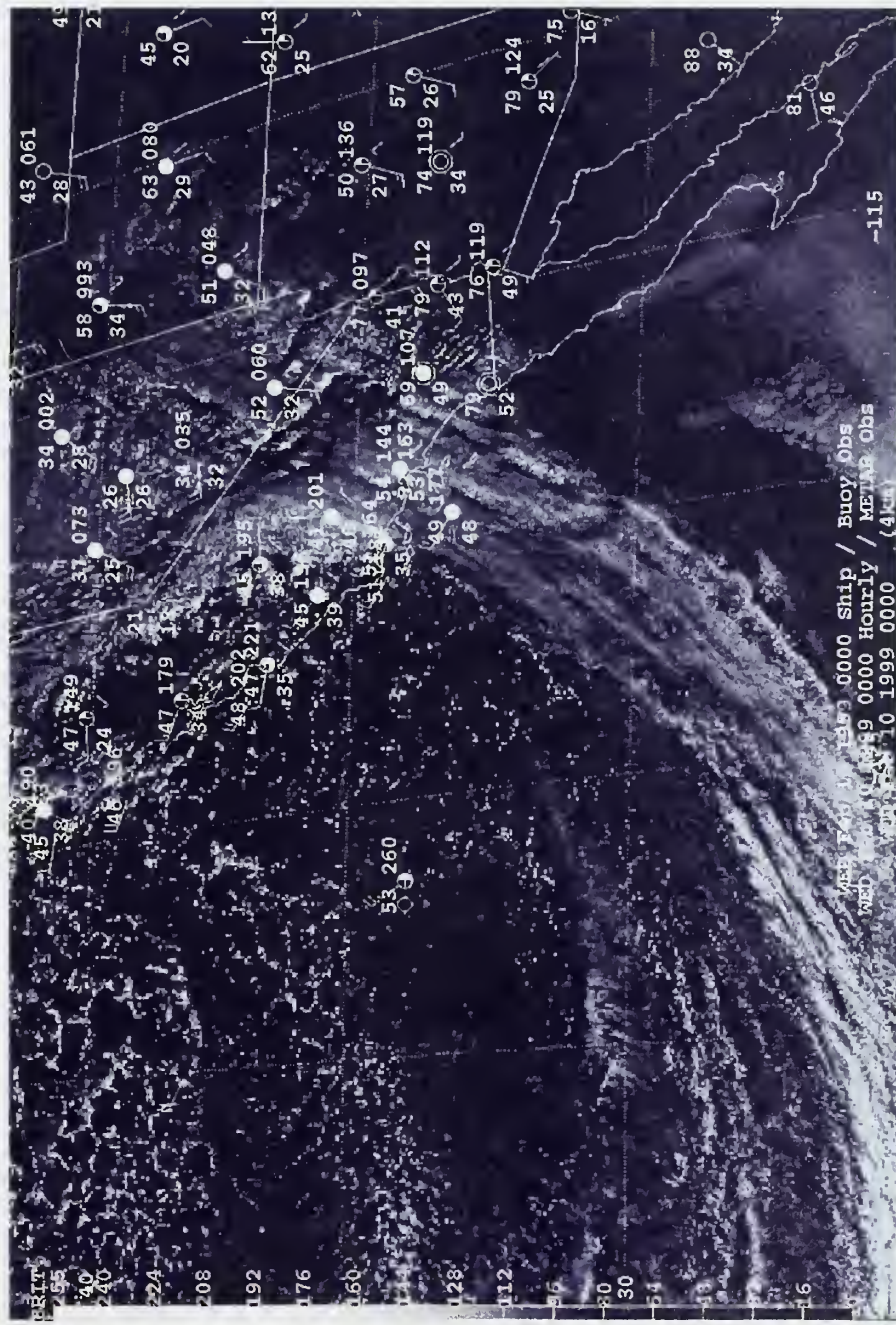
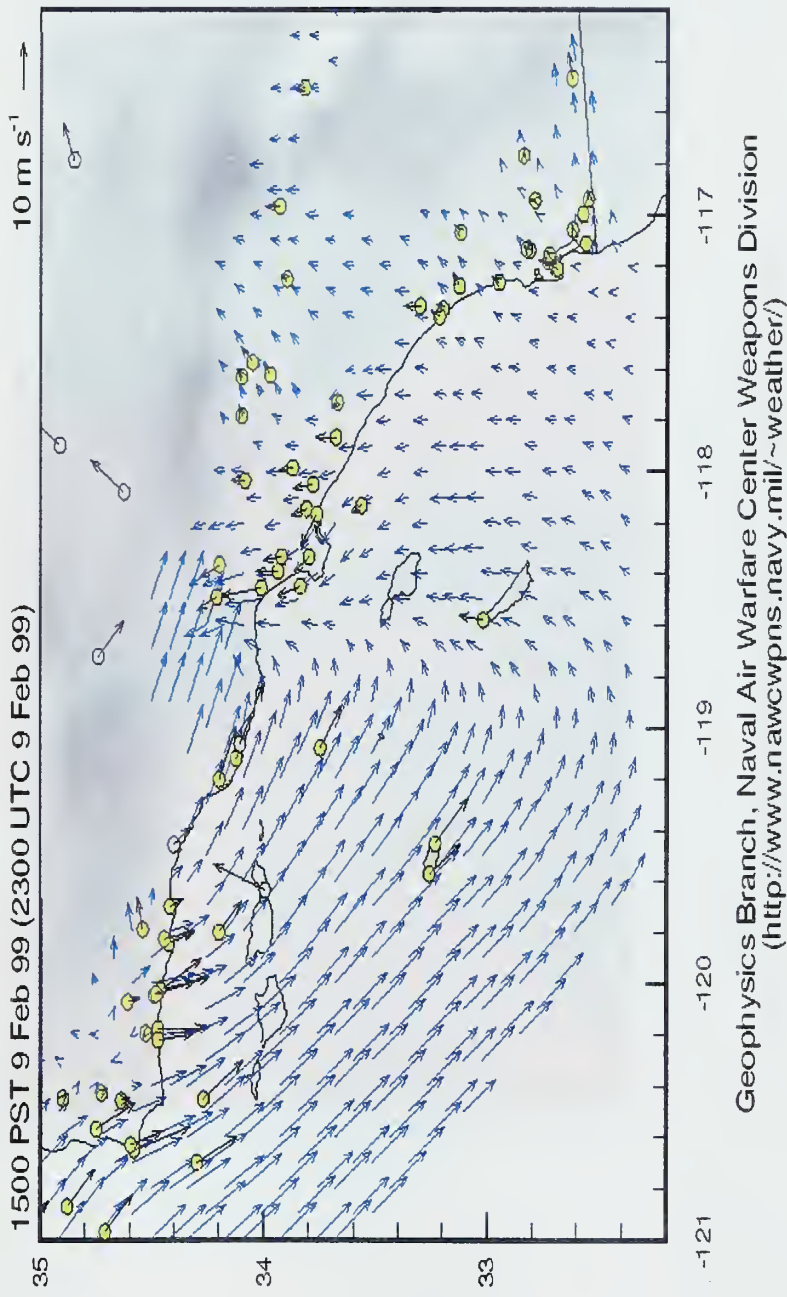


Figure 3-1. Satellite imagery from 0000 UTC 10 February showing the cloud signature of the actual front as it passes through the bight.



## SURFACE WIND VECTORS

(blue vectors are interpolated from yellow observation sites)



Geophysics Branch, Naval Air Warfare Center Weapons Division  
(<http://www.awcwpns.navy.mil/~weather/>)

Figure 3-2. Mesoscale analysis clearly depicting the front over the waters between San Nicolas Island and Santa Catalina and San Clemente Islands (NAWC Pt. Mugu)



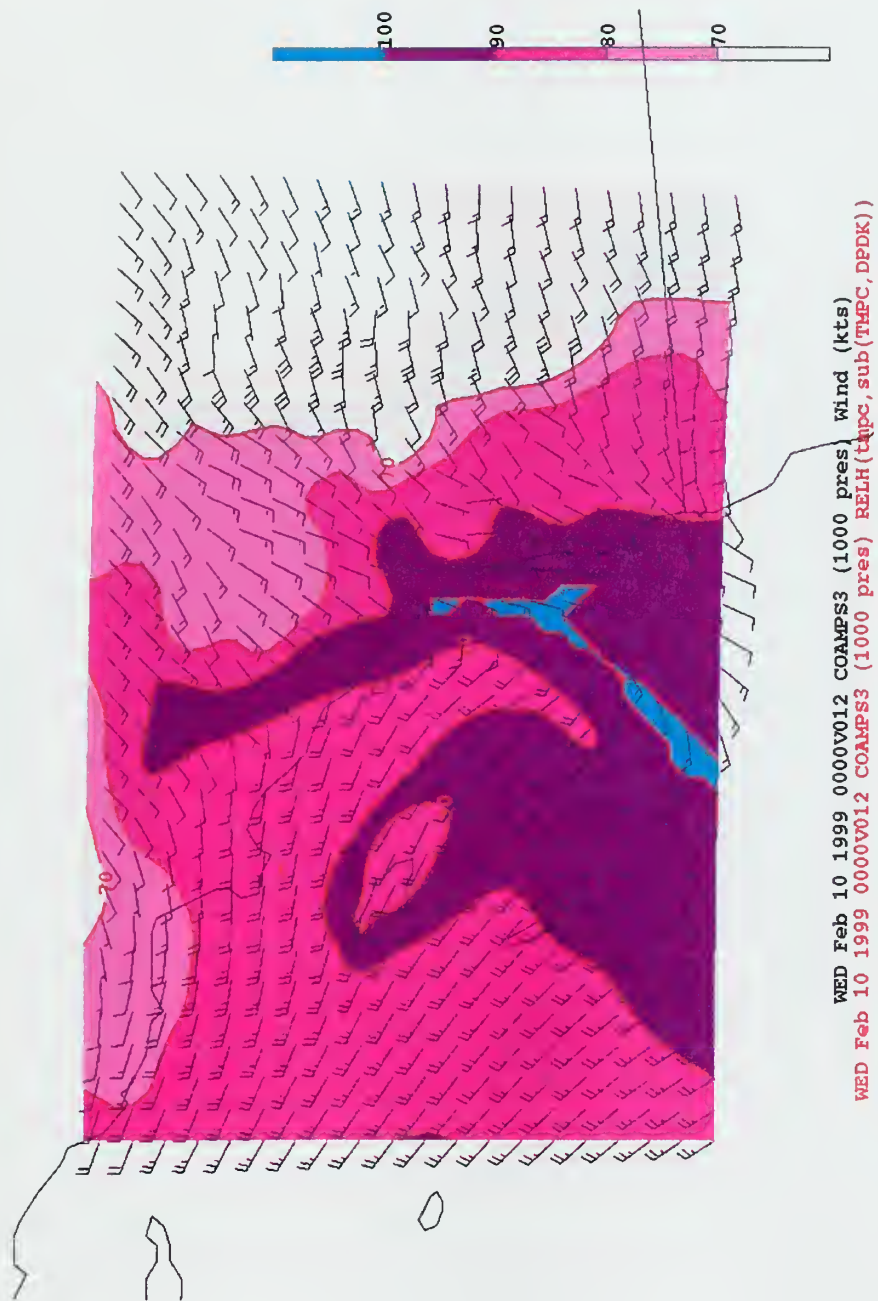


Figure 3-3. A 12-h forecast based on an accurate analysis, where COAMPS not only propagates the position of the larger-scale front accurately down to the high-resolution nest, but also skillfully depicts the mesoscale structure of and the response to the front.



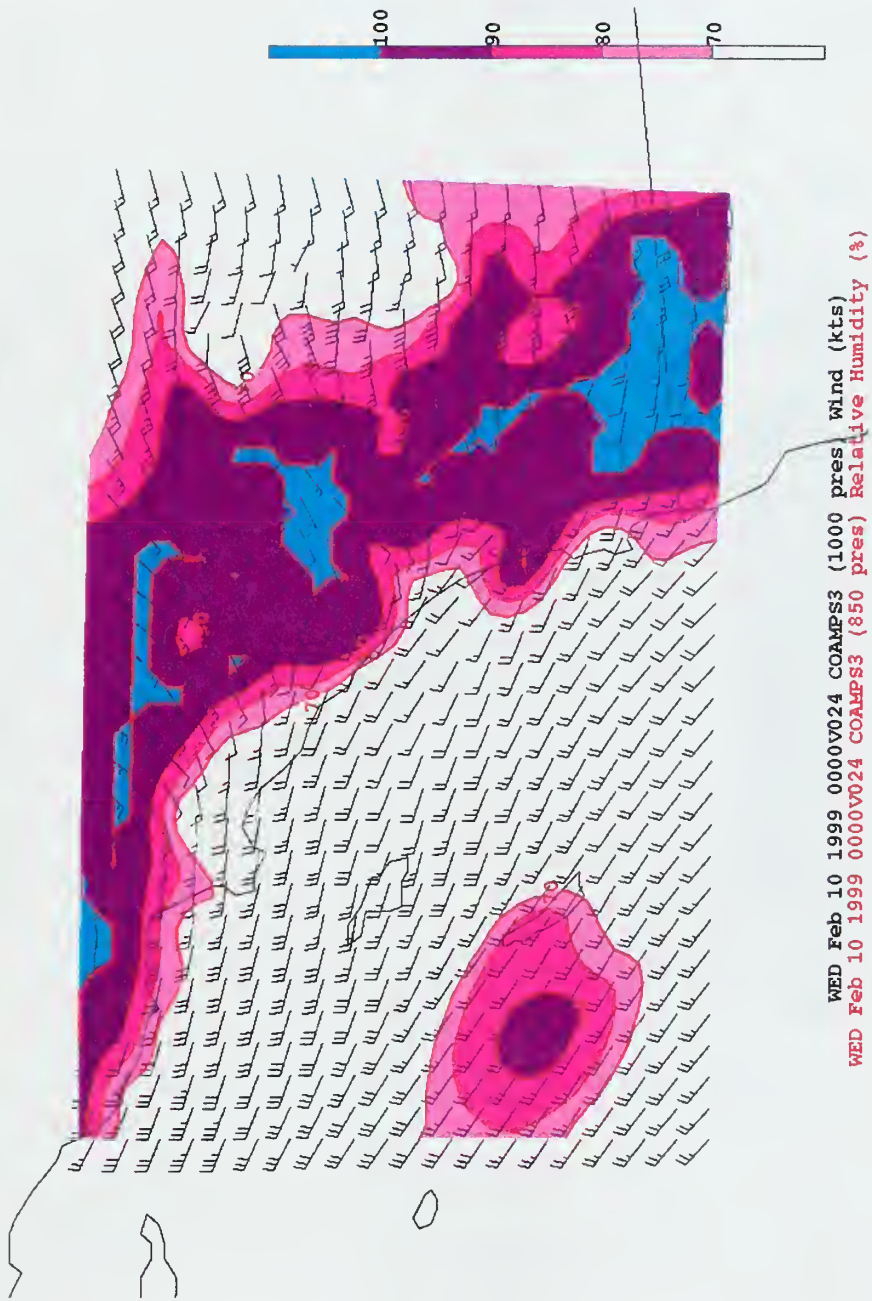


Figure 3-4. This 24-hr COAMPS forecast initialized from an erroneous analysis and demonstrates the danger of unequivocally accepting the guidance provided by a mesoscale model.



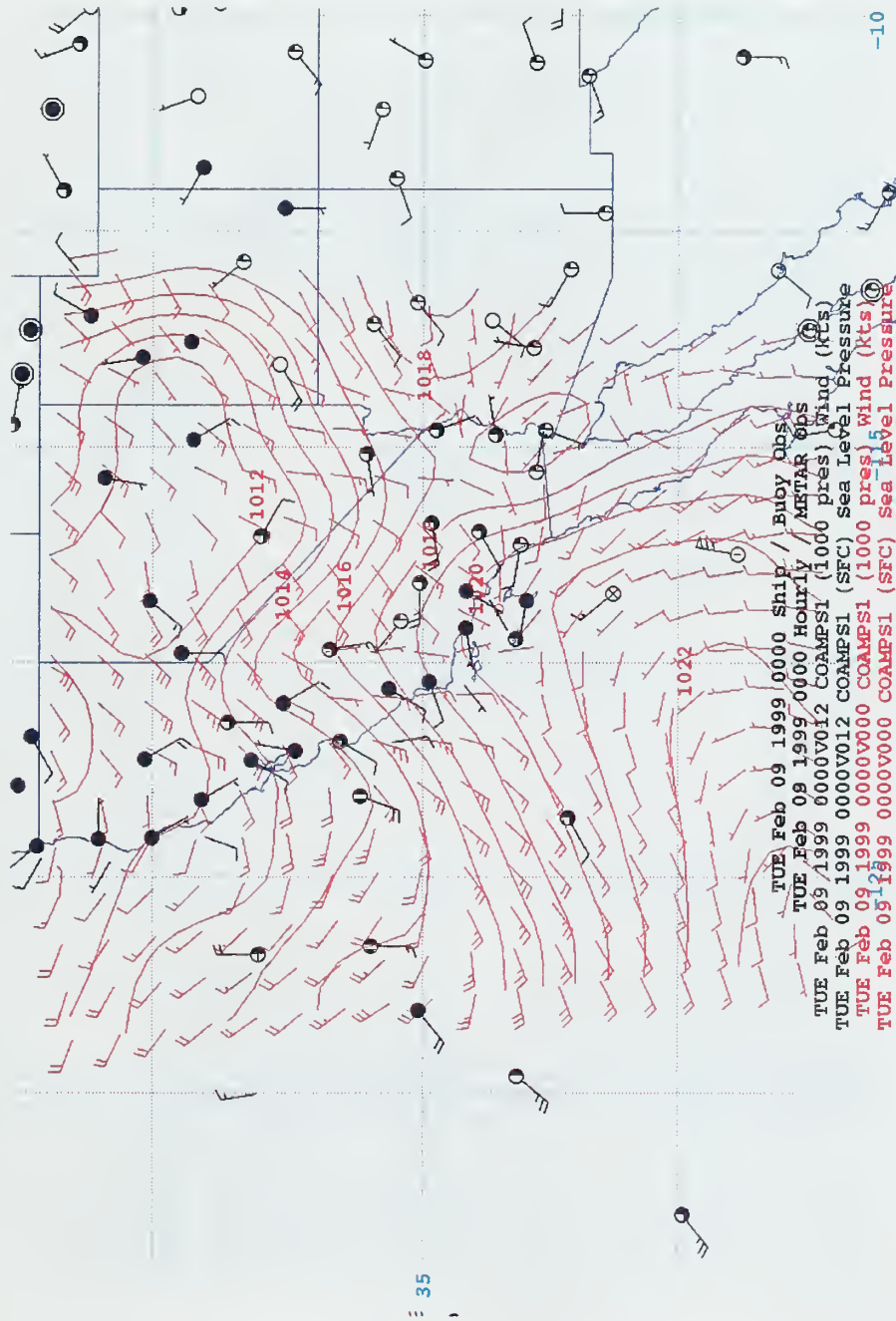


Figure 3-5. The initial analysis (for the erroneous COAMPS 24-h forecast) appears to be disregarding most of the surface observations, especially the ship reports in the vicinity of the actual front. The analyzed front is too fast and is located approximately 120 nm to the southeast of the actual front.



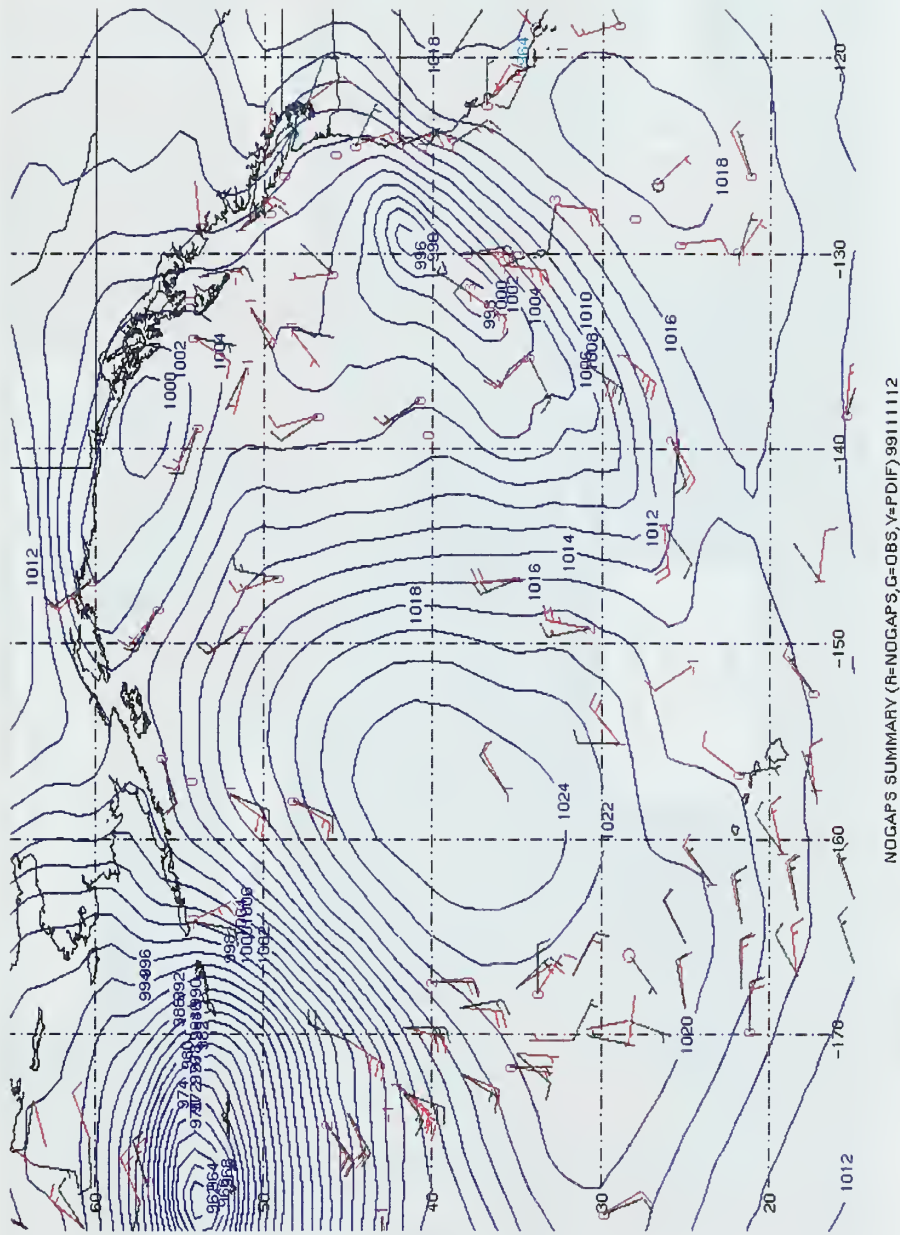


Figure 3-6. An example of analysis verification of selected NOGAPS fields against ship and buoy data (NWS Seattle, WA). NOGAPS surface pressure is contoured blue, while the wind data is red, and the actual observations are green. Pressure differences are violet. Comparisons between model output and observations are also available at various levels for cloud track/water vapor data, ACARS data, Rawinsonde data, scatterometer data, and precipitable water data from GOES.



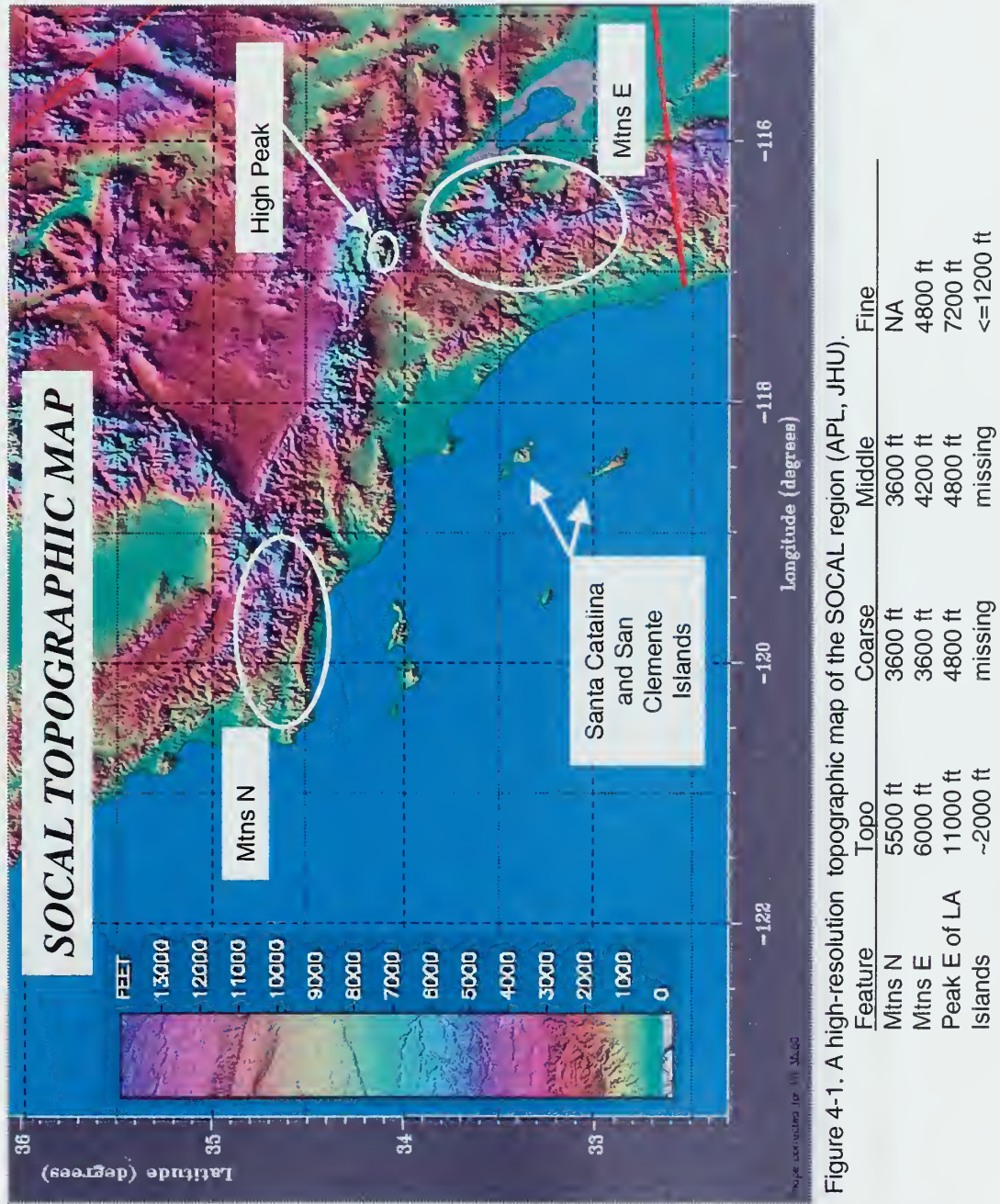


Figure 4-1. A high-resolution topographic map of the SOCAL region (APL, JHU).



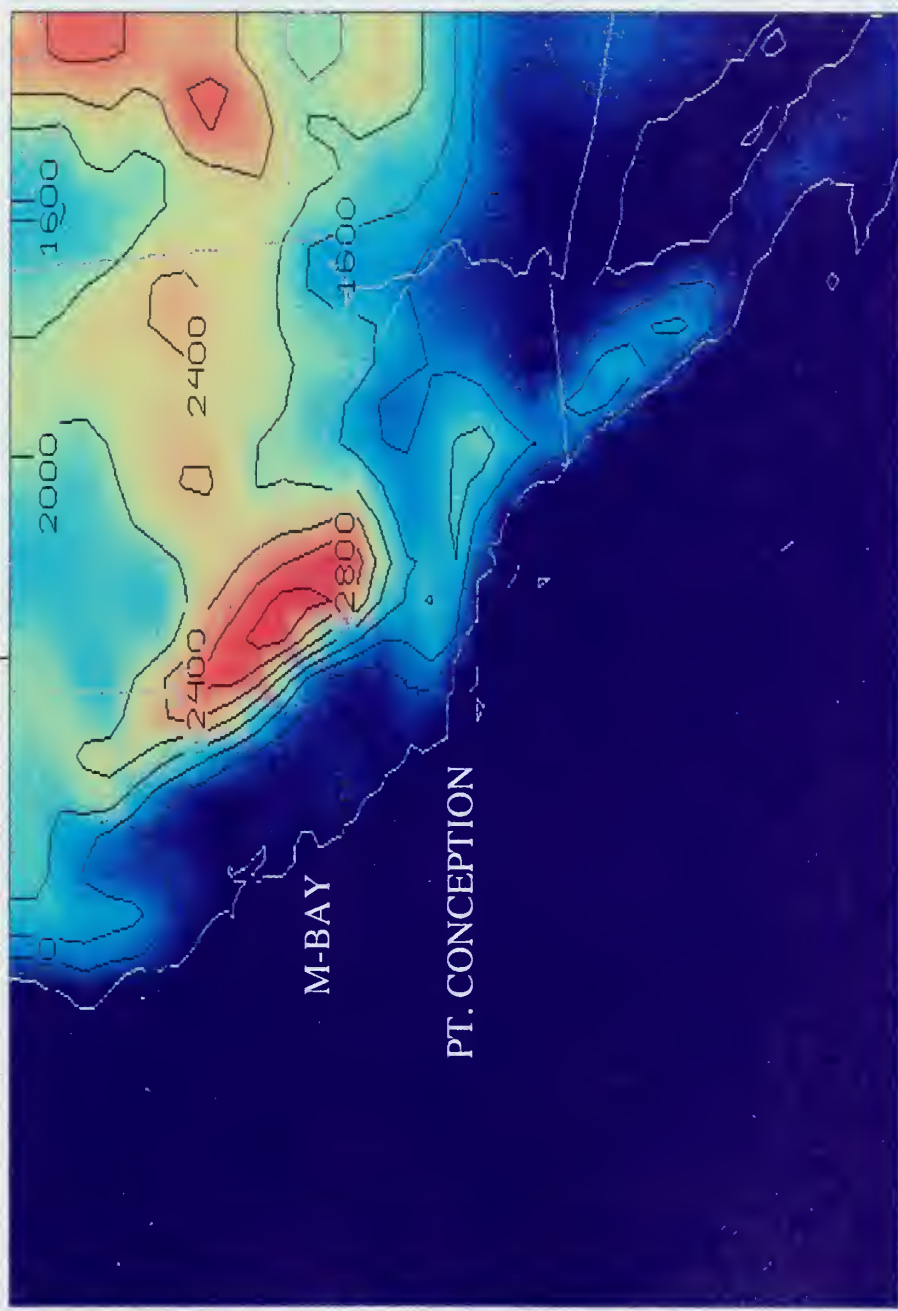


Figure 4-2. NPMOC San Diego's TAMS-RT COARSE mesh topography (m).



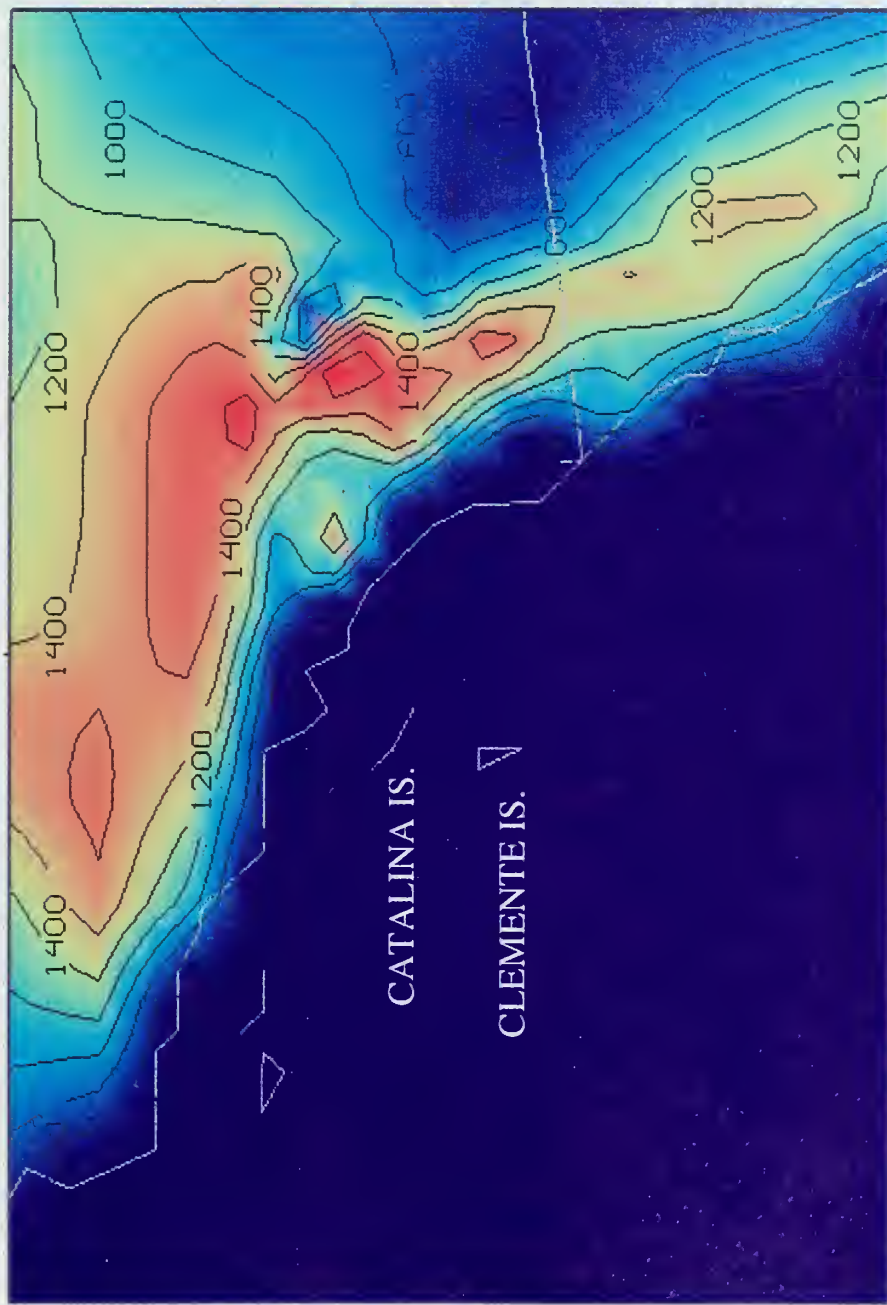


Figure 4-3. NPMOC San Diego's TAMS-RT INTERMEDIATE mesh topography (m).



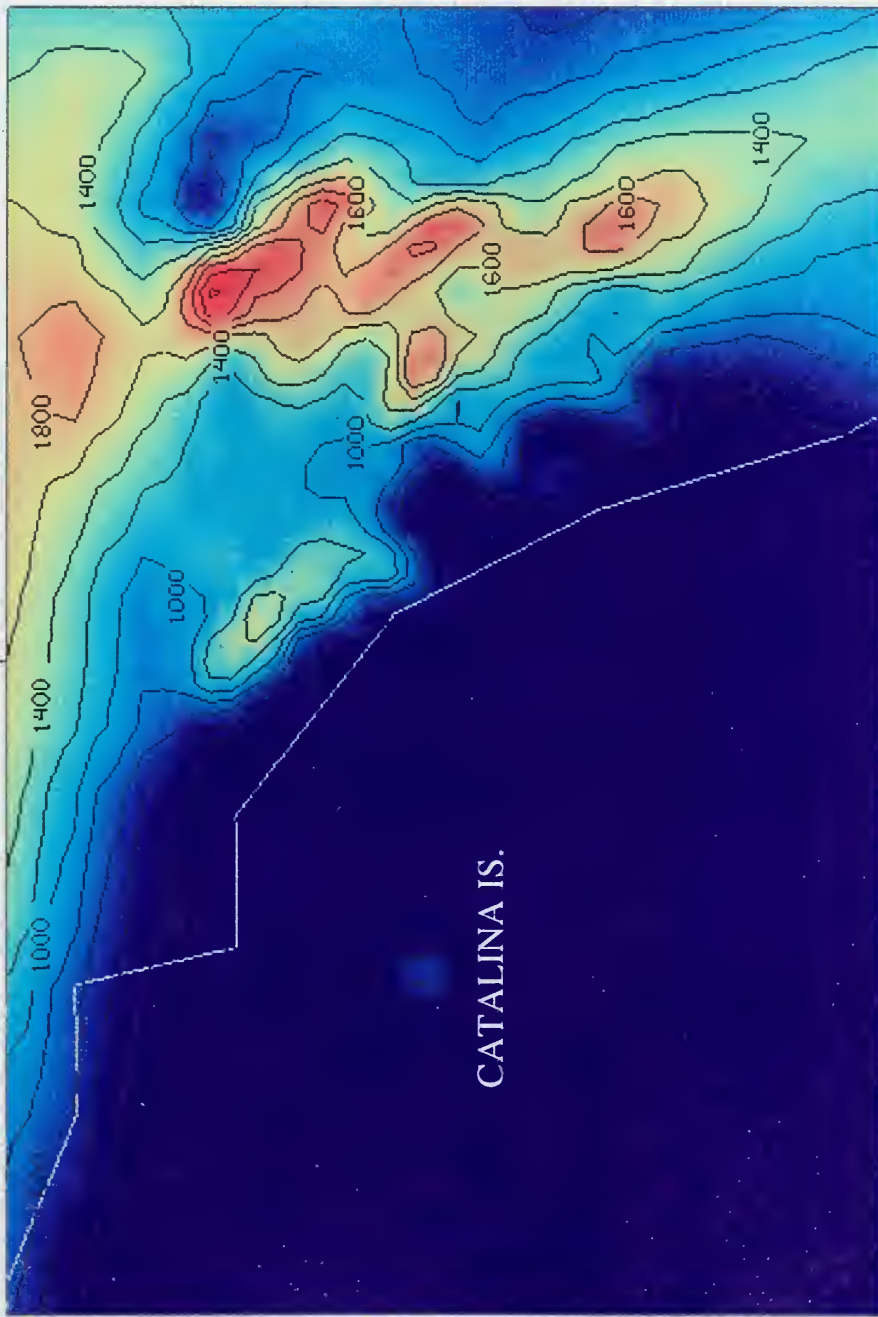


Figure 4-4. NPMOC San Diego's TAMS-RT FINE mesh topography (m).



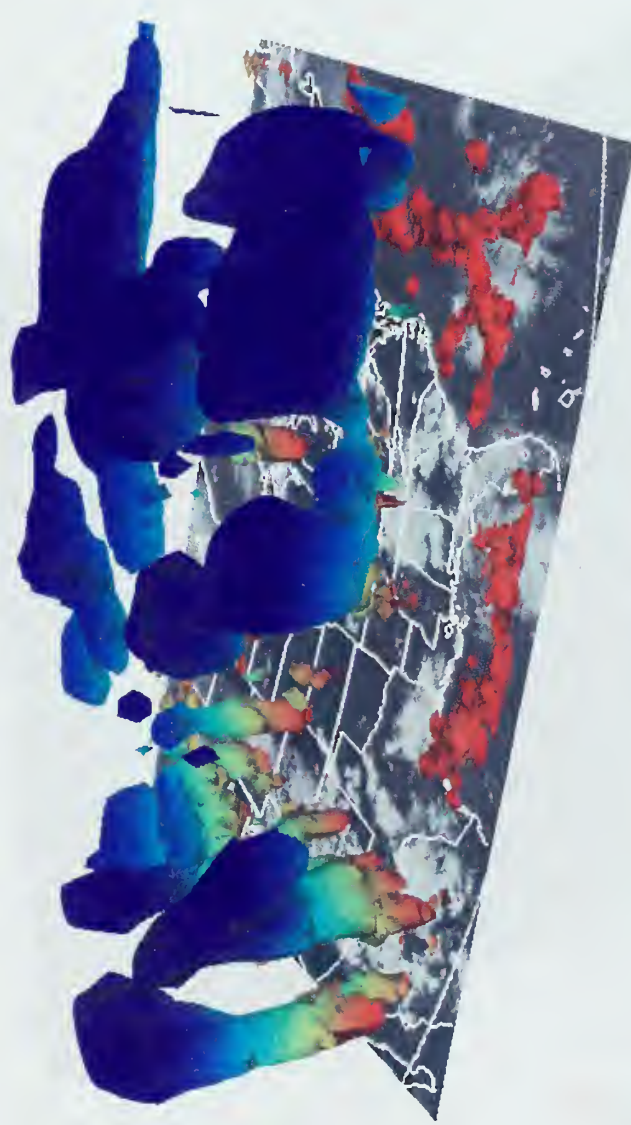


Figure 4-5. “Texture Mapping” in Vis5D. Here, cloud liquid water (with a temperature /altitude color scheme) at analysis time is being displayed over the corresponding satellite imagery. When evaluated against the COAMPS analysis or first-guess fields (or even Vis5D formatted NOGAPS fields), the comparison can reveal key information about the utility of a particular forecast (EPA Scientific Visualization Center (SvC)).



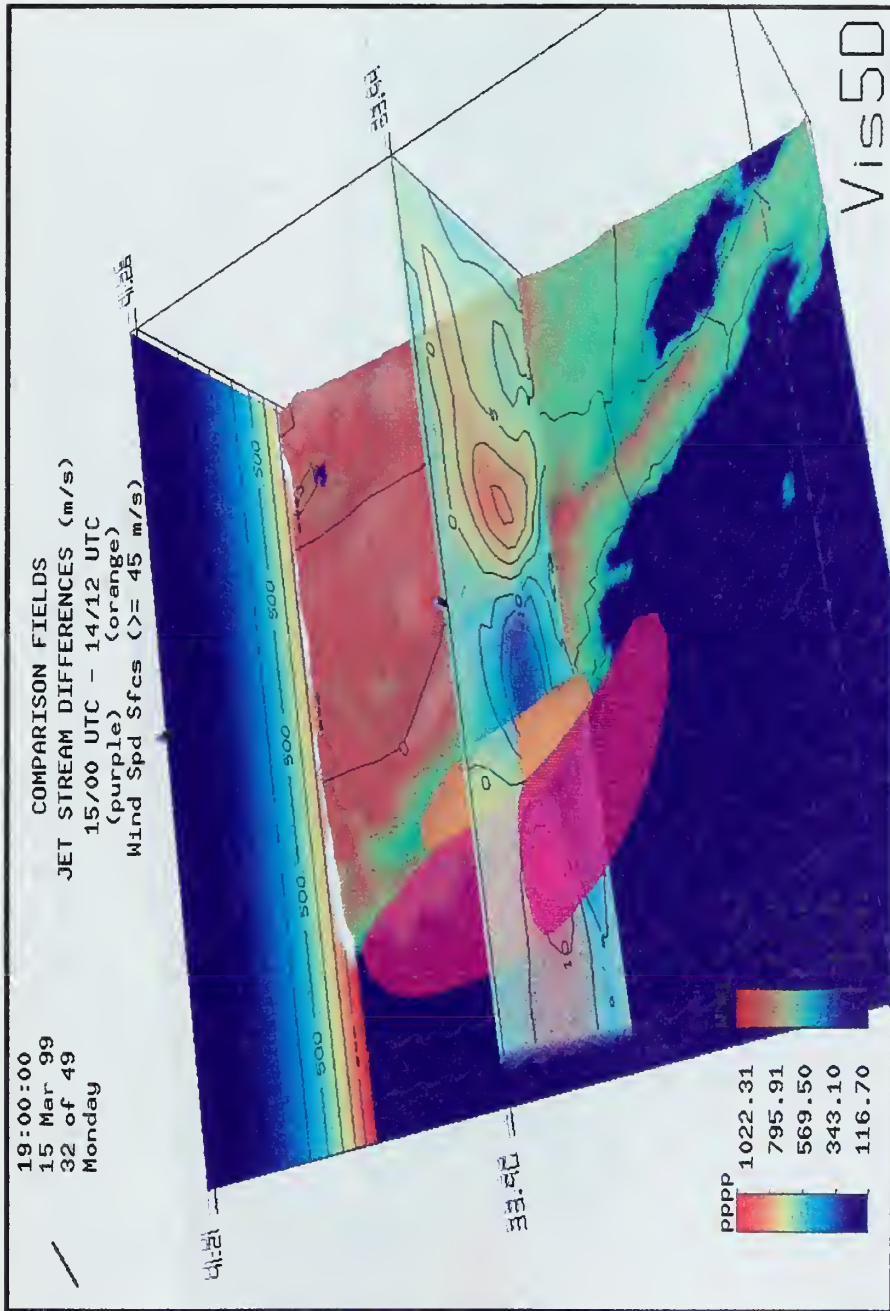


Figure 4-6. Vis5D Comparison Technique. The jet stream has changed in location and intensity from the previous run (orange) to the current run (purple). The vertical slice is a wind difference comparison that subtracts the previous forecast values from the current one. Positive values (yellow to red) are areas where the jet stream intensity in the current run is greater than in the previous model run, whereas negative (blue) regions are of the opposite effect.



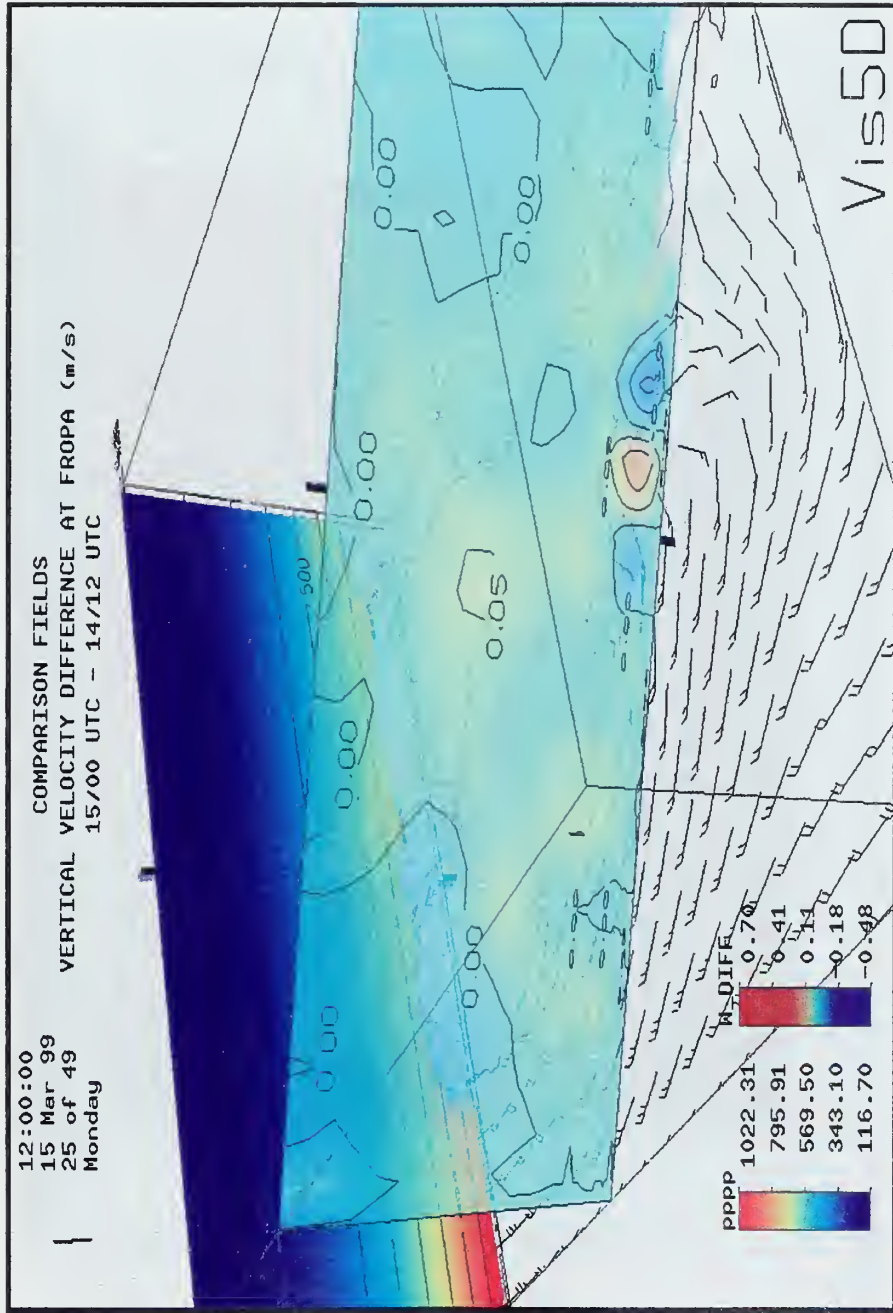


Figure 4-7. A vertical velocity difference cross-section for the current forecast minus the previous forecast. In this graphic, positive areas (red) denote areas of greater ascent (or less descent) by as much as 4 cm/s in the region just ahead of the surface front, thereby indicating the front is more active in the current forecast.



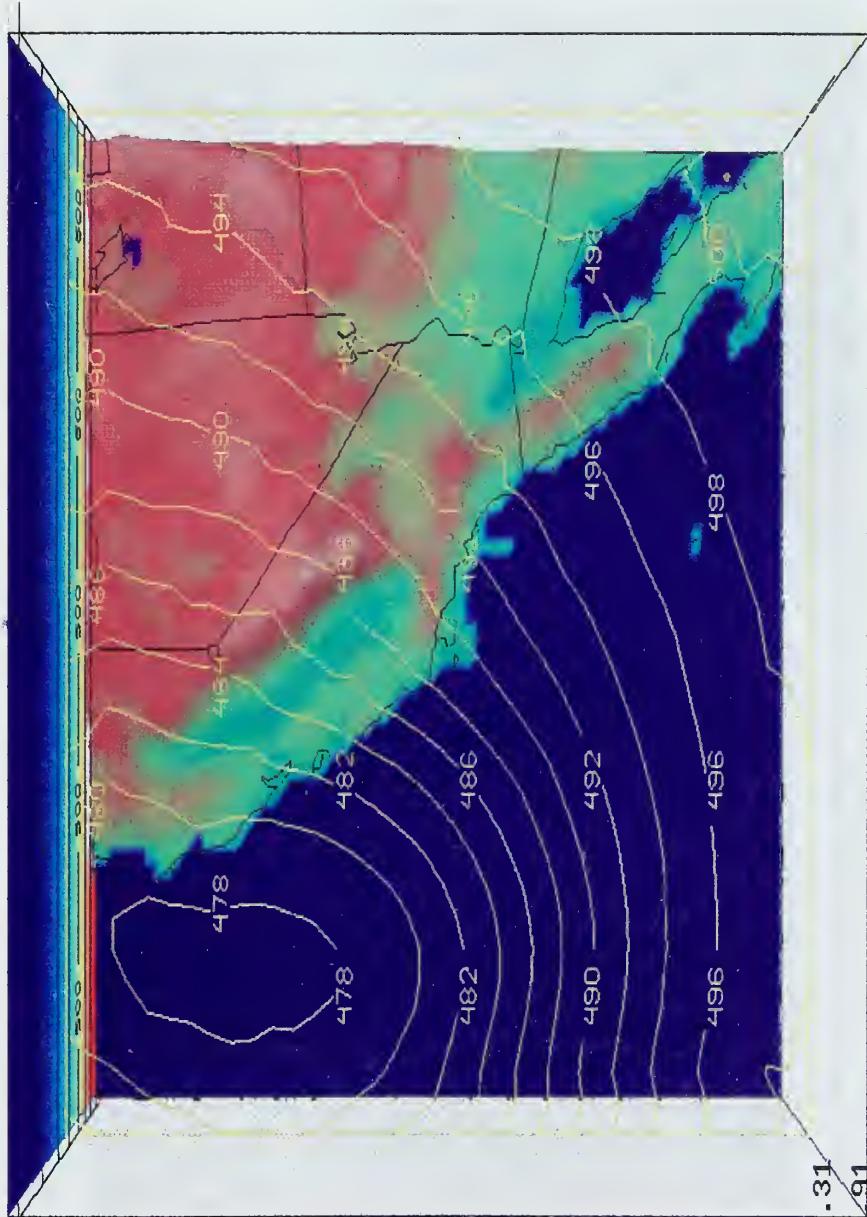


Figure 4-8. A “synoptic orientation” chart depicting a mid-level pressure slice (~500 mb according to the vertical reference slice) and the surface wind barbs. Note that the pressure slice is the display of all the pressure values at a constant height and is unlike the conventional display of isoheights of a constant pressure surface. A “TCP” view option is selected to give the familiar 2-D display.



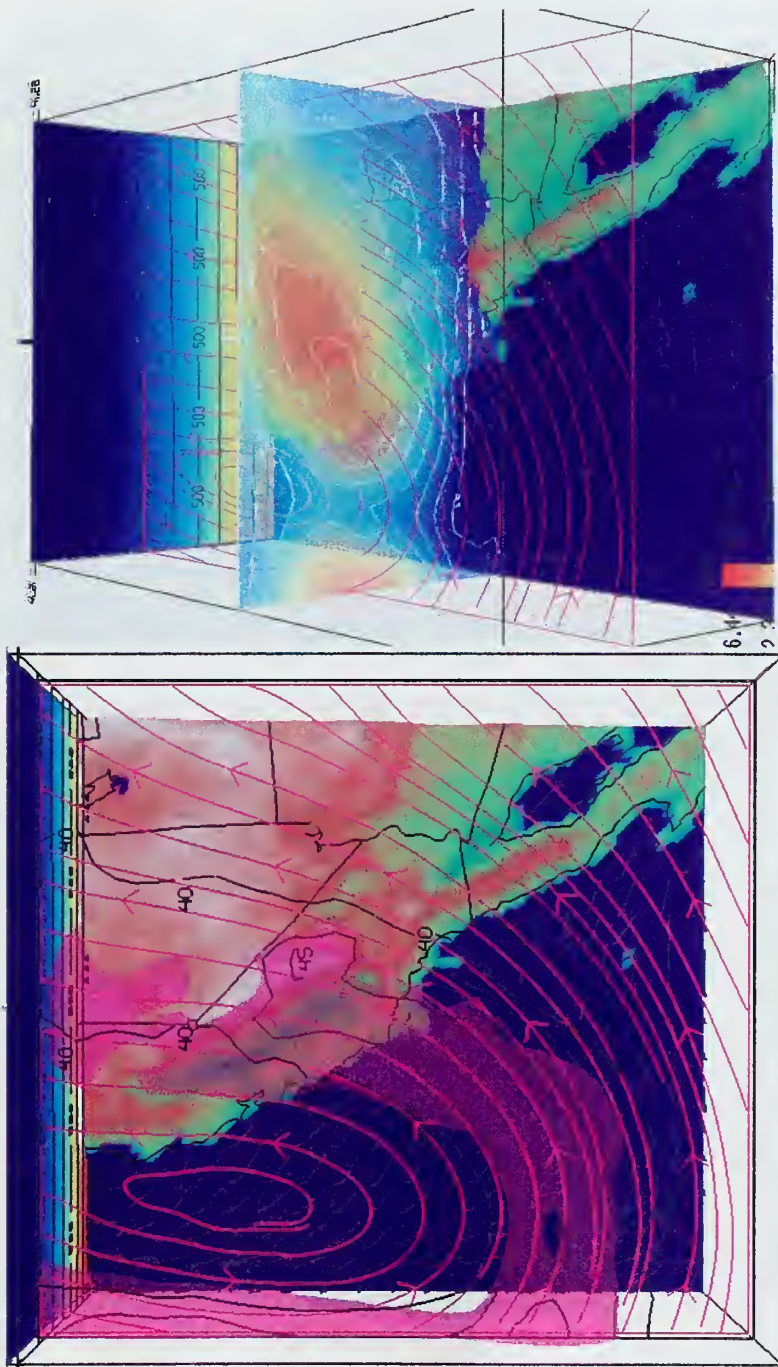


Figure 4-9. Jet Stream Analysis. A 45 m/s (90 kts) jet core (purple) extending throughout the base of a long-wave trough alongside a vertical slice depicting the intensity and vertical extent of the jet stream.



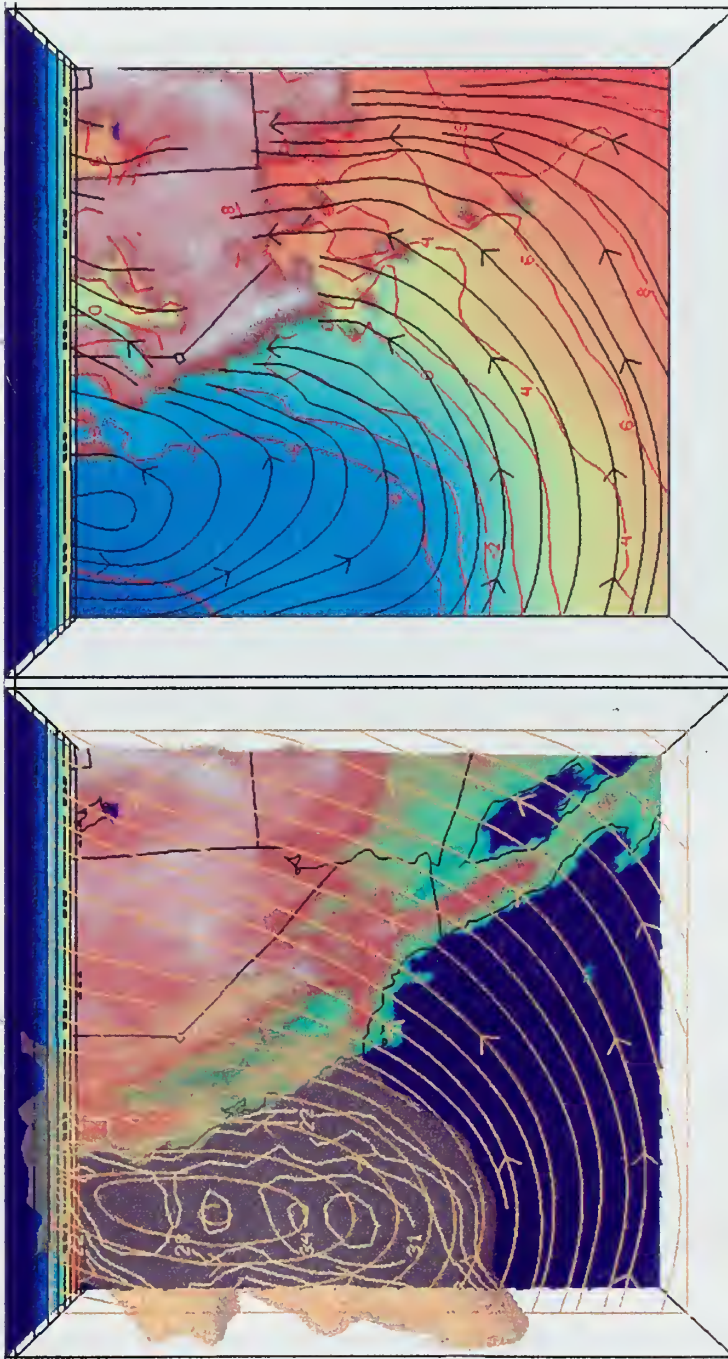


Figure 4-10. Vorticity (left) and thermal (right) forcing analysis. PVA is occurring east of the upper-level trough, while CAA is occurring into the base of the long-wave trough and WAA is occurring out ahead of the surface front. Both PVA and WAA regions coincide with the upper-level divergence associated with the jet stream in figure 4-9. These three factors considered together give a pretty clear indication of where to expect the model to develop strong ascent regions from quasi-geostrophic considerations.



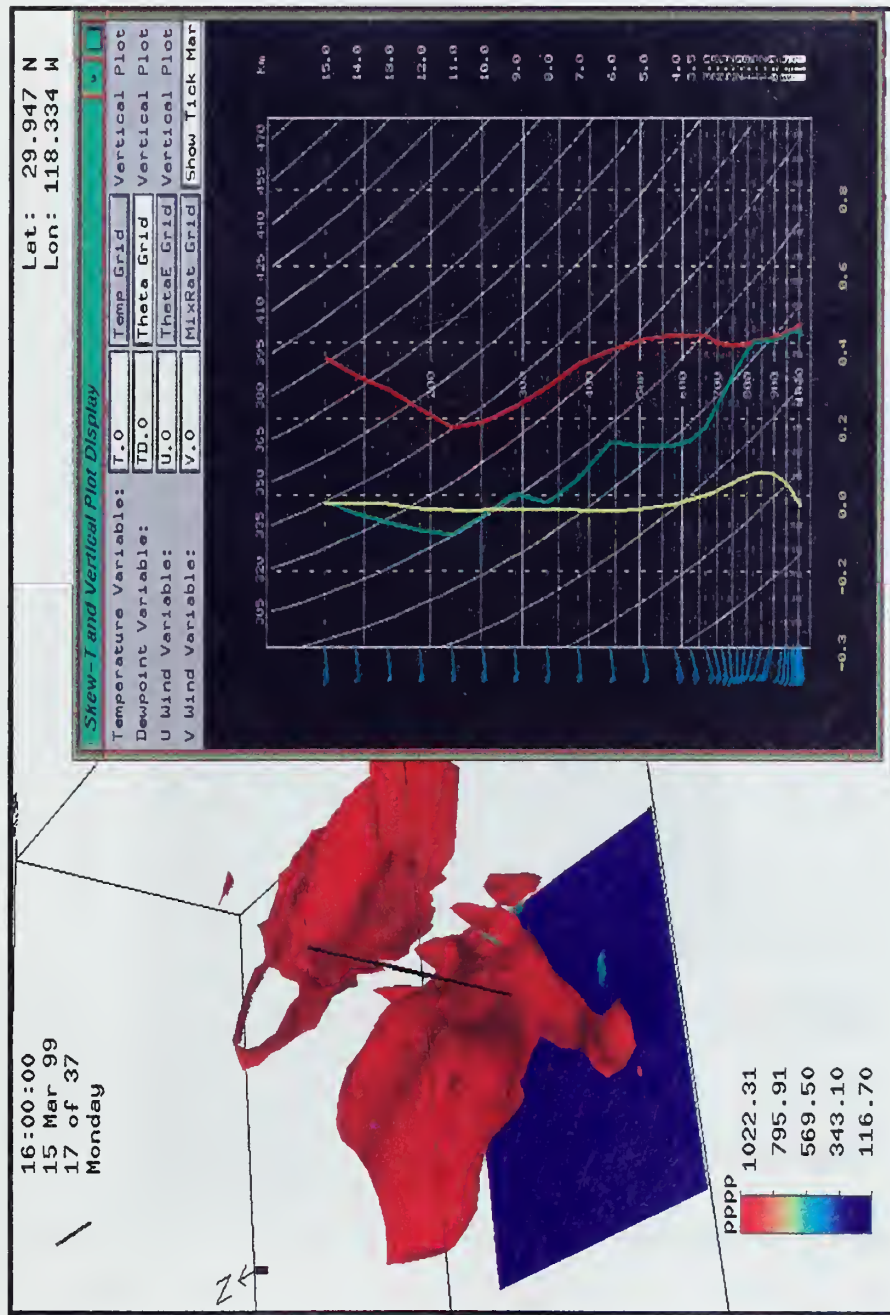


Figure 4-11. Vertical Motion Analysis. A zoomed-in view of the vertical velocity associated with a front passing through the SOCAL bight. Vis5D's sounding feature captures the "forecast sounding" alongside the vertical velocity (yellow) in the Skew-T graphic.



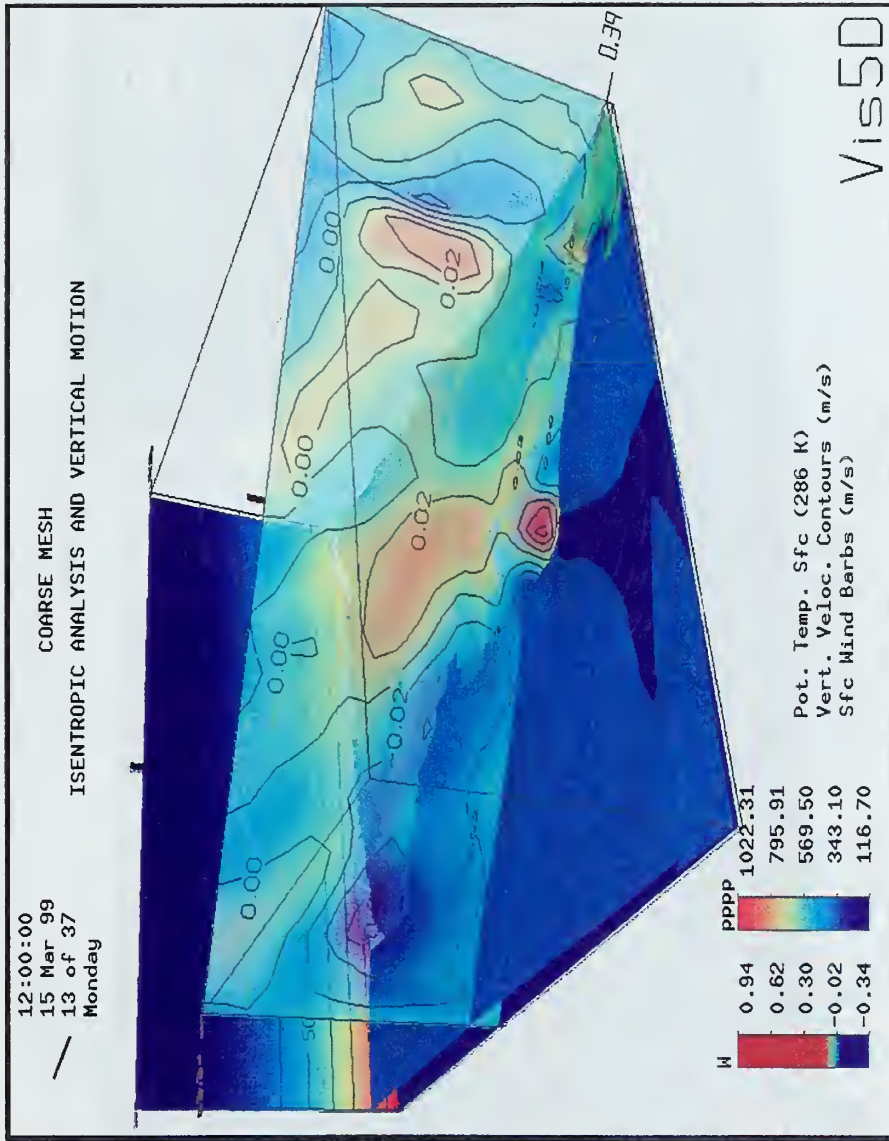


Figure 4-12. Isentropic Analysis. A  $286^{\circ}$  K potential temperature isosurface and a vertical slice of vertical velocity. Note how the ascent region (yellow to red) arches back over the frontal surface as inferred from the orientation of the potential temperature surface and has a maximum value of +8 cm/s in the vicinity of the upper-level front. Also note the upward motion associated with the mountainous terrain in the upper levels out ahead of the front as well as the broad descent (blue) region of -6 cm/s in the cold air behind the front.



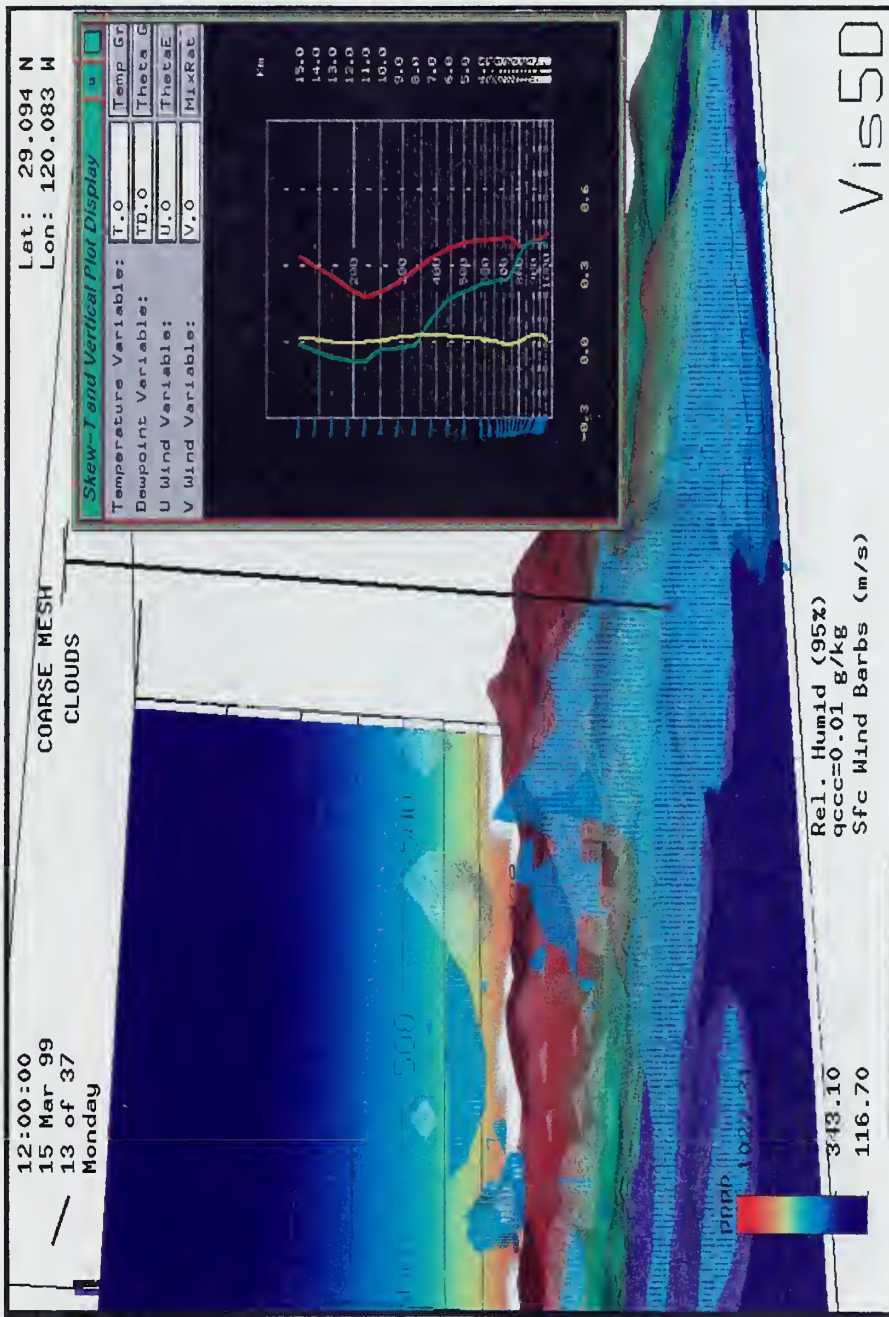


Figure 4-13. Cloud Comparison and Analysis. An example of a comparison of the two types of cloud renditions. Forecasters will be comforted to see general agreement between the two and thus increase their confidence in cloud depictions as defined by cloud droplet and ice crystal mixing ratios.



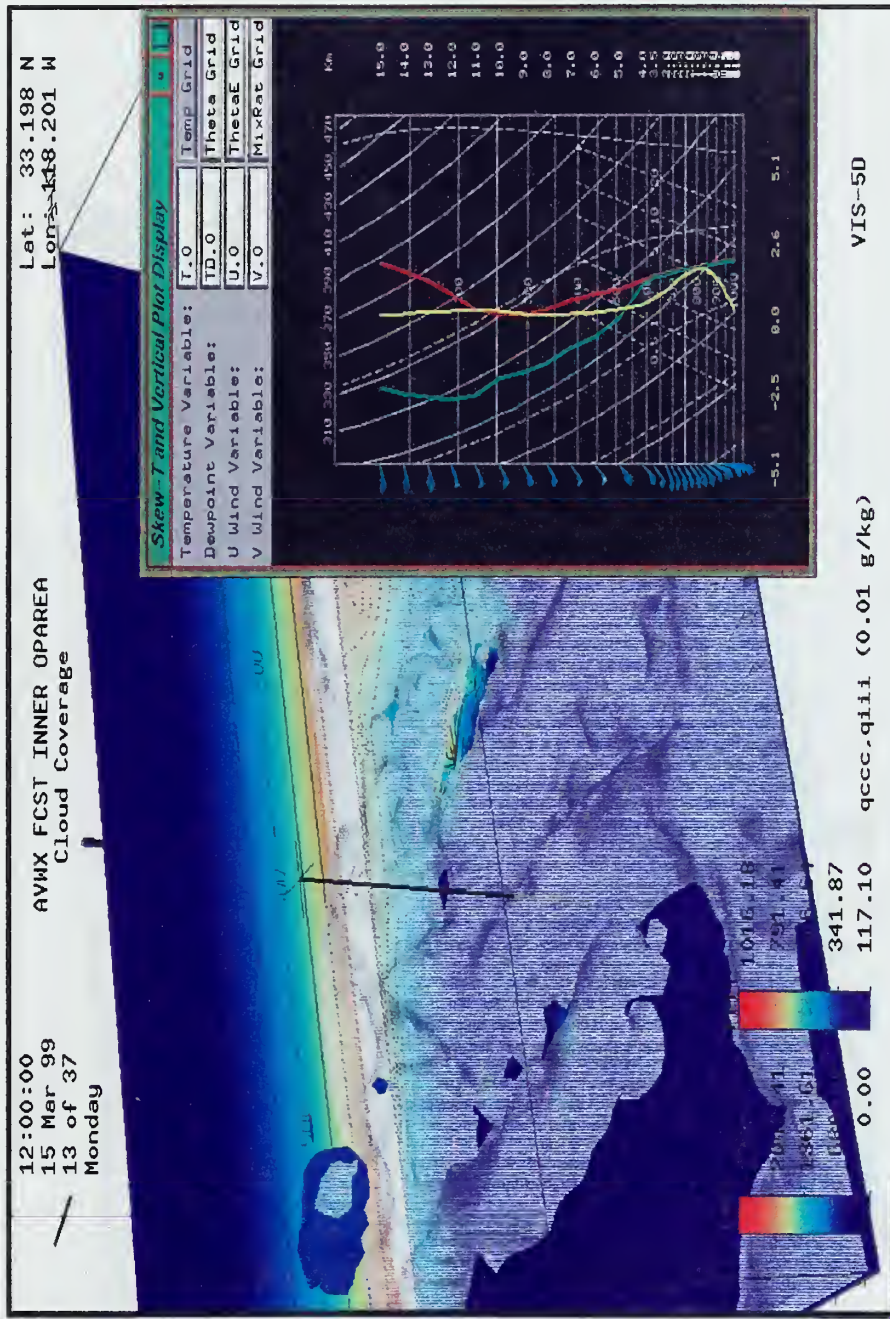


Figure 4-14. Aviation Forecasting. Detailed mesoscale structure in the fine mesh cloud fields associated with a front passing through the SOCAL bight.



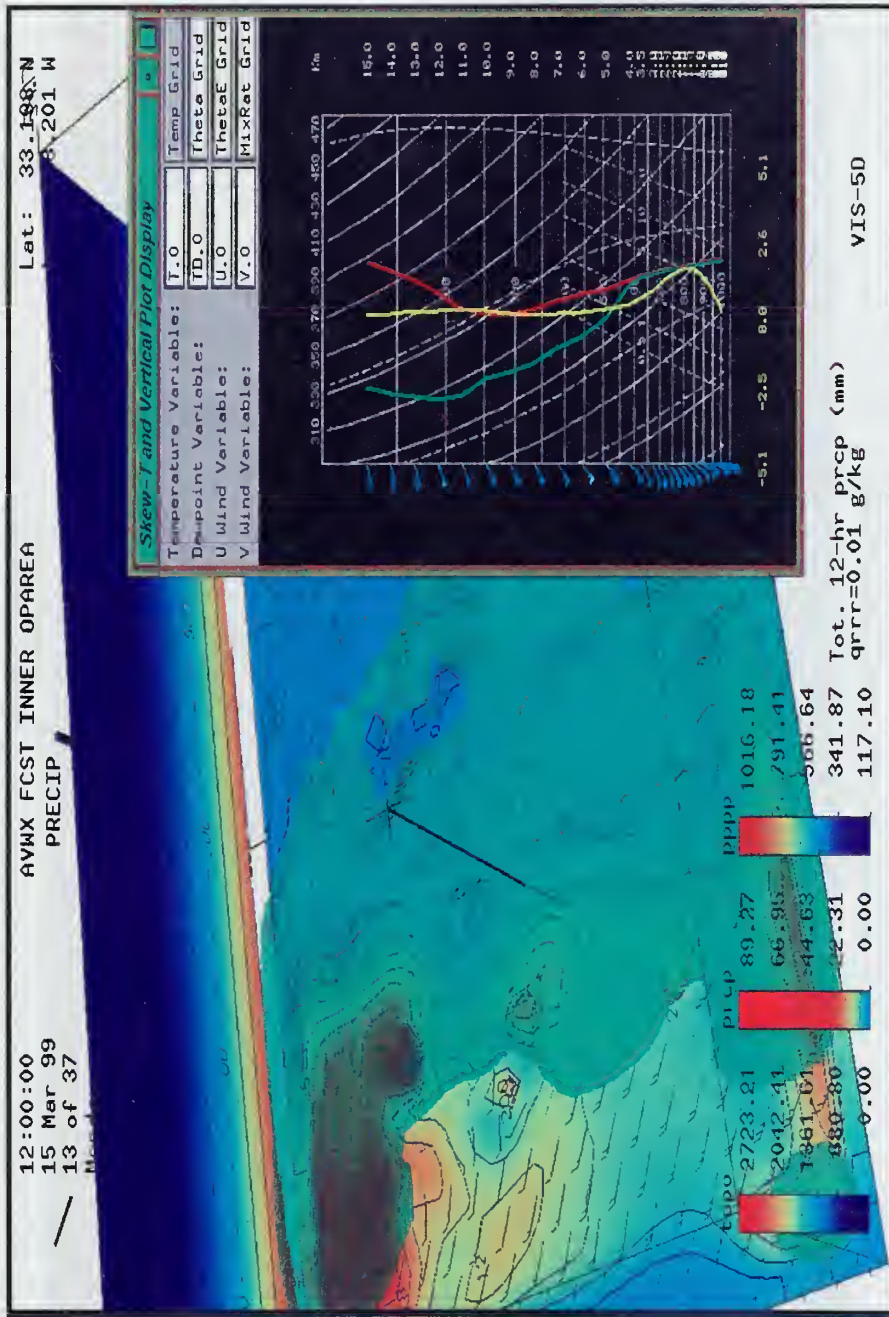


Figure 4-15. Aviation Forecasting. Rain droplet mixing ratio (large transparent green cloud) over the 12-hr total accumulated precipitation fields. The heaviest 12-hr accumulation regions (orange to red areas) are most likely associated with orographic lifting of the pre-frontal flow.



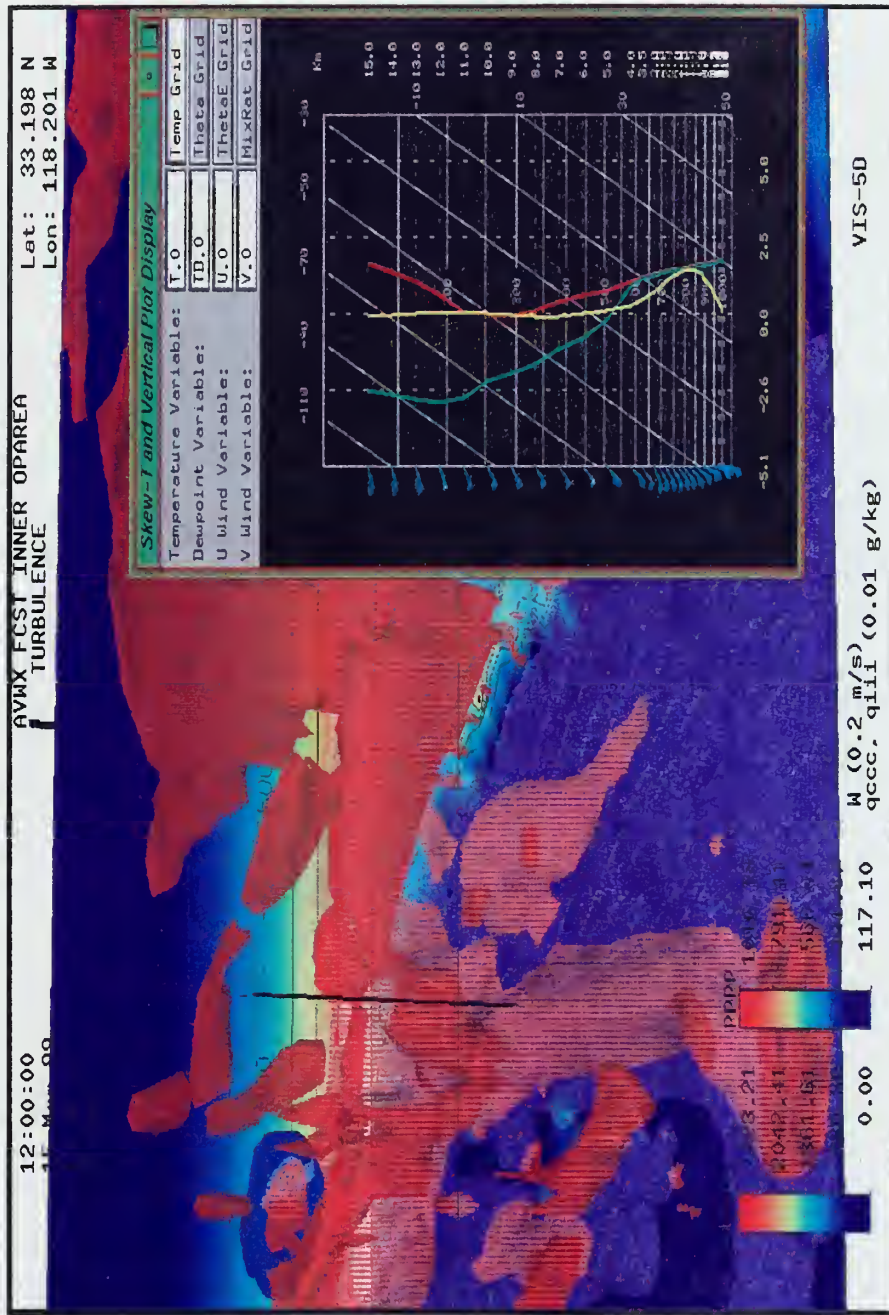


Figure 4-16. Forecast guidance for turbulence in a Vis5D graphic. Turbulence is indicated anywhere within a vertical velocity isosurface. Turbulence intensity can be inferred by varying the vertical velocity threshold. In-cloud versus clear-air turbulence (CAT) can be distinguished by whether or not the vertical motion is occurring within a cloud field isosurface. Turbulent kinetic energy (tke) was not studied in this thesis but could also provide turbulence forecast guidance.



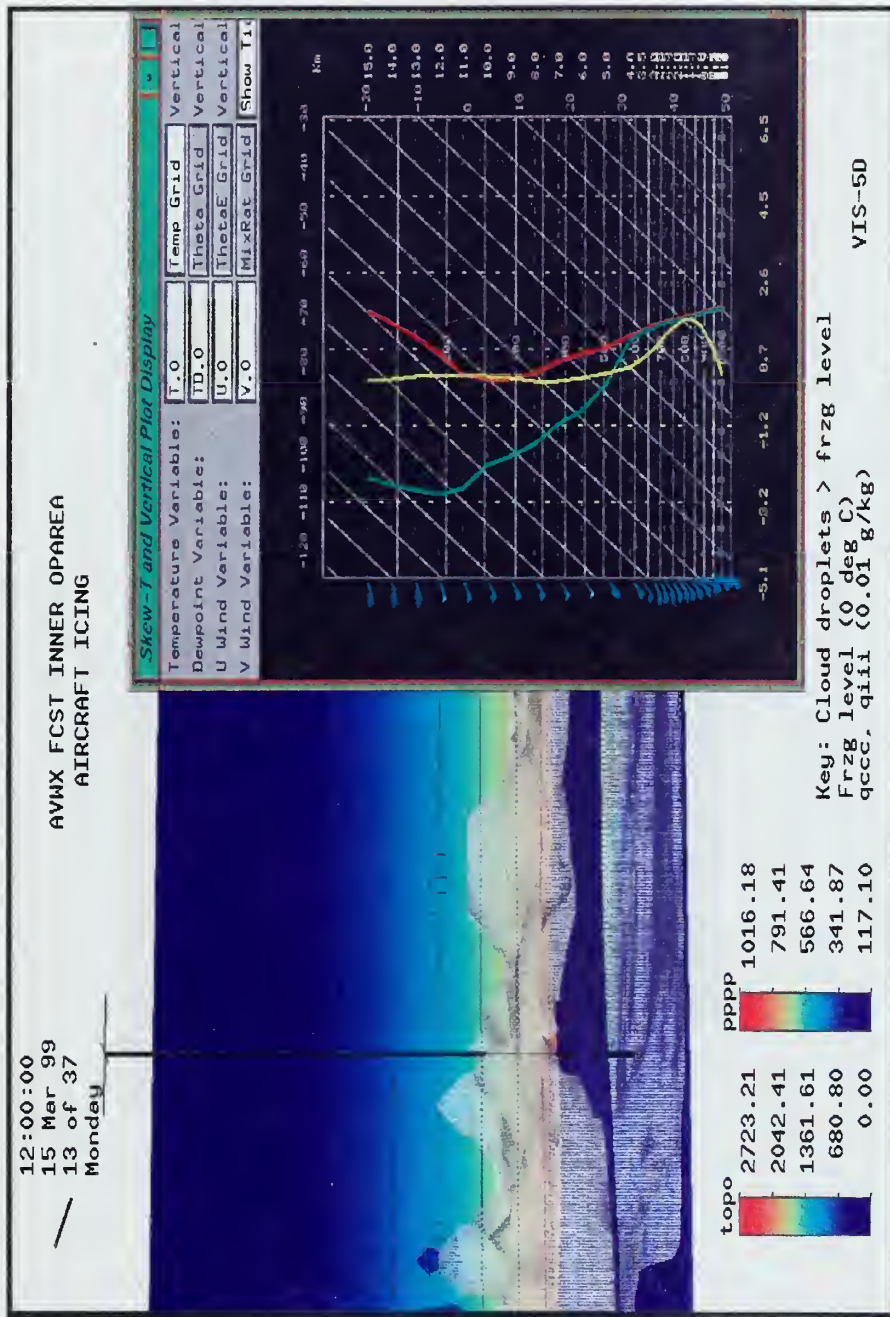


Figure 4-17. Forecast guidance for icing in a Vis5D graphic. Icing is inferred wherever cloud droplets (akin to cloud liquid water and indicated by the cloud droplet mixing ratio isosurface) are located within sub-freezing air (demarcated and indicated by the 0° C air temperature isosurface).



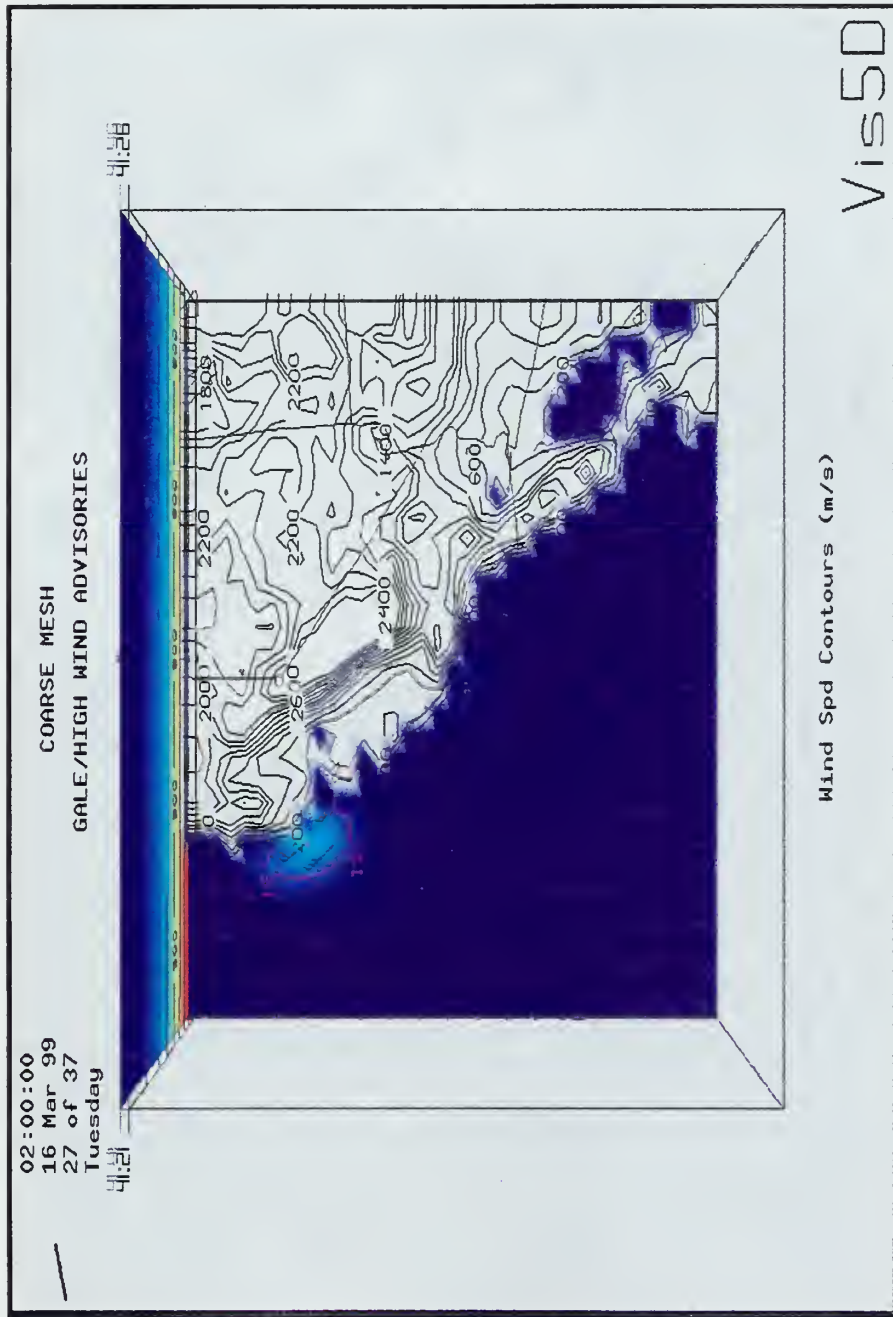


Figure 4-18. Low-level winds/warnings. Wind barbs and horizontal color and contour slices highlighting areas of near-gale force winds ( $15 \text{ m/s} = \sim 30 \text{ kts}$ ) in the vicinity of Point Conception.



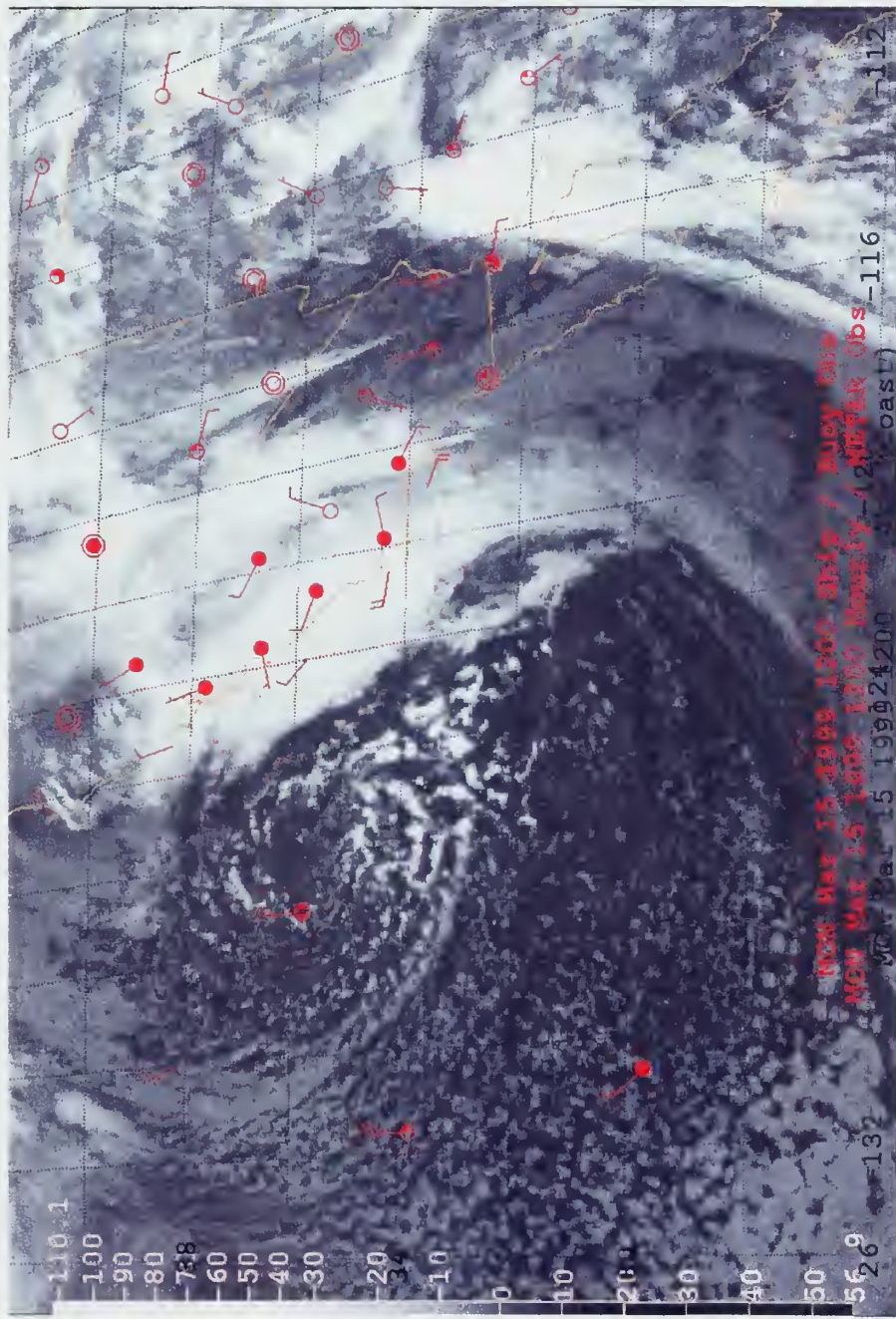


Figure 5-1. Extratropical cyclone and frontal system passing through the SOCAL bight at 1200 UTC on 15 March 1999. Los Angeles, Santa Barbara, and marine observations reveal the location of the front in the northern bight, while the imagery and a lone ship report 27N 125W hint at its seaward location.



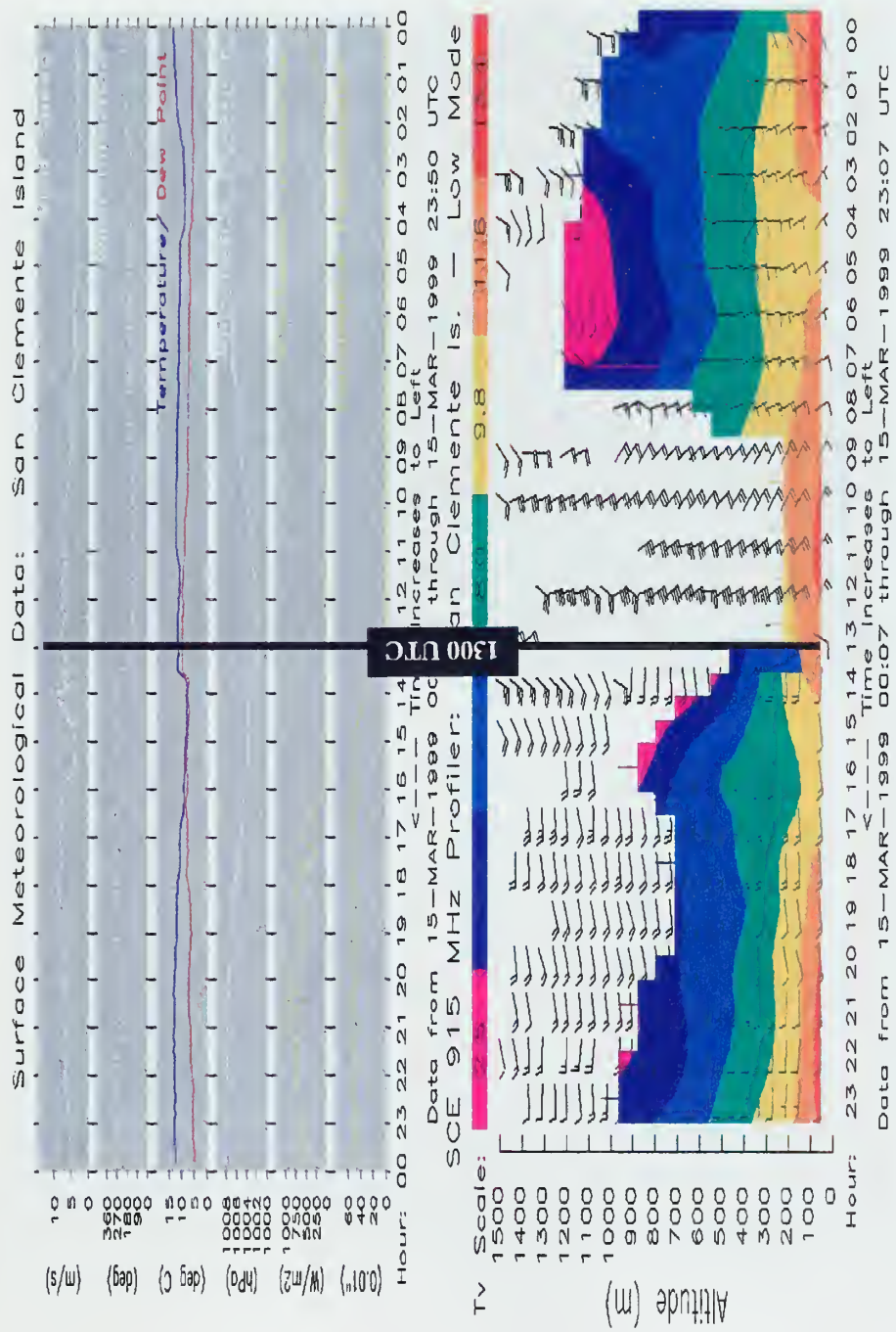


Figure 5-2. Surface instruments (left) and at WP/RASS data at San Clemente show frontal passage ~1330 UTC as indicated by the rapid wind shift, sharp drop in temperature, minimum pressure, and the onset of precipitation (left) and corresponding wind shift and drop in low-level temperature (right). Note also the strong low-level pre-frontal winds in the WP data.



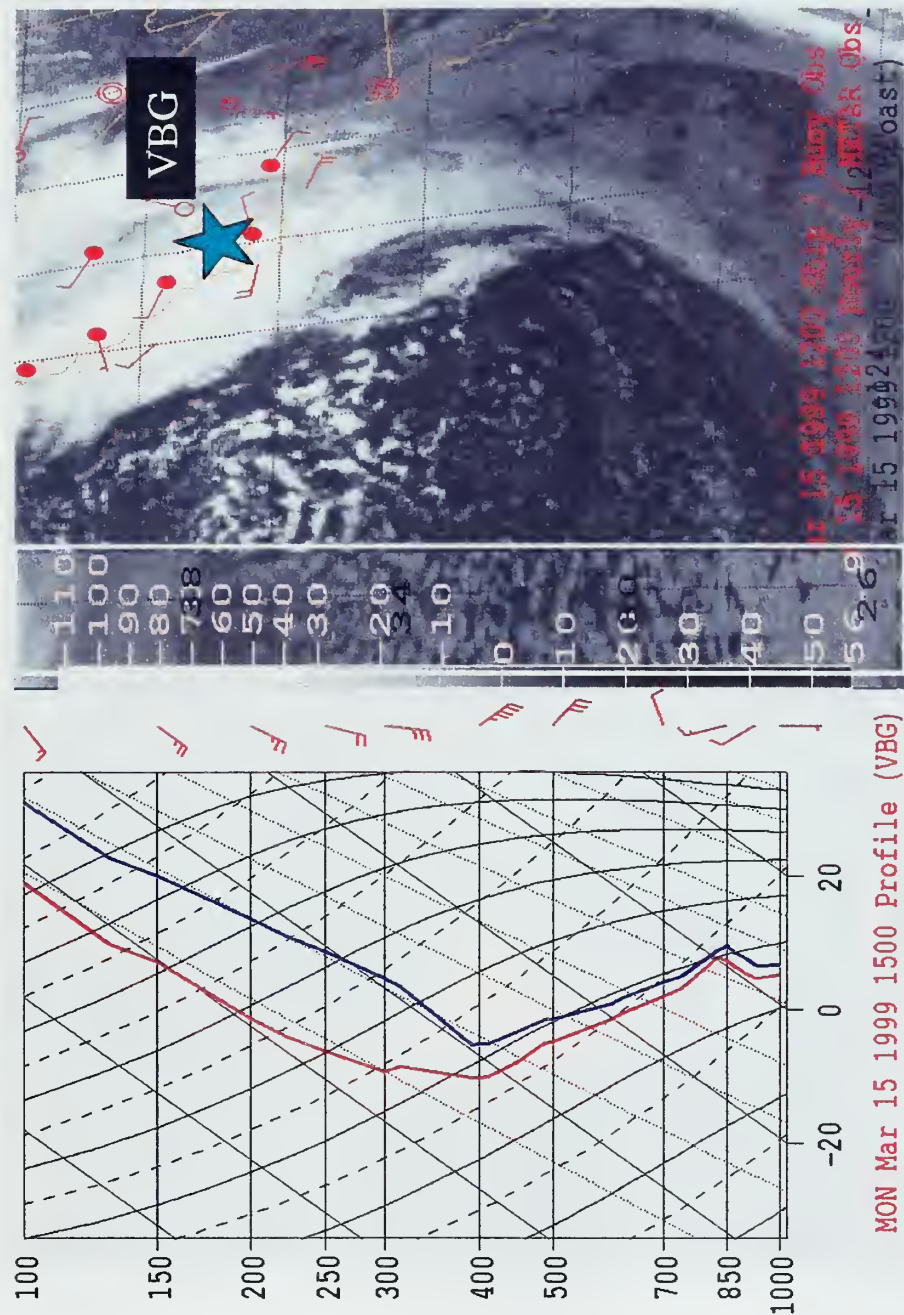


Figure 5-3. The post-frontal Vandenberg AFB (VBF) upper-air sounding (left). The sounding and IR imagery shows cloud top temperatures of  $-40$  to  $-50$   $^{\circ}\text{C}$  with corresponding tops in the 300 mb range.



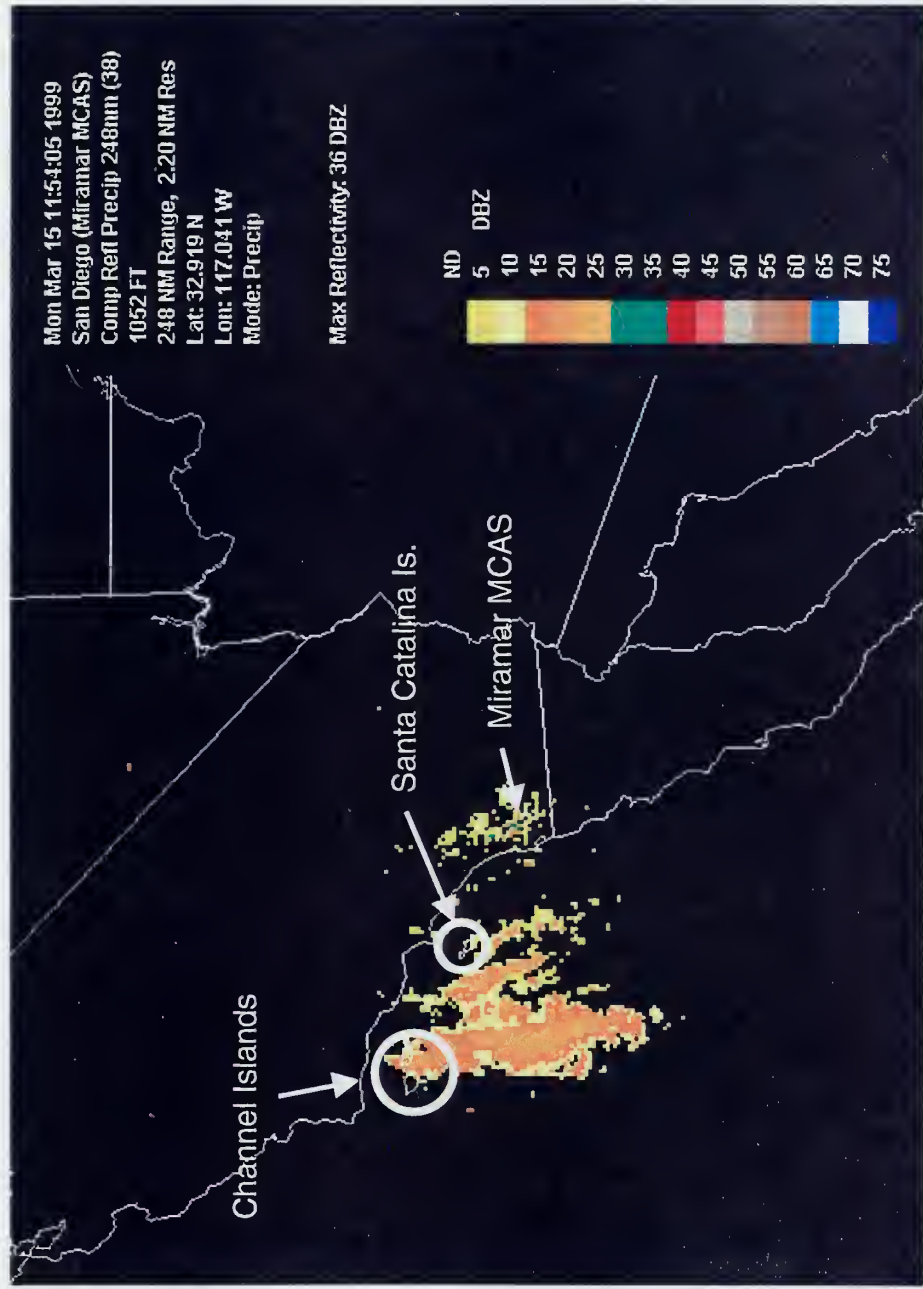


Figure 5-4. Composite reflectivity data valid at 1200 UTC from the San Diego (Miramar MCAS) WSR-88D radar site showing pre-frontal returns of 15-20 dB increasing to 20-25 dB (later 40-50 db was observed within the deep convection).



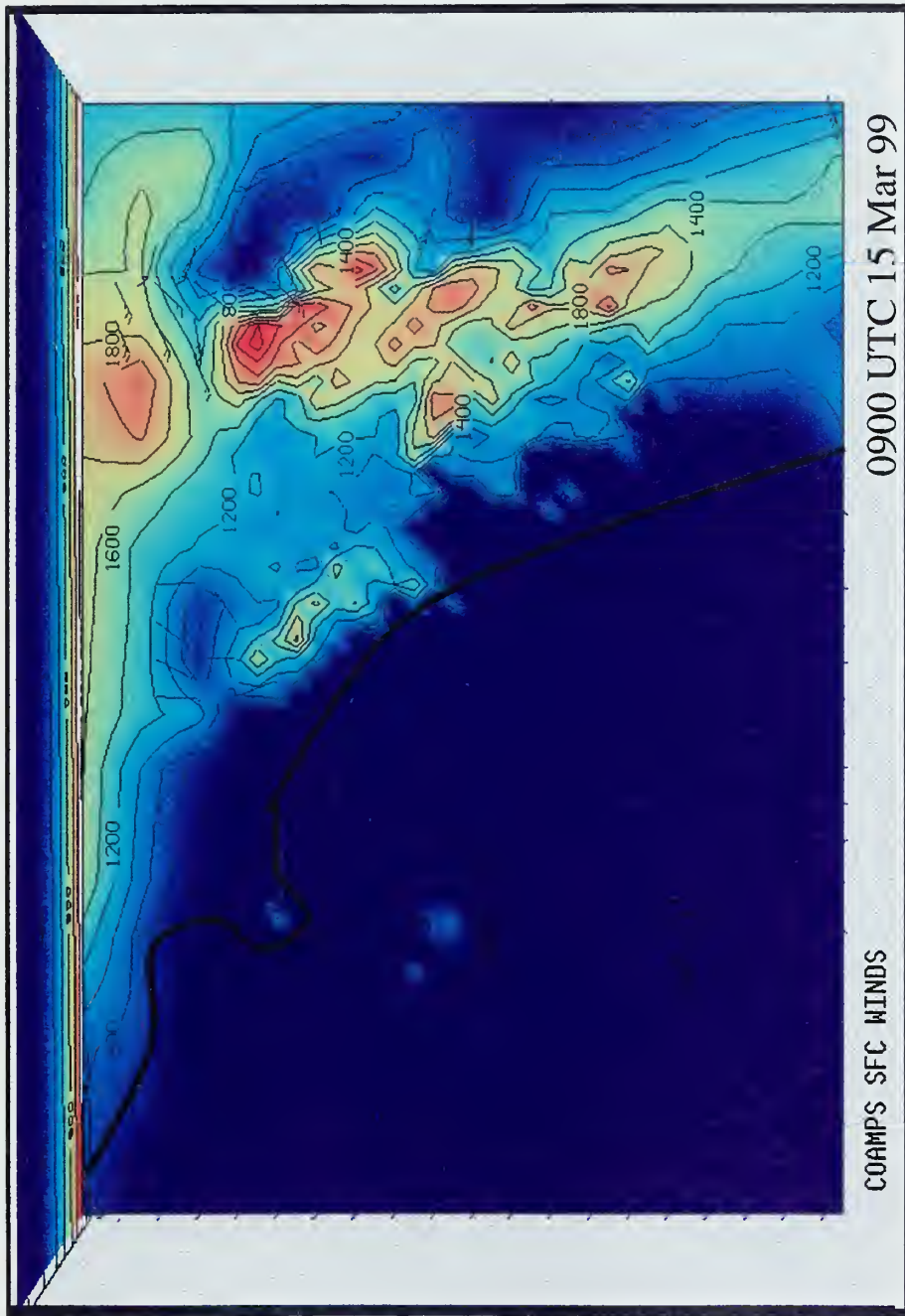


Figure 5-5. Winds. COAMPS is too fast on the front's location showing FROPA over San Clemente and Santa Catalina Islands at 0900 UTC on the 15<sup>th</sup>, ~4 1/2-h earlier than recorded by the observations.



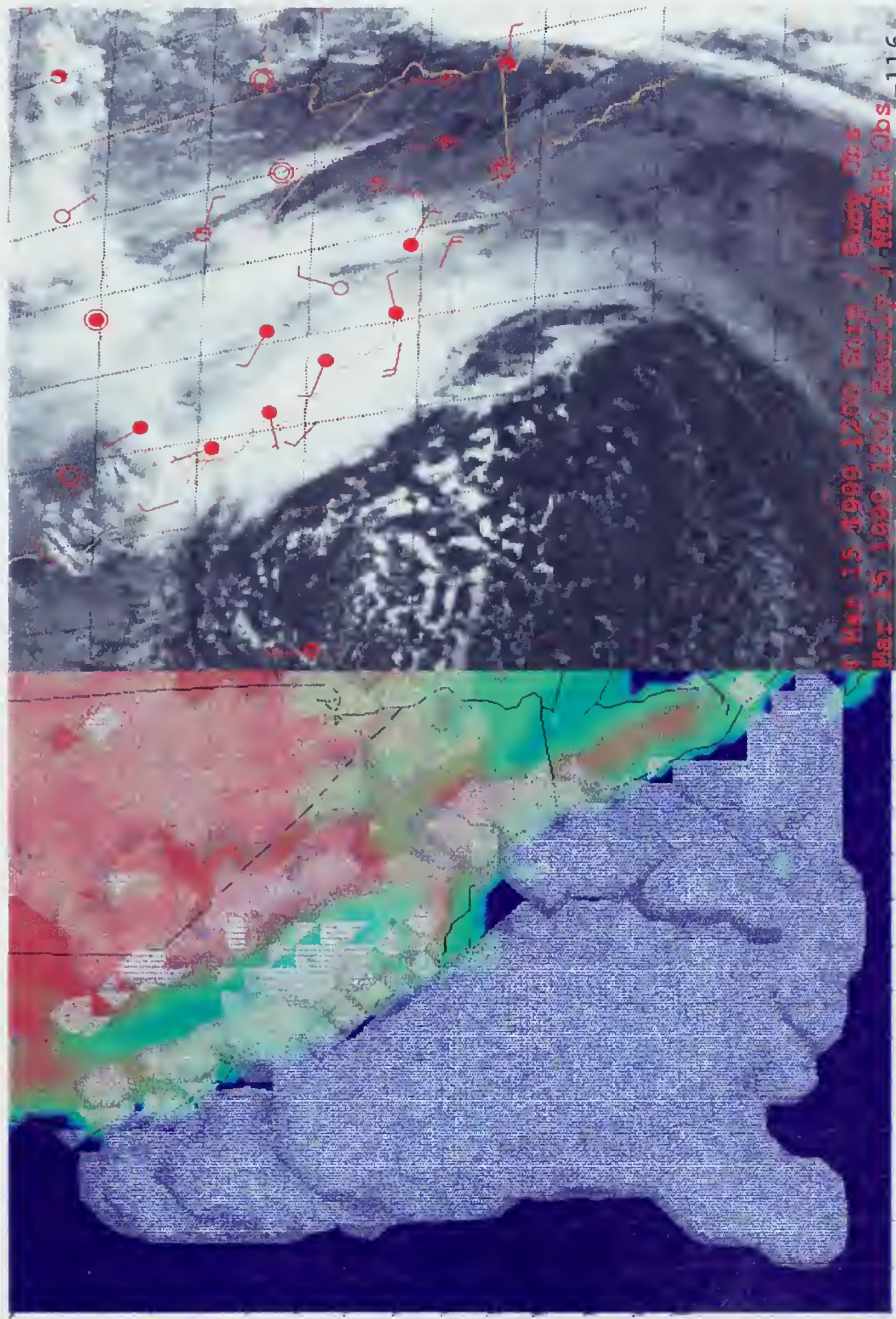


Figure 5-6. Apart from being out of phase, a *smoothing tendency* is suggested in both the pre- and post-frontal clouds (open and closed-cell cumulus and stratocumulus versus COAMPS single low-level stratus cloud). The grid resolution is too coarse (even at 5-km) to resolve the open cell nature of the actual clouds. In essence, low "stratus-like" layers in COAMPS will most likely verify as open and/or closed cell cumulus or stratocumulus. Also, COAMPS does not forecast the upper-level cirrus streak evident in the satellite imagery.



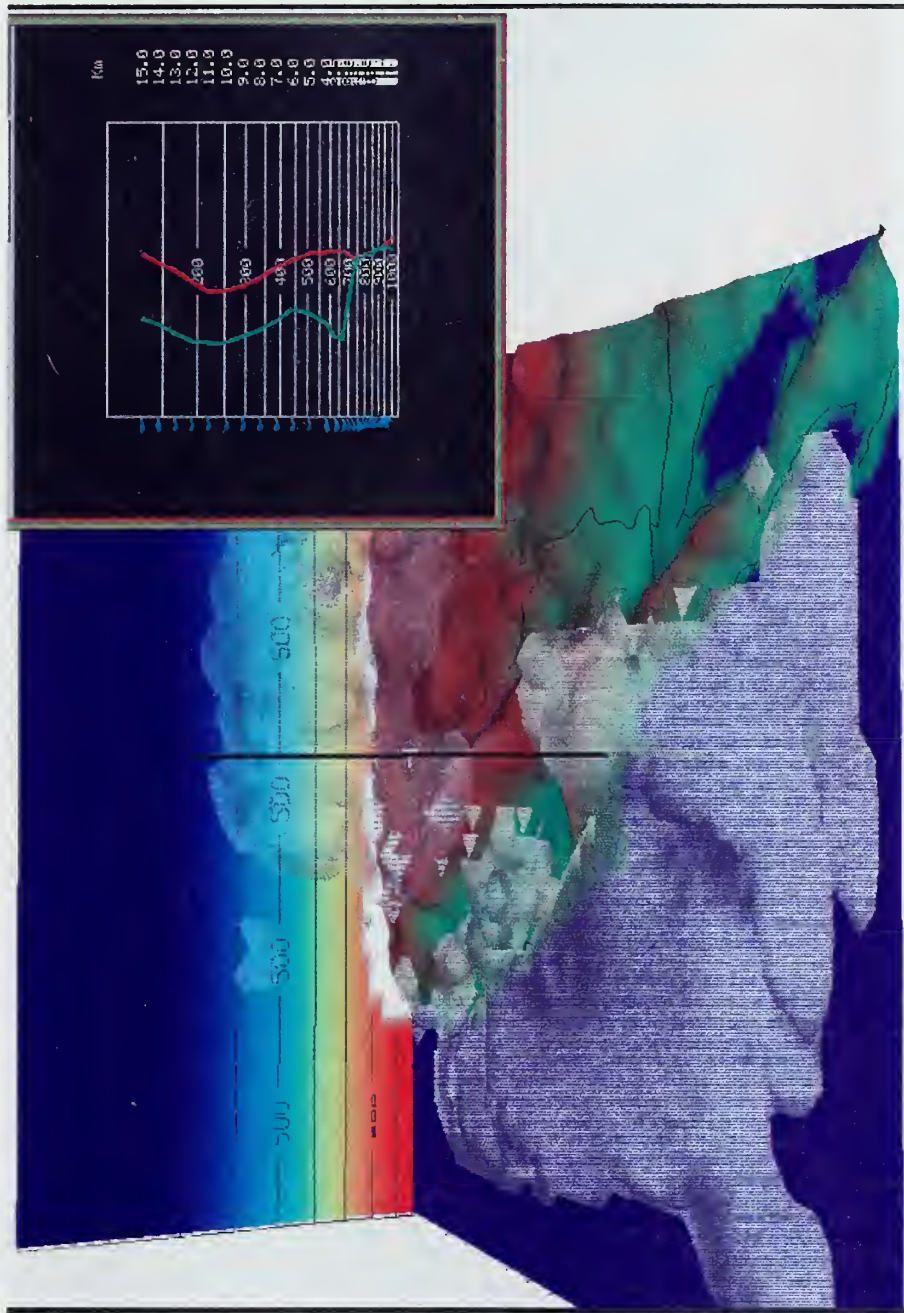


Figure 5-7. COAMPS slightly under-predicts the extent of the vertical development of the frontal clouds (400 mb vs. ~300 mb). The largest error appears to be in the under-development of the convective clouds stretching along the coast from Point Conception to the north of San Francisco Bay (Also see Figure 5-6), which may also impact (i.e., under-forecast) precipitation, turbulence, and icing forecasts.



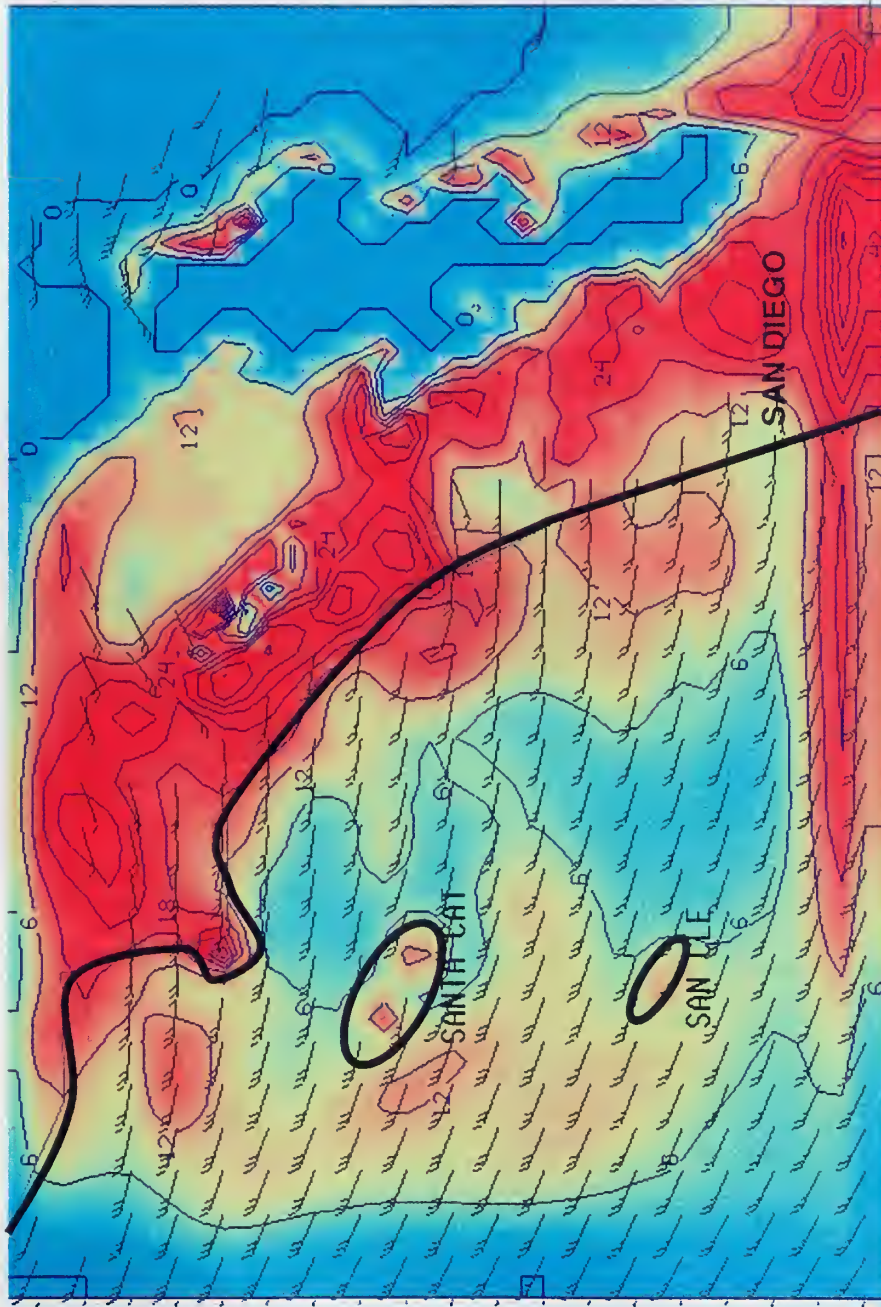


Figure 5-8. COAMPS total precipitation for the event (i.e., the 12-h precipitation totals at the end of the model run). The “smoother than reality” topography may not block the flow sufficiently and allows more onshore flow and hence precipitation than indicated (see the alongshore winds in Figure 5-1). Also, note the problem with the boundary values.



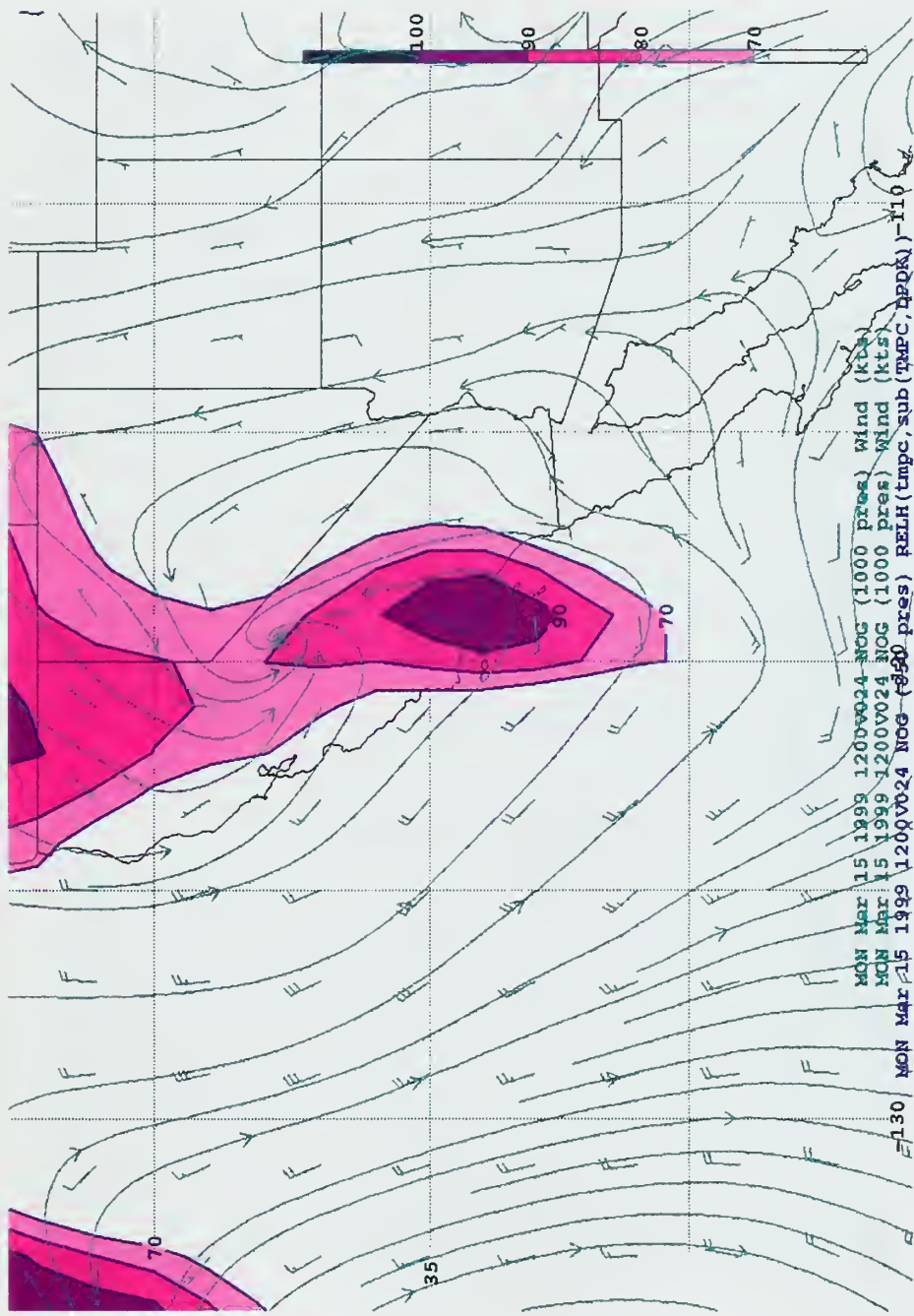


Figure 5-9. The 24-hour NOGAPS forecast valid at 1200 UTC on 15 March verified accurately compared to the observations and satellite imagery. The cloud rendering in NOGAPS (chosen as a relative humidity threshold of 70%) shows skill in the pattern and extent of the well-developed multi-layer clouds associated with the front, however there is little to no indication of the low-level stratus.



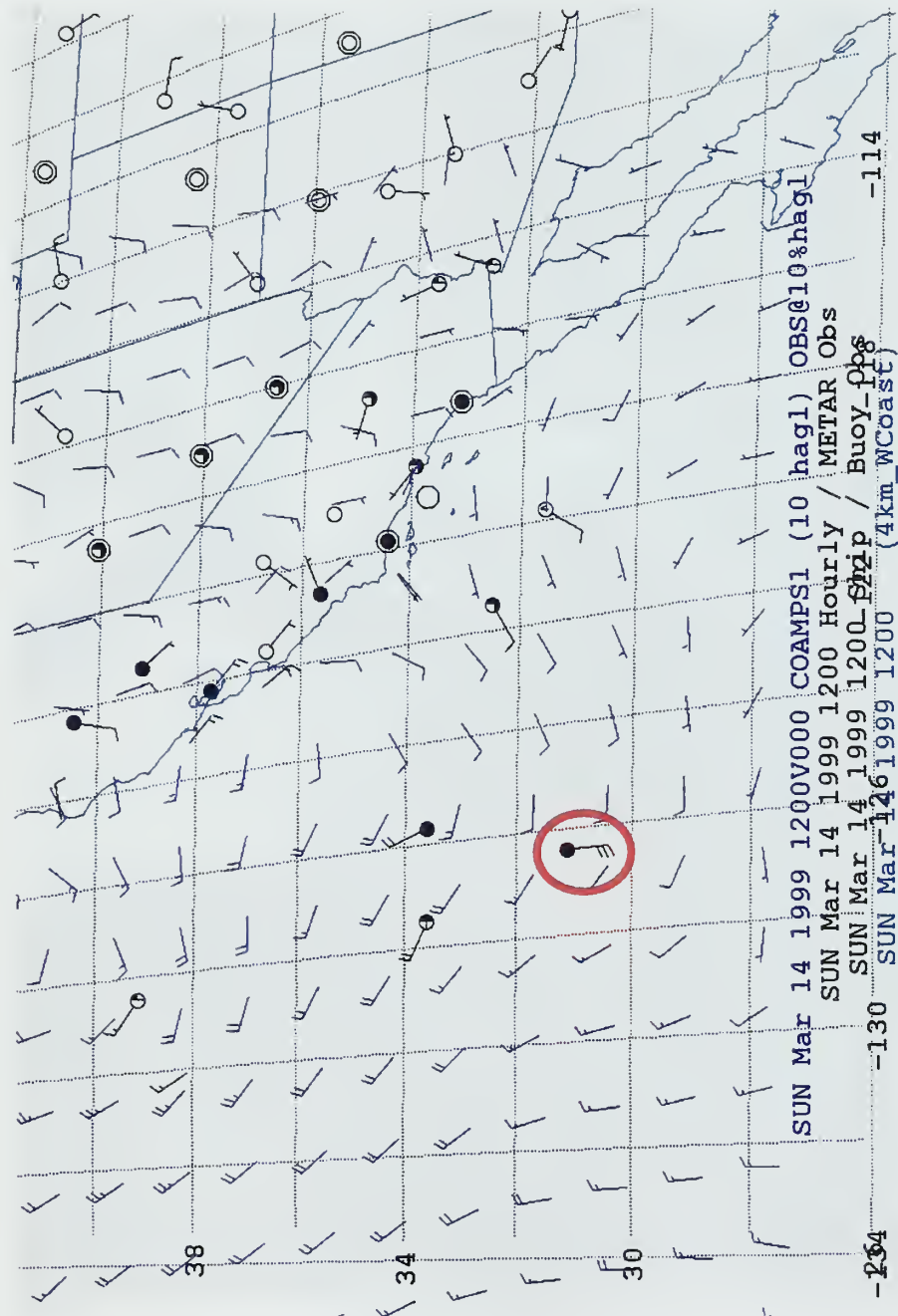


Figure 5-10. The COAMPS analysis for the 24-h forecast with analysis observations.



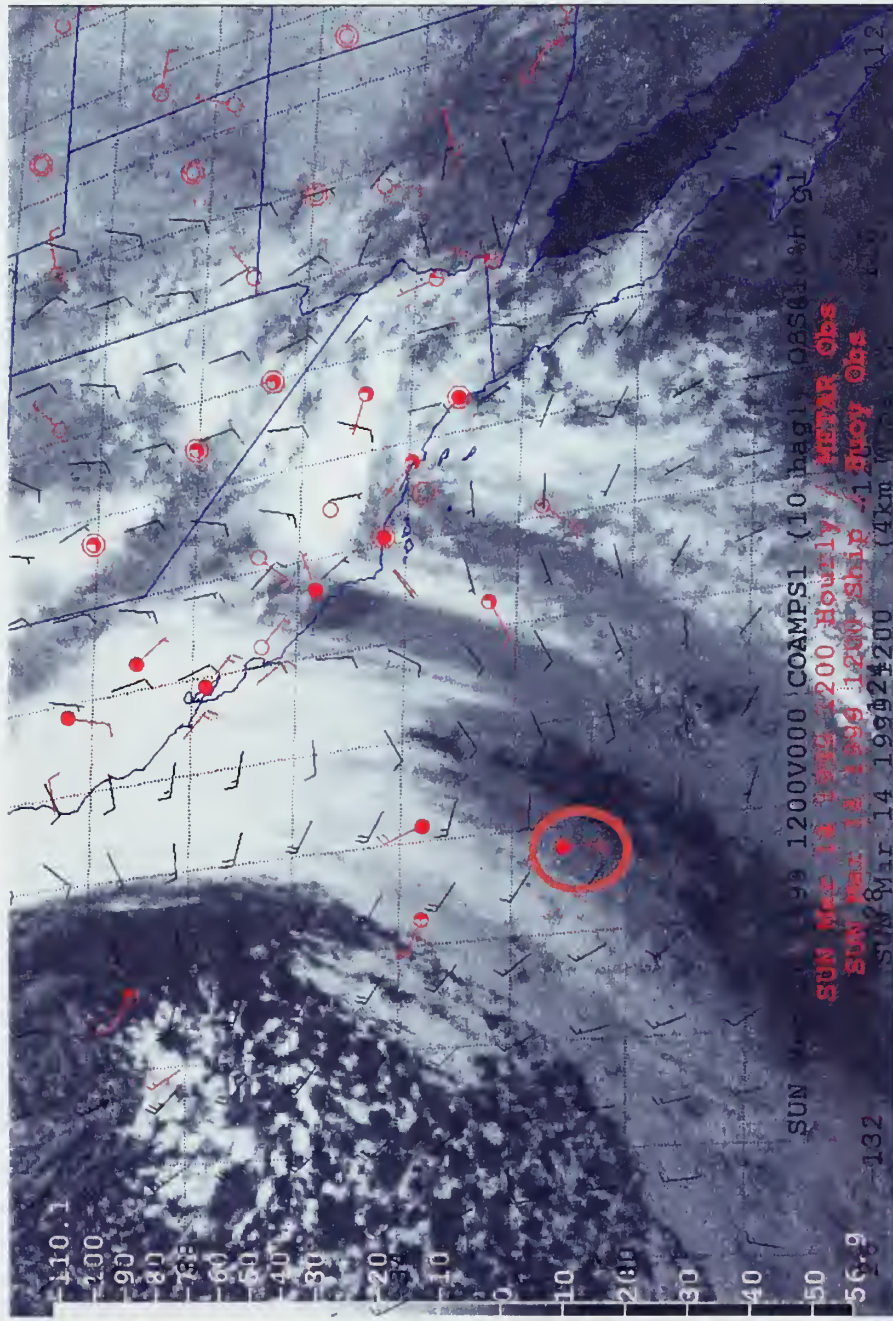


Figure 5-11. The COAMPS mis-analysis for the 24-hr forecast with analysis observations and satellite imagery. Note that the 30-kt southerly wind observation seems to be in error until fused with IR imagery. In fact, this observation is critical for correctly locating the position of the surface front and stresses the importance of verifying the analysis against all available data at analysis time as in the method described in chapter 3.



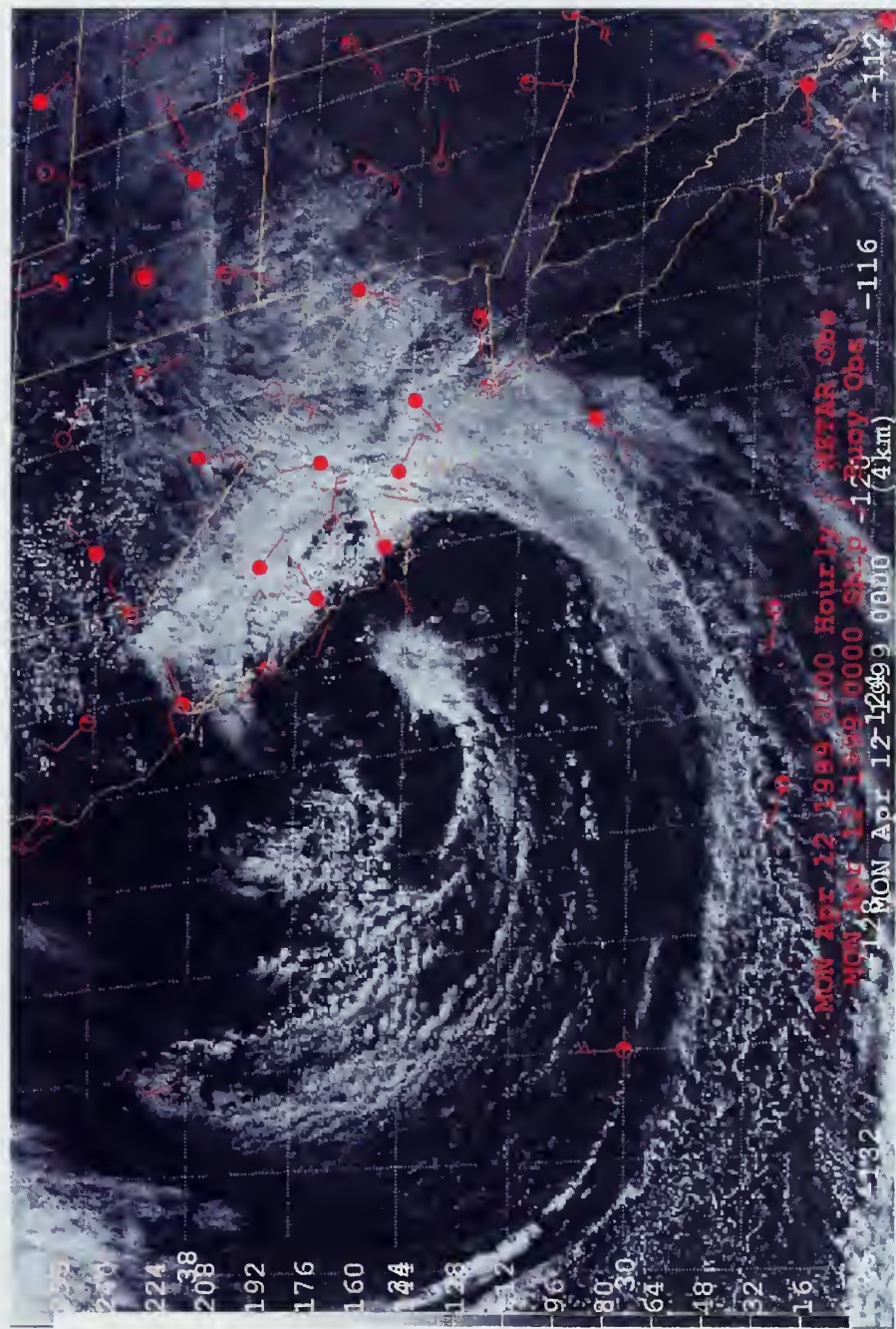


Figure 5-12. A well-defined frontal system passing through the SOCAL bight at 0000 UTC on 12 April 1999 with a pronounced trough located just off of Point Conception and trailing behind the actual front. The frontal signature is complex and certainly the cloud pattern at 130 W supports the possibility of a dual frontal passage.



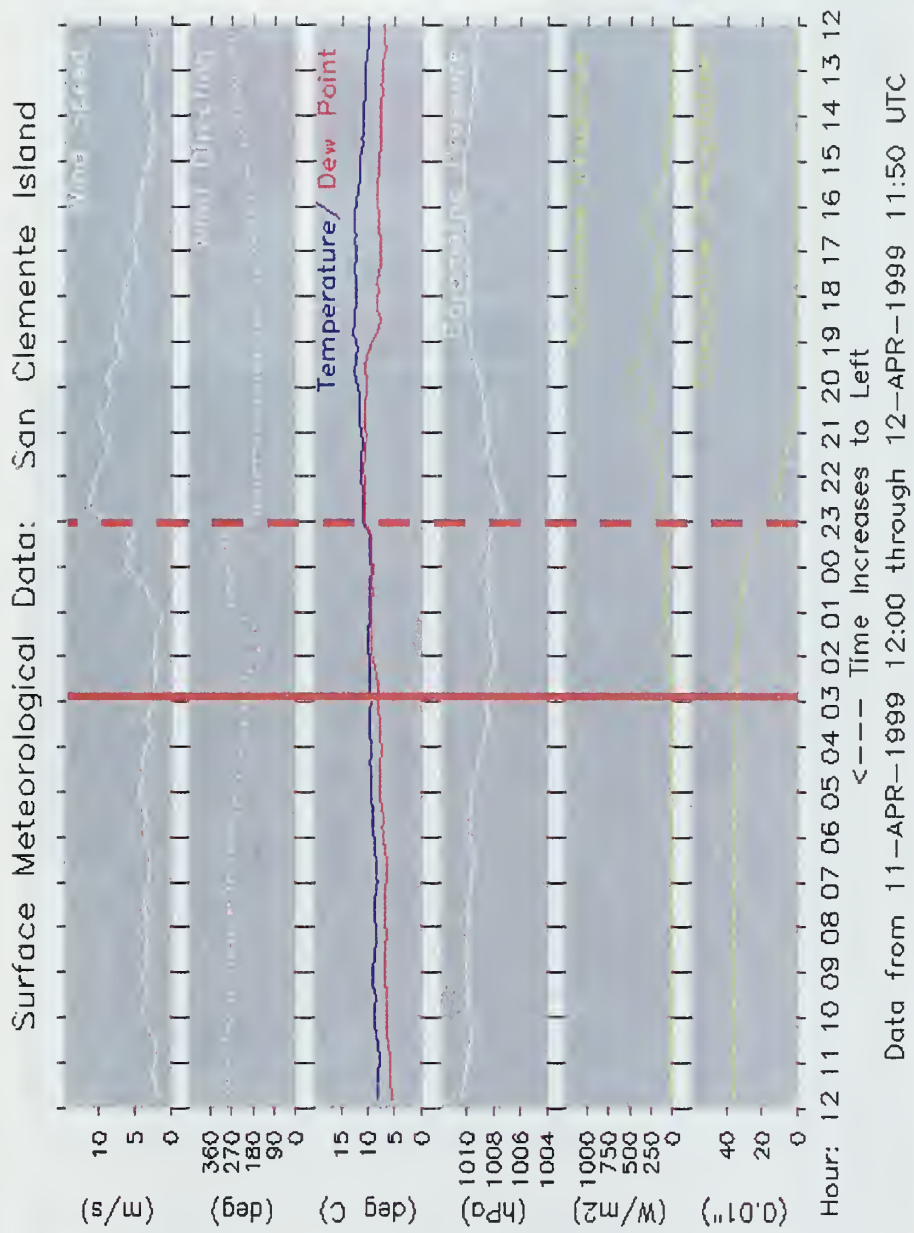


Figure 5-13. Surface data from the San Clemente wind profiler site shows ambiguity in the actual time of frontal passage at that station and even suggests the possibility of two frontal passages between 2300 and 0300 UTC (Figure 5-13).



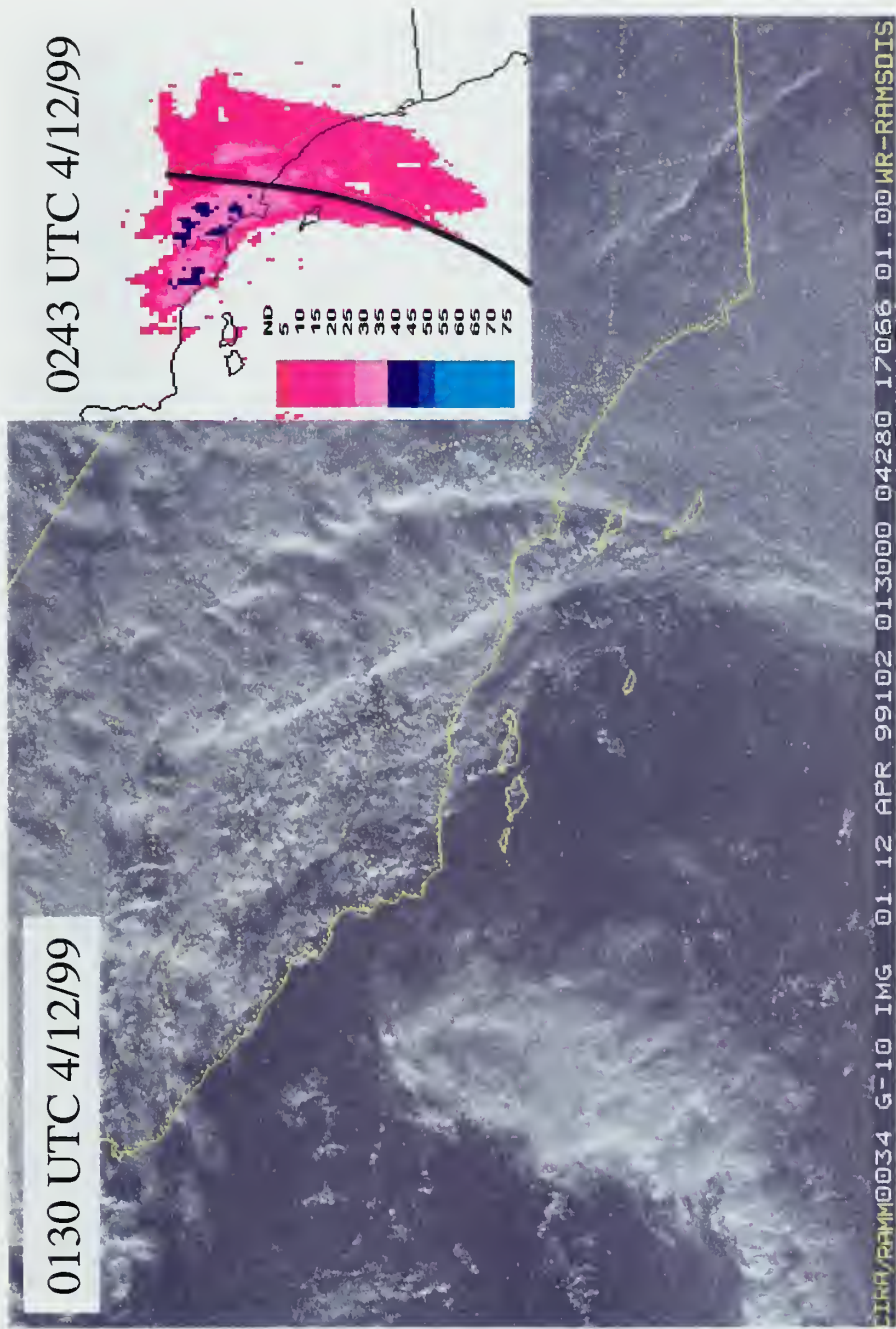


Figure 5-14. Visible satellite imagery valid at 0130 UTC and Doppler radar data valid at 0243 UTC suggest a complex frontal structure and a considerable amount of pre-frontal clouds and precipitation associated with this front (note that only Santa Catalina Island appears in the radar graphic).



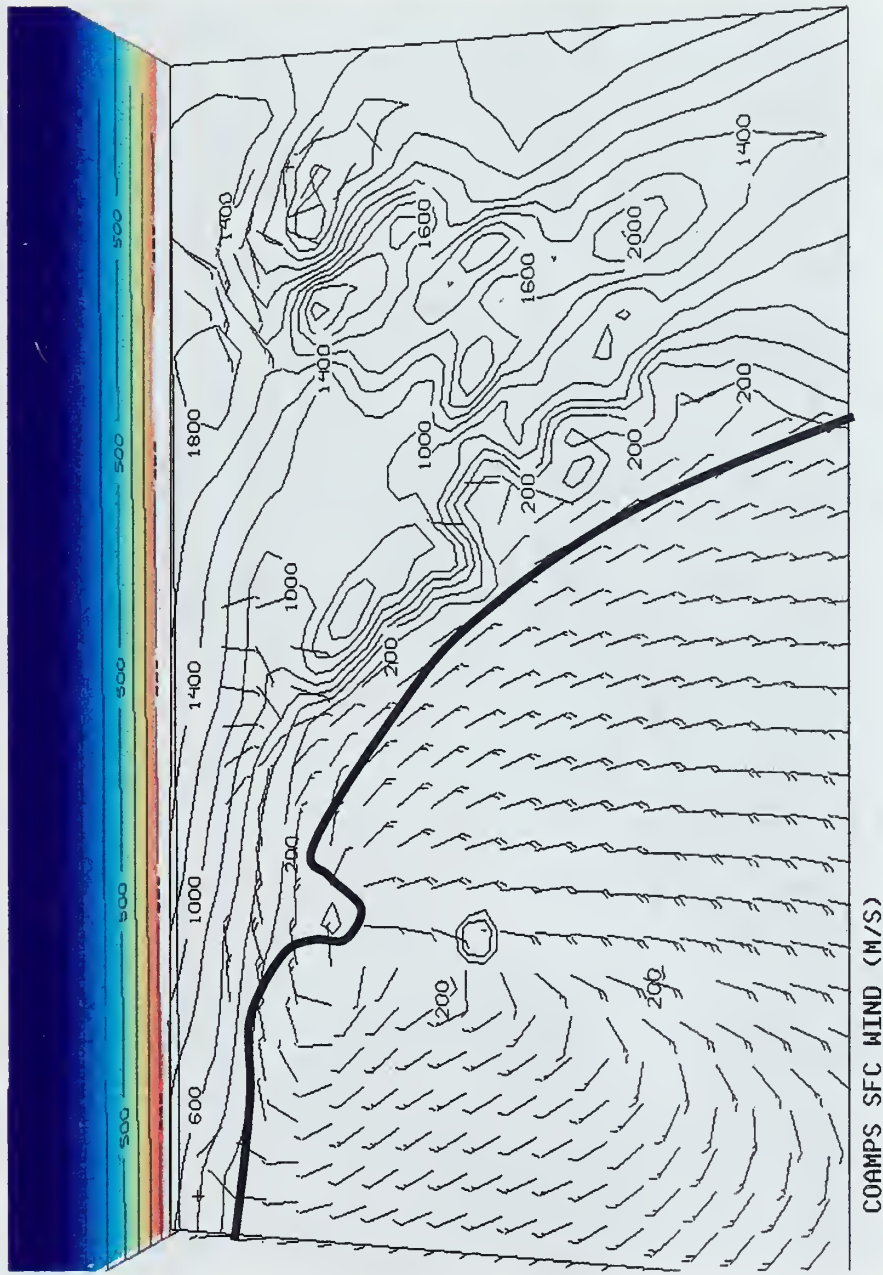


Figure 5-15. A clearly defined front passing through San Clemente and Santa Catalina Islands at 0400 UTC, or within 1-h of the actual frontal passage as determined above. COAMPS has over-forecast by approximately 5 and 10 kts respectively the pre- and post-frontal winds, but verifies well on the winds during the passage of the front.



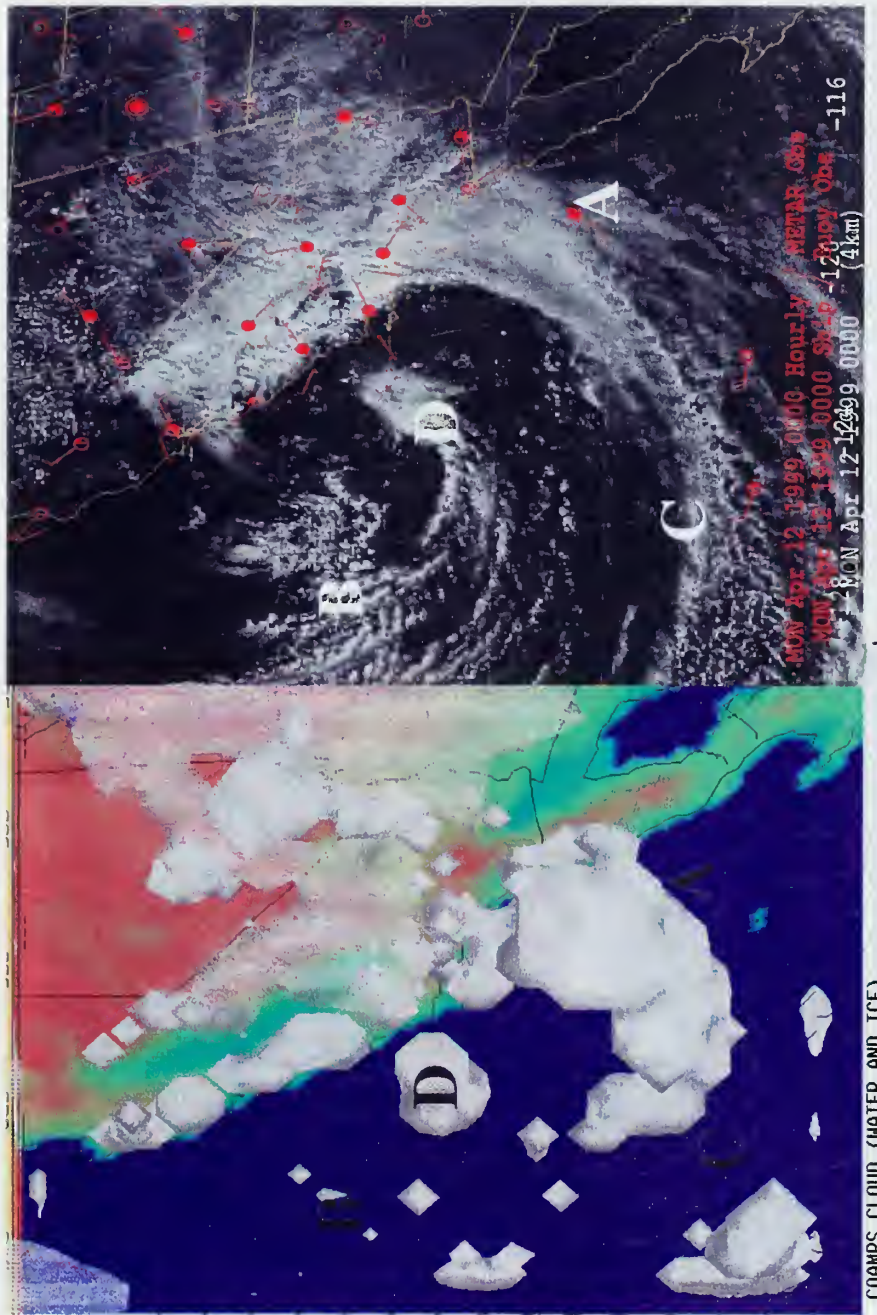


Figure 5-16. Clouds: COAMPS versus actual. COAMPS under-forecasts low-level clouds over the Central Valley, pre-frontal convergence bands ("A"), the filling in of low-level clouds further behind the short-wave trough ("B"), and depicts an erroneous gap ("C") in the front seaward. COAMPS accurately forecasts the immediate post-frontal clearing and even indicates vertically developed clouds up to 600 mb ( $\sim 4$  km) in the general vicinity of the short-wave trough ("D") that trails behind the front.



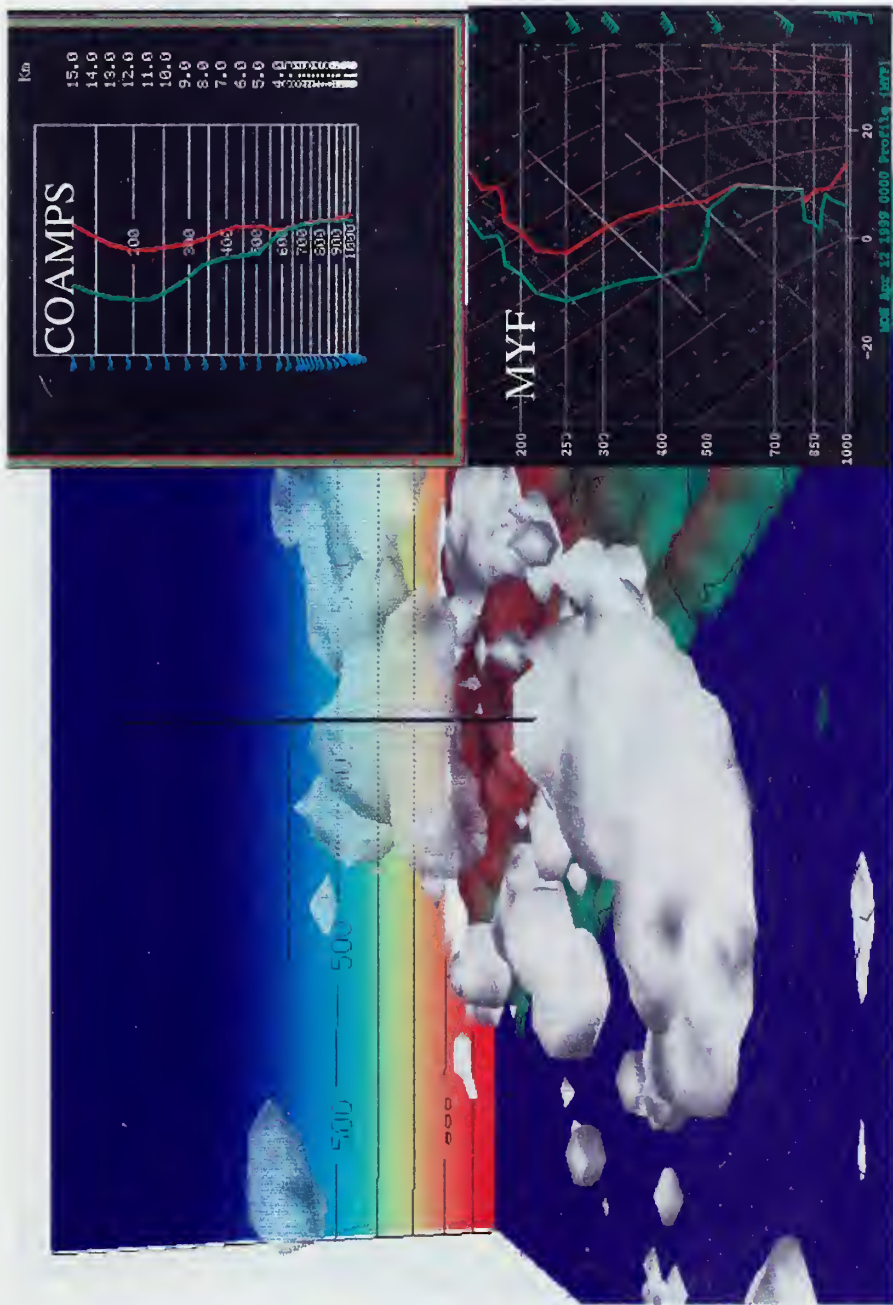


Figure 5-17. COAMPS cloud fields and forecast sounding (VT 0400 UTC) compared to the actual Montgomery Field (MYF) sounding. COAMPS verifies fairly well on the vertical extent of the pre-frontal cloud shield (~600 mb).



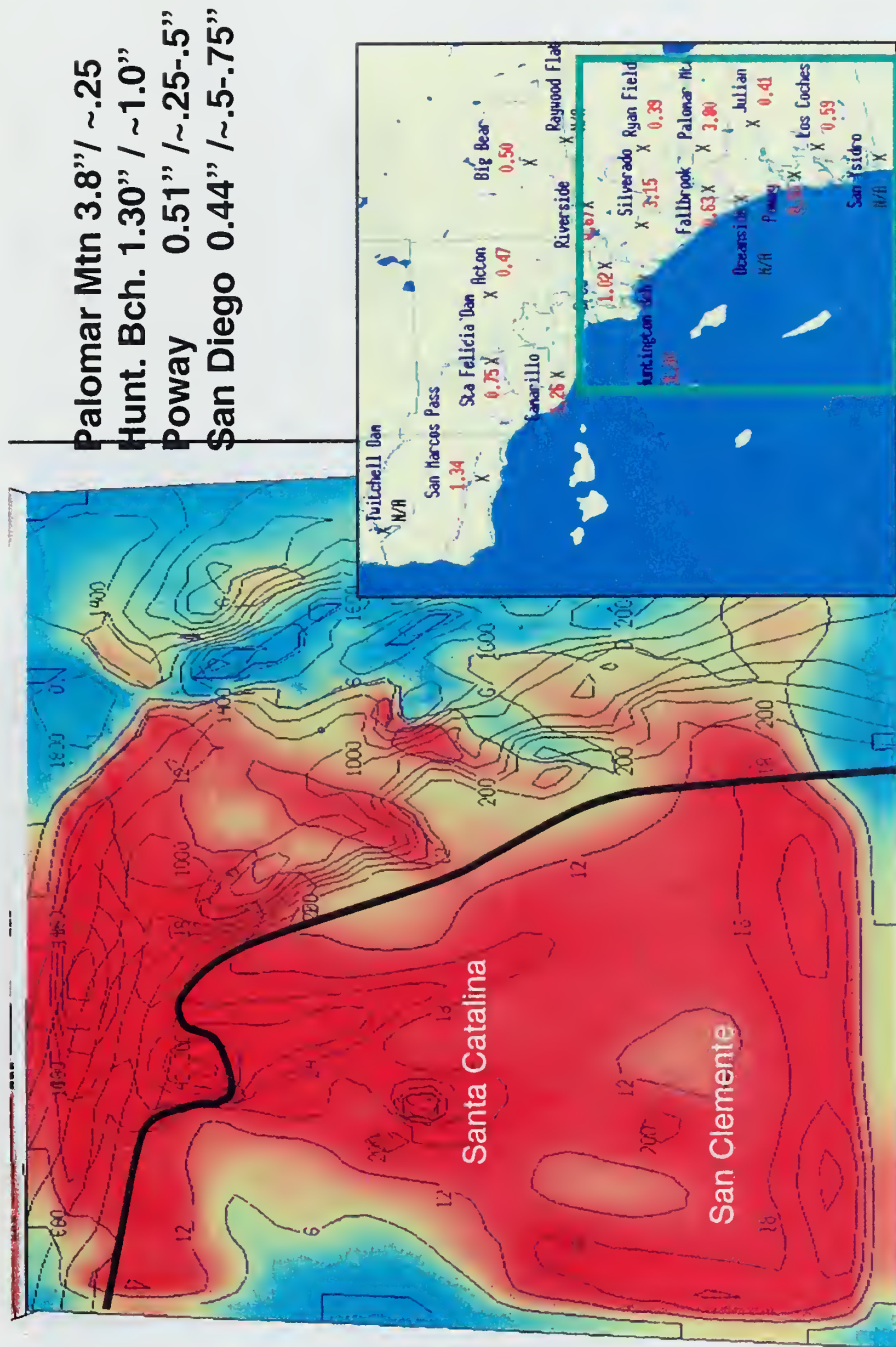


Figure 5-18. COAMPS 12-h total accumulated precipitation for the entire event in mm (left) and NWS 24-h total precipitation values (right). COAMPS demonstrated skill in the relative distribution of the rainfall, but showed less precipitation than was recorded by rainfall gauges for most stations (CA/NV River Forecast Center). Note the green box approximates the COAMPS area depicted to the left.



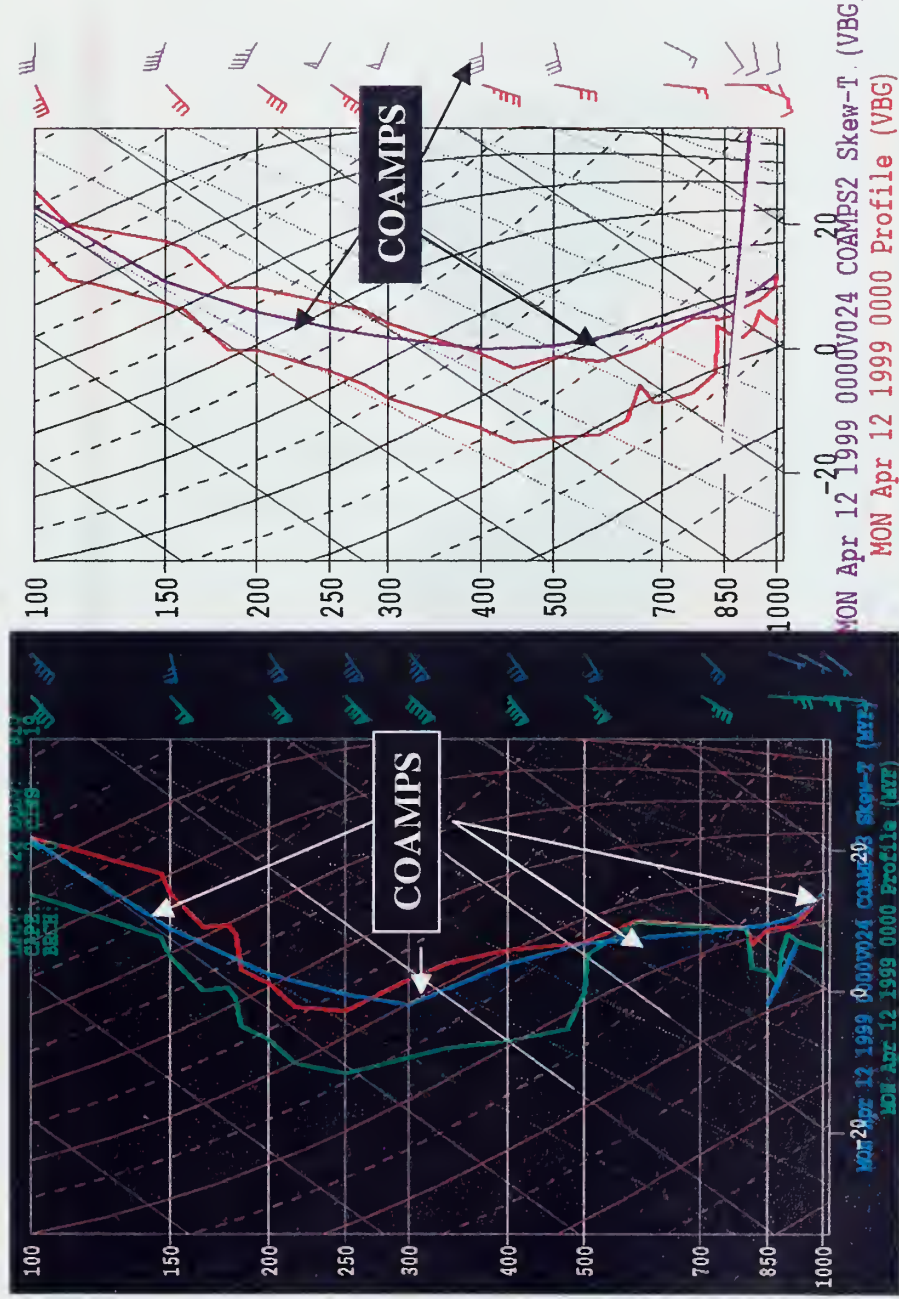


Figure 5-19. Forecast soundings. COAMPS 24-h forecast sounding against the verifying upper-air soundings at pre-frontal and post-frontal sites, Montgomery Field (MYF) and Vandenberg AFB (VBG) respectively. Note that COAMPS' lapse rate near the surface remains stable. Stronger cold air advection on the backside of this front than COAMPS was able to resolve.



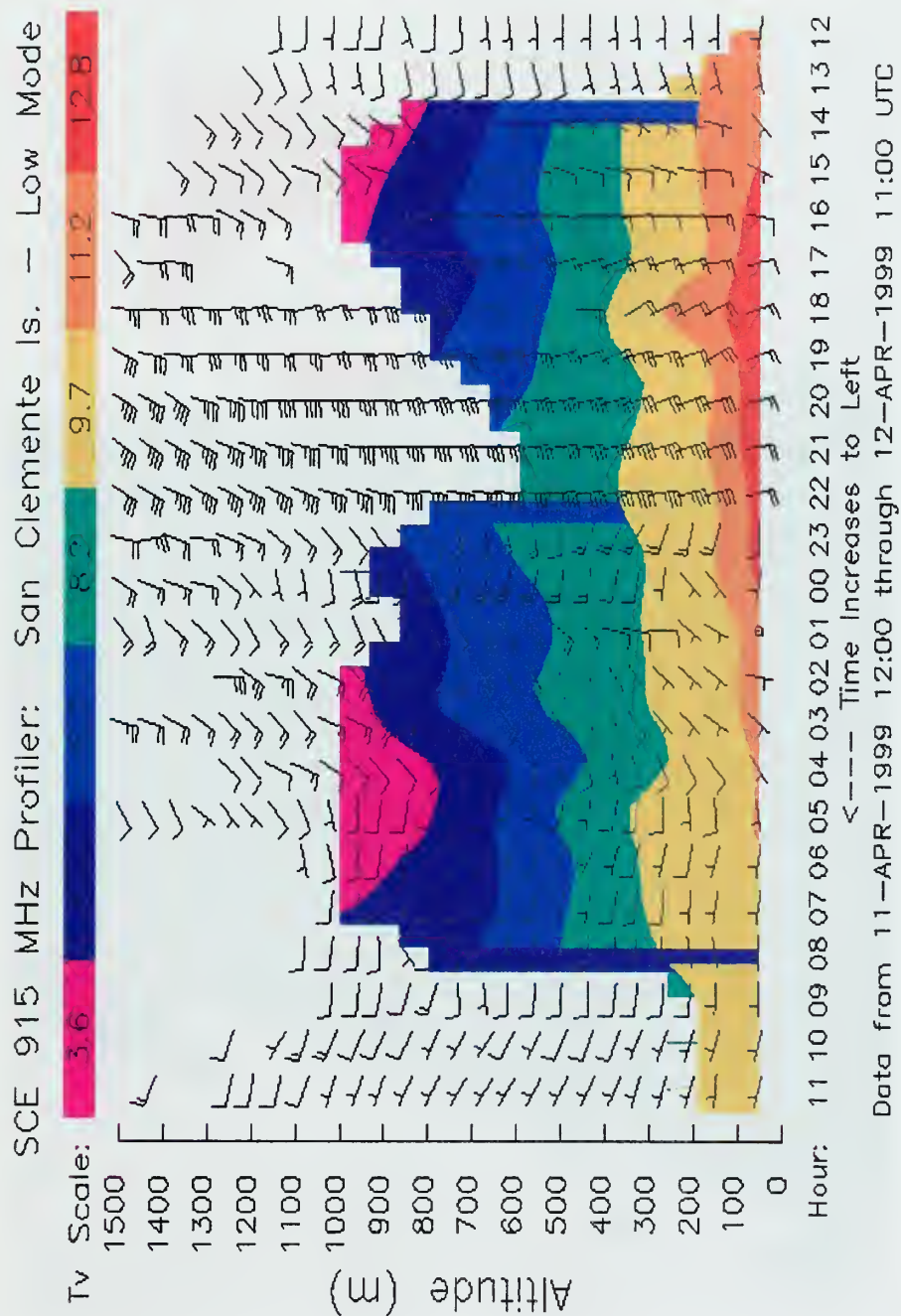


Figure 5-20. The RASS on the San Clemente Island profiler depicts a low-level lapse rate of about  $8^{\circ}$  C/km, which is more in line with the COAMPS forecast.



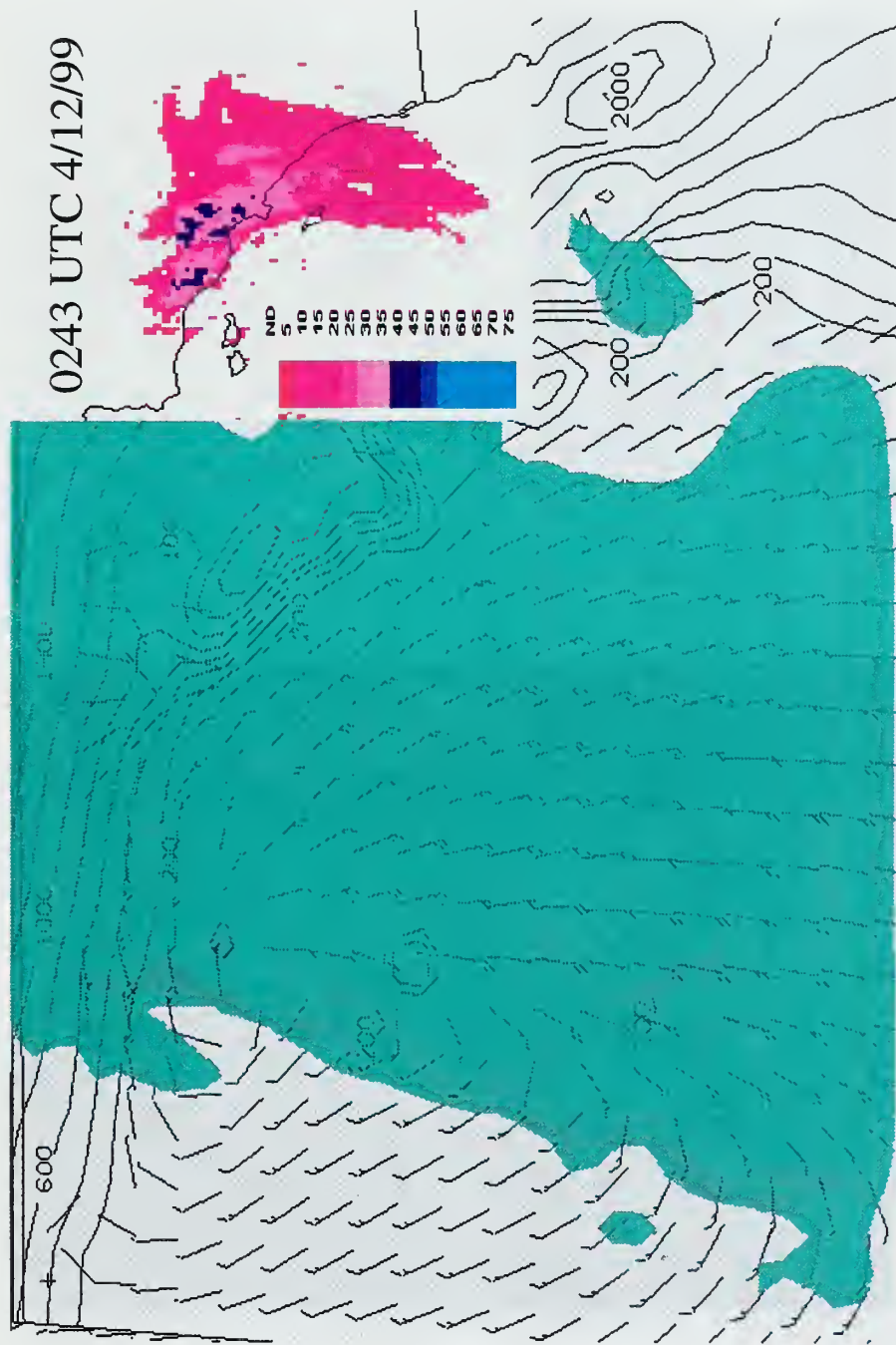


Figure 5-21. Compare COAMPS depiction of instantaneous rainfall to the verifying radar image image.



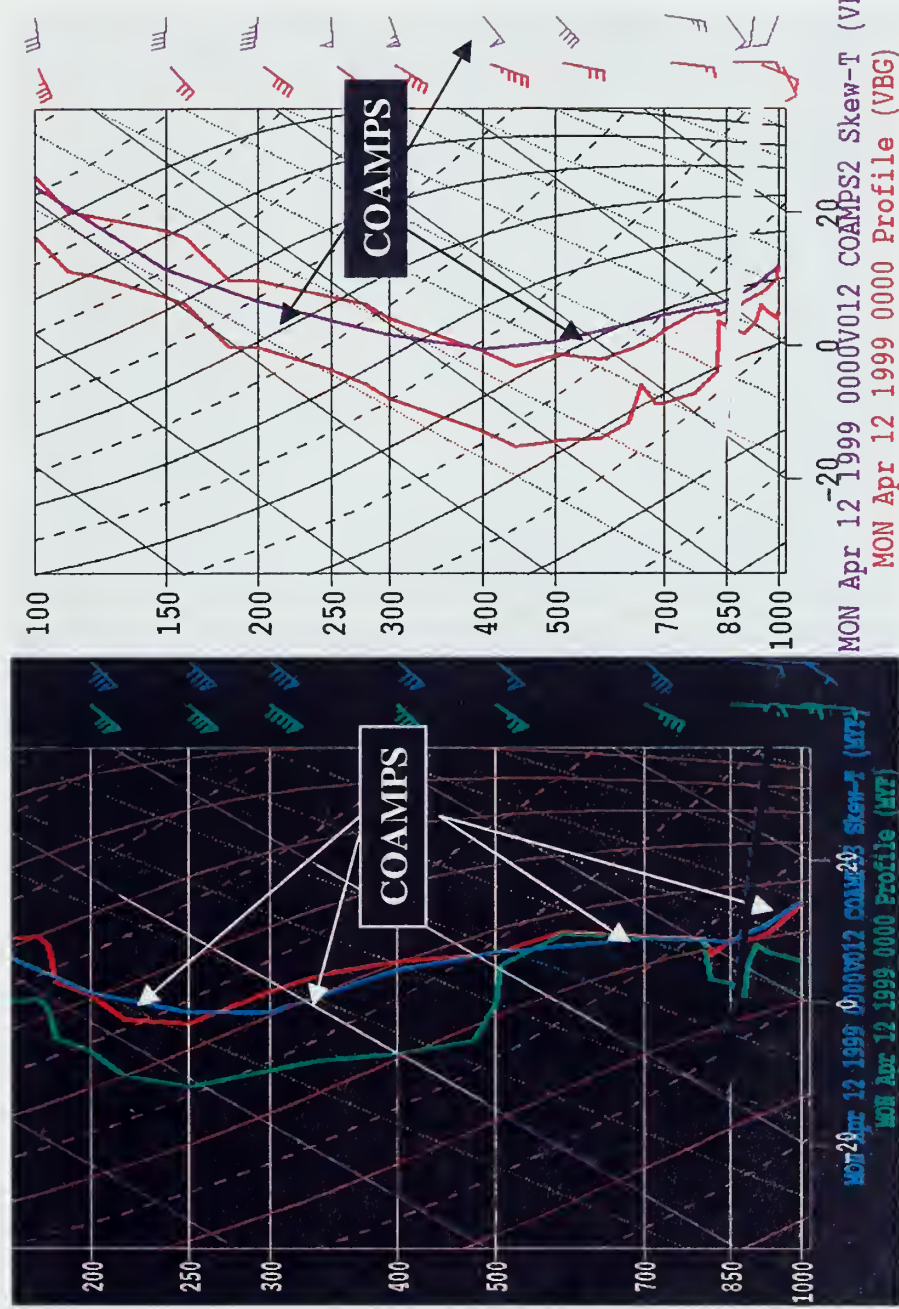


Figure 5-22. The COAMPS 12-h forecast sounding and the verifying upper-air soundings at pre-frontal and post-frontal sites, Montgomery Field (MYF) and Vandenberg AFB (VBG) respectively.



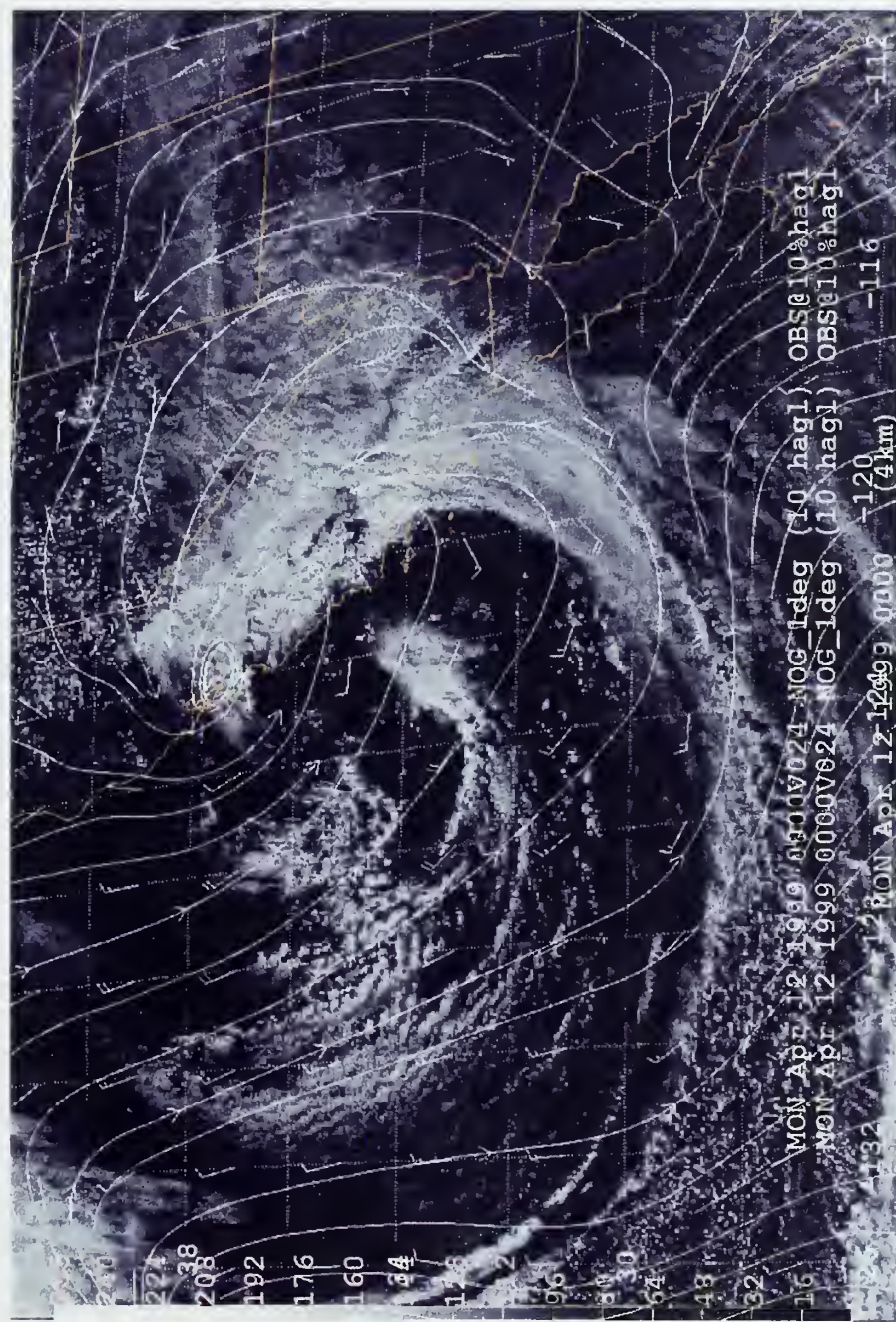


Figure 5-23. The 24-h NOGAPS forecasts was successful in verifying accurately the position of the front against the observations and satellite.



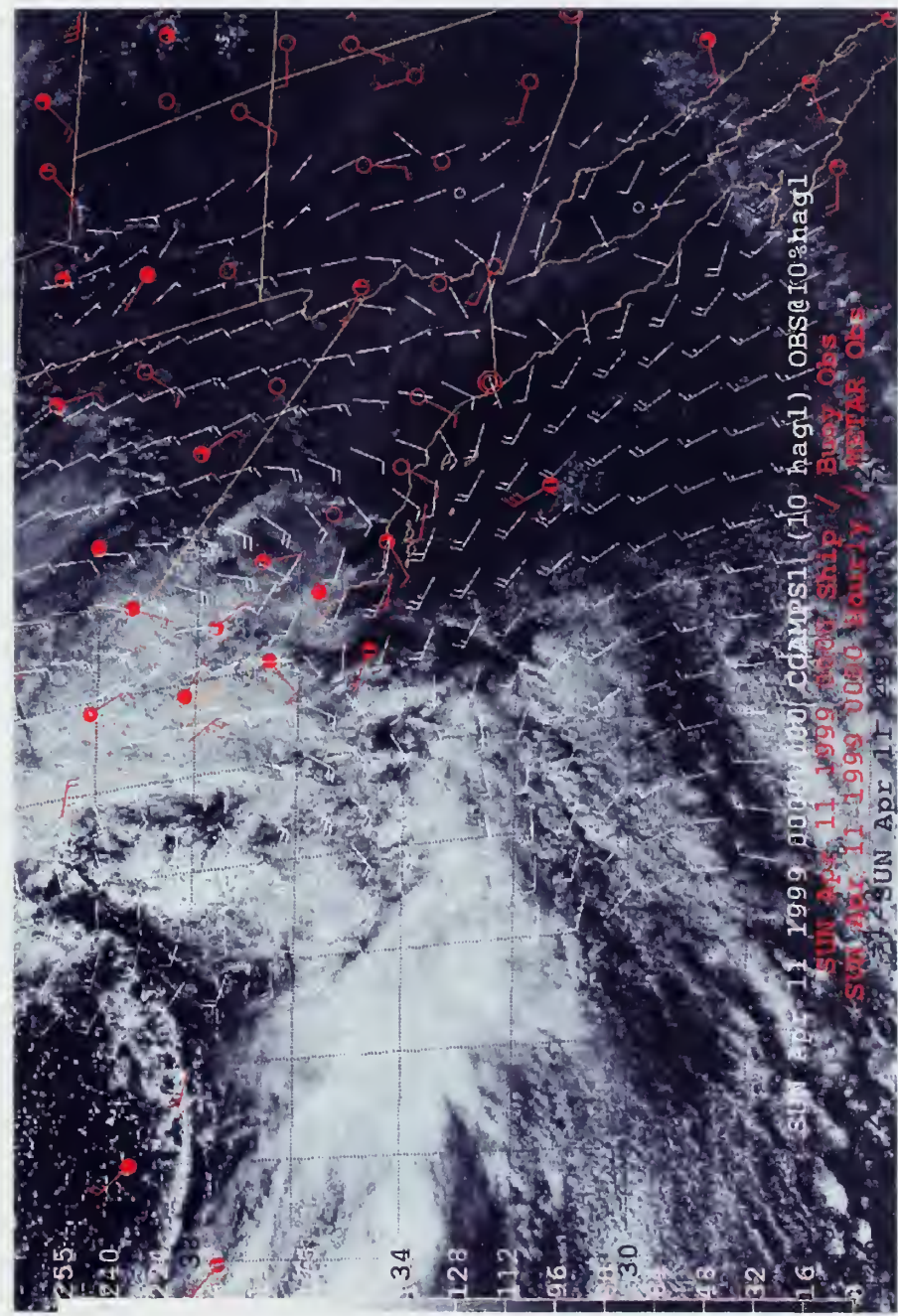


Figure 5-24. COAMPS analysis for the 24 to 30-h forecast with the analysis observations and satellite imagery.



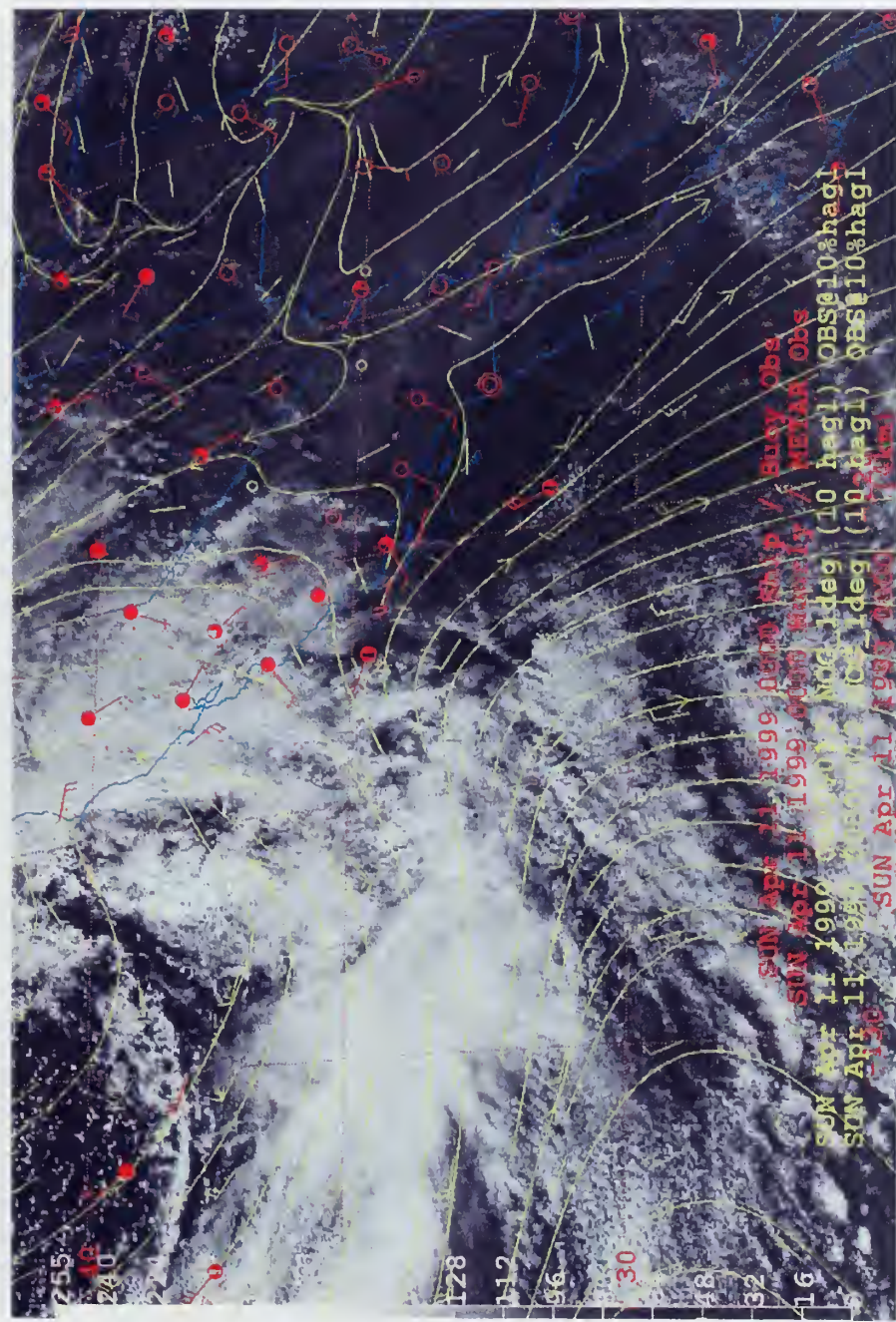


Figure 5-25. NOGAPS has analyzed the trough accurately, therefore, since it will be the first-guess to some subsequent COAMPS analysis, the COAMPS analysis should be skillful.



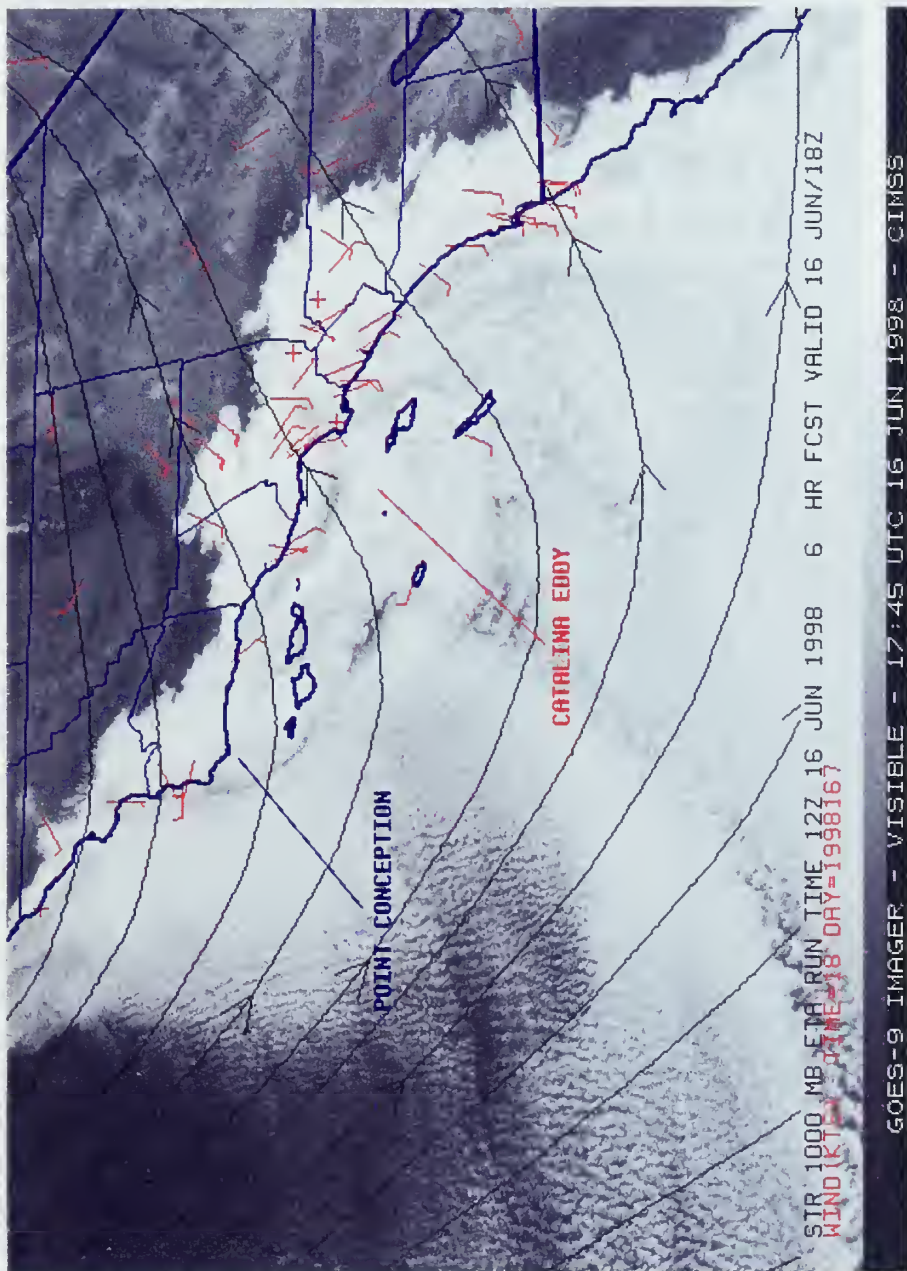


Figure 5-26. GOES-9 visible imagery from 16 June 1745 UTC (above) showing a Catalina Eddy circulation just off the southern California coast. This eddy began to form on 15 June 1998, as northerly low-level flow off Point Conception began to interact with the complex topography of the southern California coastline. Note the normal fog and stratus along the coast, which retreated toward the ocean as the day progressed.



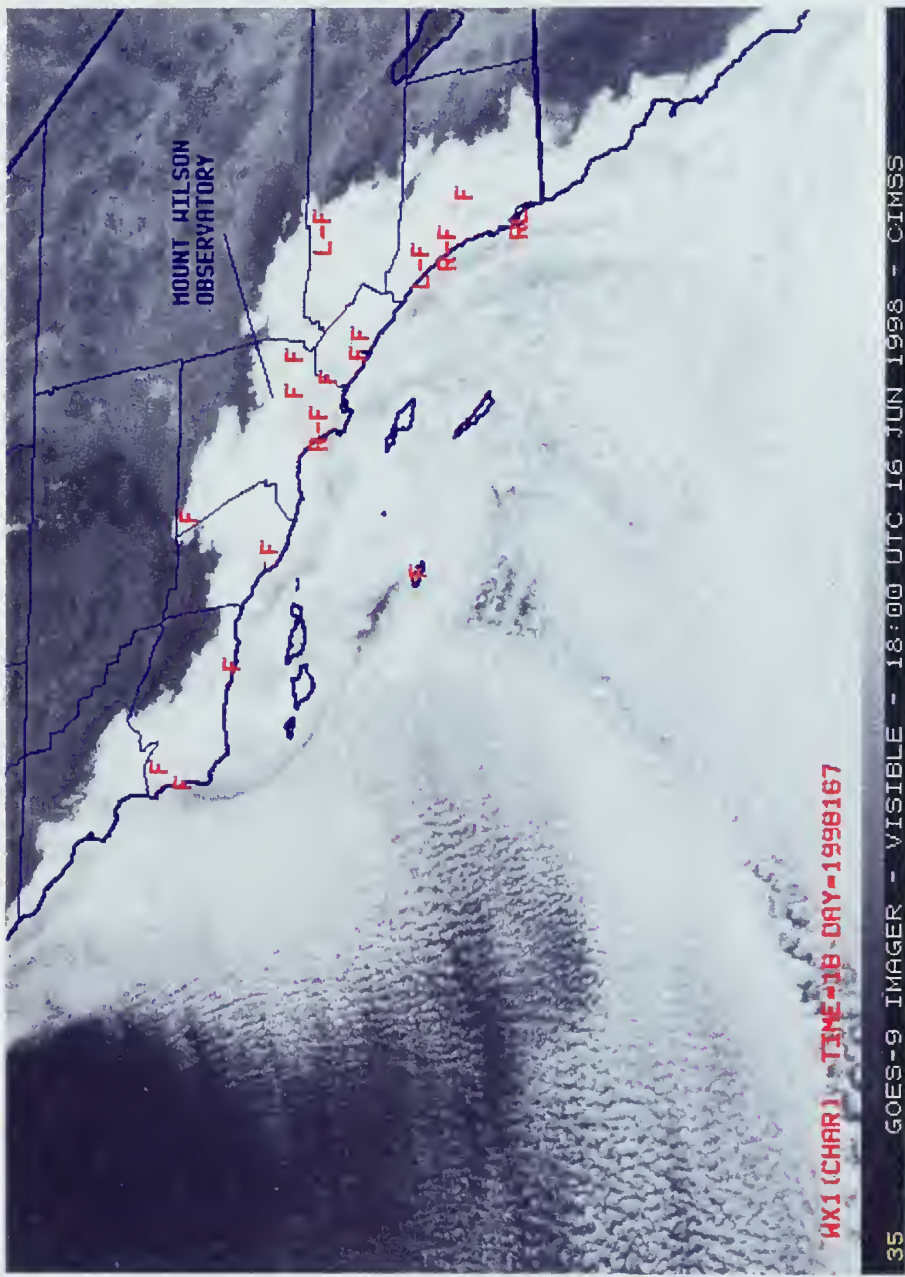


Figure 5-27. The eddy circulation intensified on 16 June and helped to induce a persistent onshore flow of marine air into the coastal counties during the entire day. Drizzle and rain was reported at several stations across the region. High altitude fog was even reported at the Mount Wilson Observatory (in the San Gabriel Mountains northeast of Los Angeles), indicating that the depth of the marine layer reached the 6000-foot level.



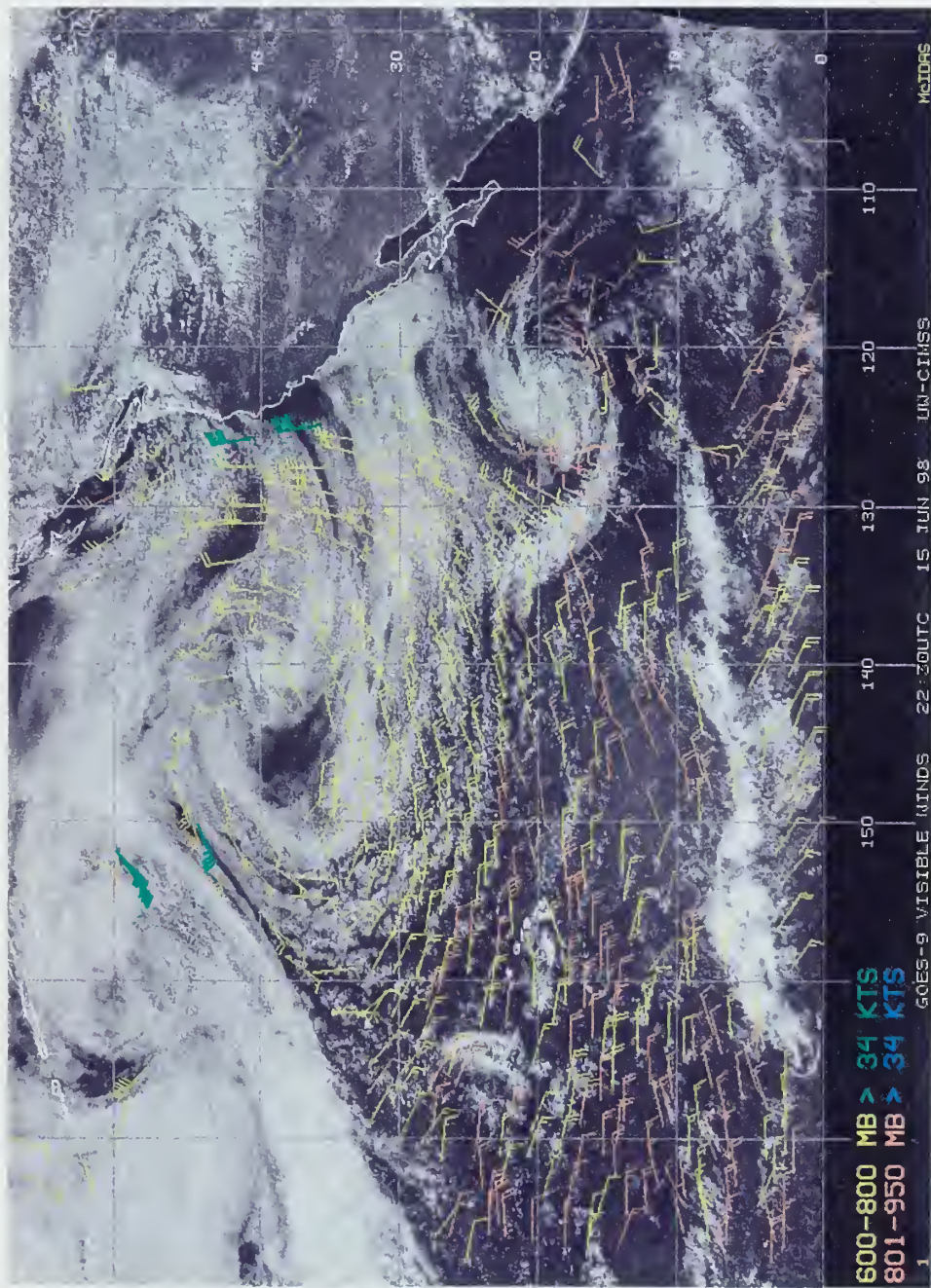


Figure 5-28. Satellite cloud derived winds revealing the strong northerly flow off of the central California coast. The interaction of this flow with the complex topography of the northern SOCAL bight induced the Catalina Eddy resulted in the 15-16 June eddy.



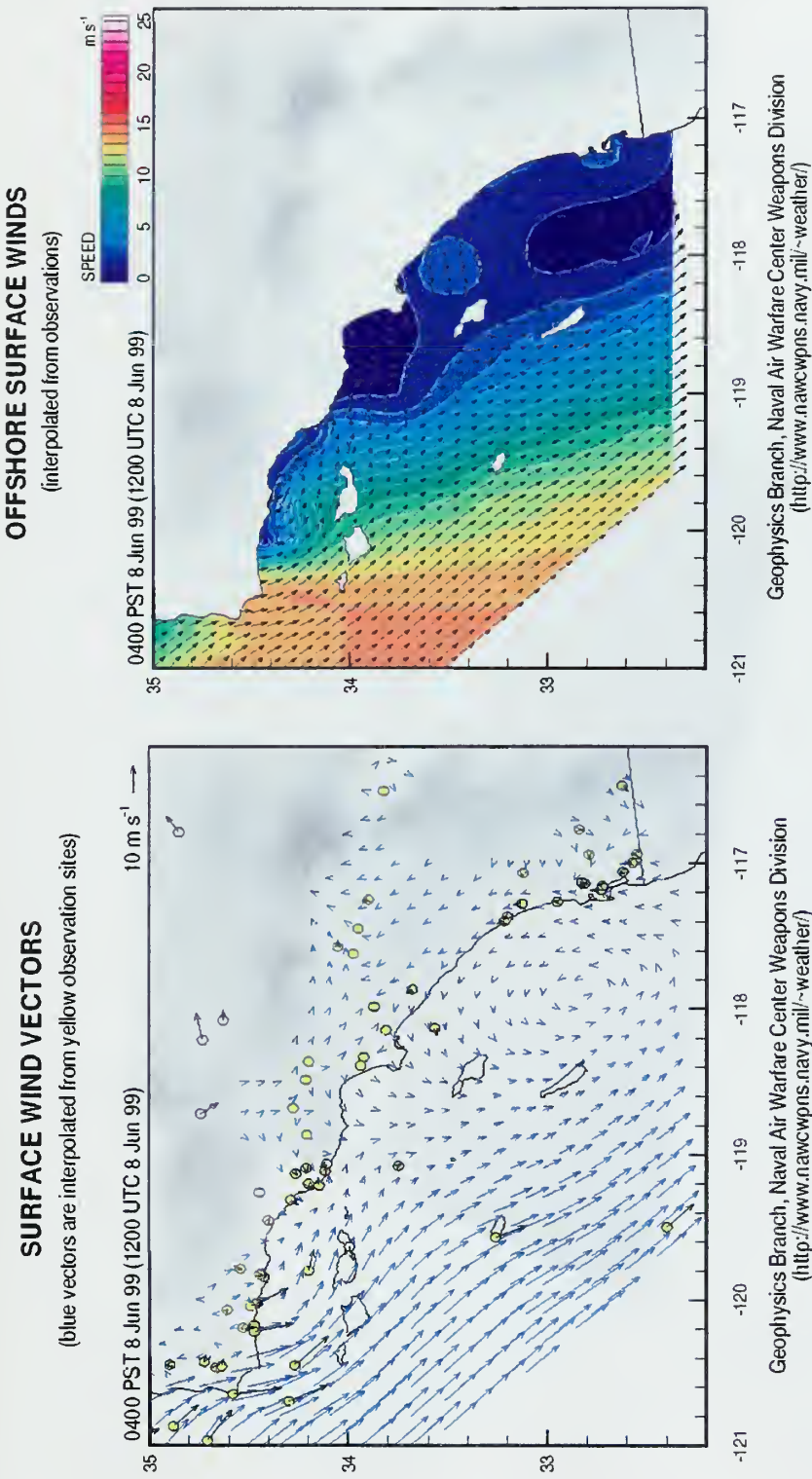


Figure 5-29. Naval Air Warfare Center Weapons (NAWC) Division version of a meso-analysis of the wind field. The blue vectors in the first plot represent the surface wind flow in the offshore marine layer and the adjacent basins of Southern California. The wind field is derived by interpolating the hourly wind observations taken at the stations denoted by the yellow circles. The stations denoted by the white circles are not included in the interpolation analysis as they are considered unrepresentative of the marine layer or low-level basin flow due to their location or elevation (NAWC 1999).





Figure 5-30. Wind profiler/Radio Acoustic Sounding System network in the SOCAL bight (NPS 1999).



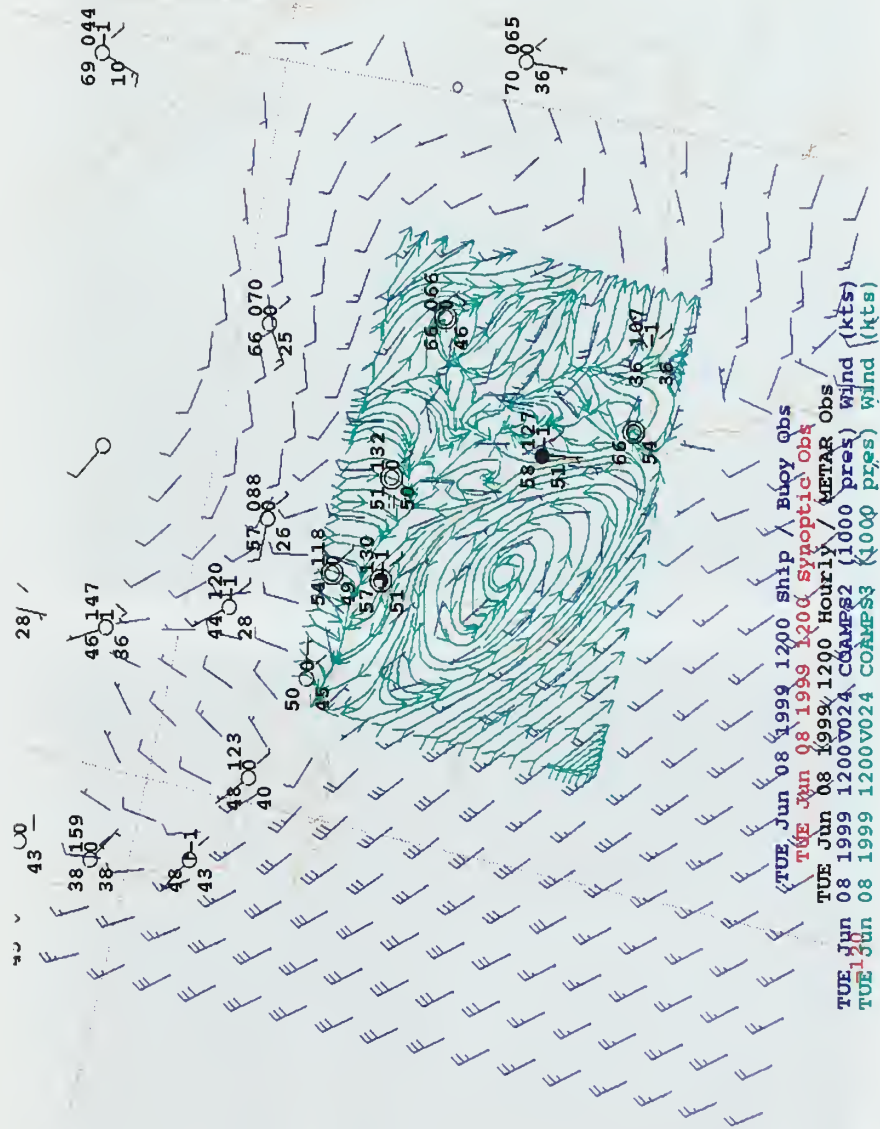


Figure 5-31. A depiction of the Catalina Eddy as resolved and forecast by COAMPS for 08 June 1200 UTC. The blue wind barbs (kts) are from the medium mesh (15 km resolution) and the green streamlines are from the innermost mesh (5 km resolution).



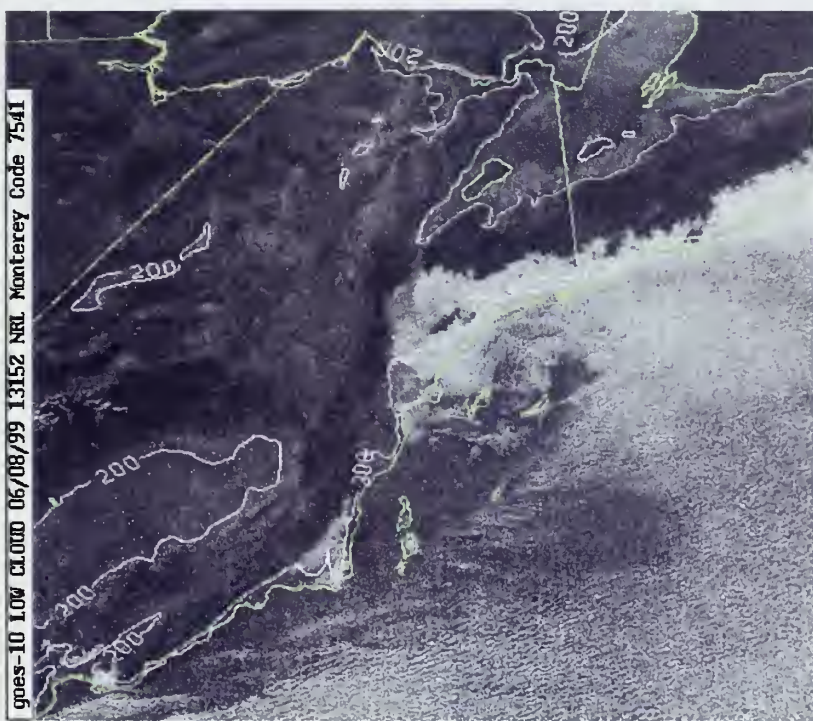
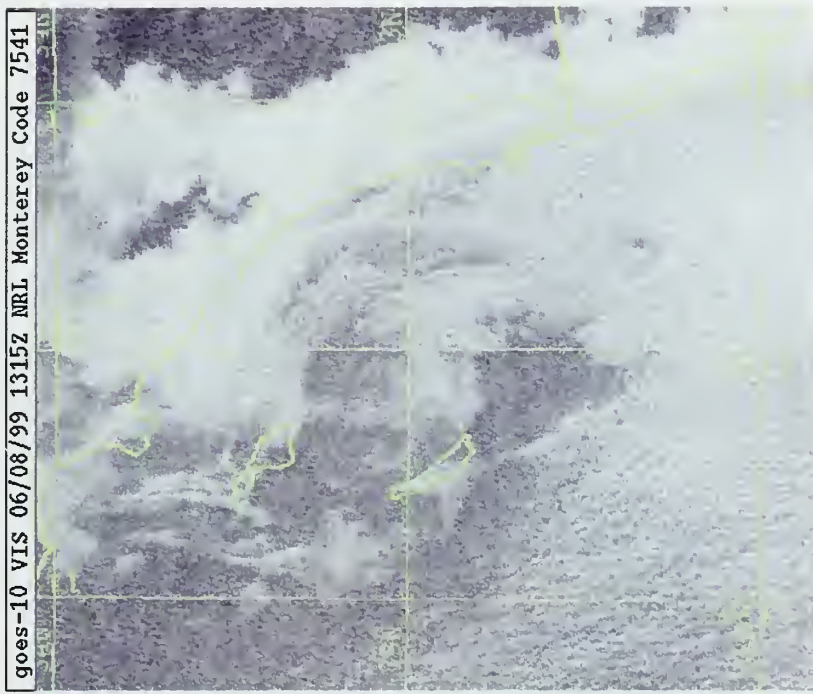


Figure 5-32. GOES 10 visible imagery from Naval Research Lab Monterey depicting a Catalina Eddy on 08 June 1315Z. A comparison of this imagery with the COAMPS 24-forecast depicted in figure 6 shows that COAMPS displayed considerable skill in forecasting this event (NRL 1999).



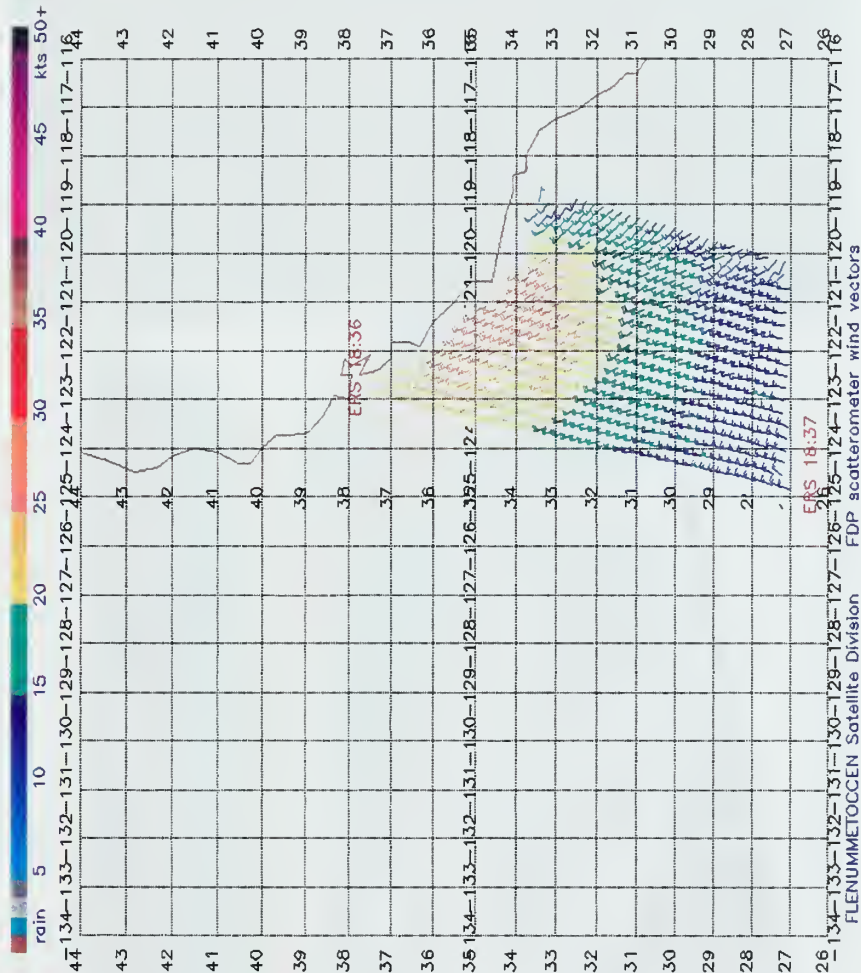


Figure 5-33. Scatterometry data valid just 6-h after the Eddy that supports the stronger winds (~30 kts) that COAMPS is showing in the outer bight.



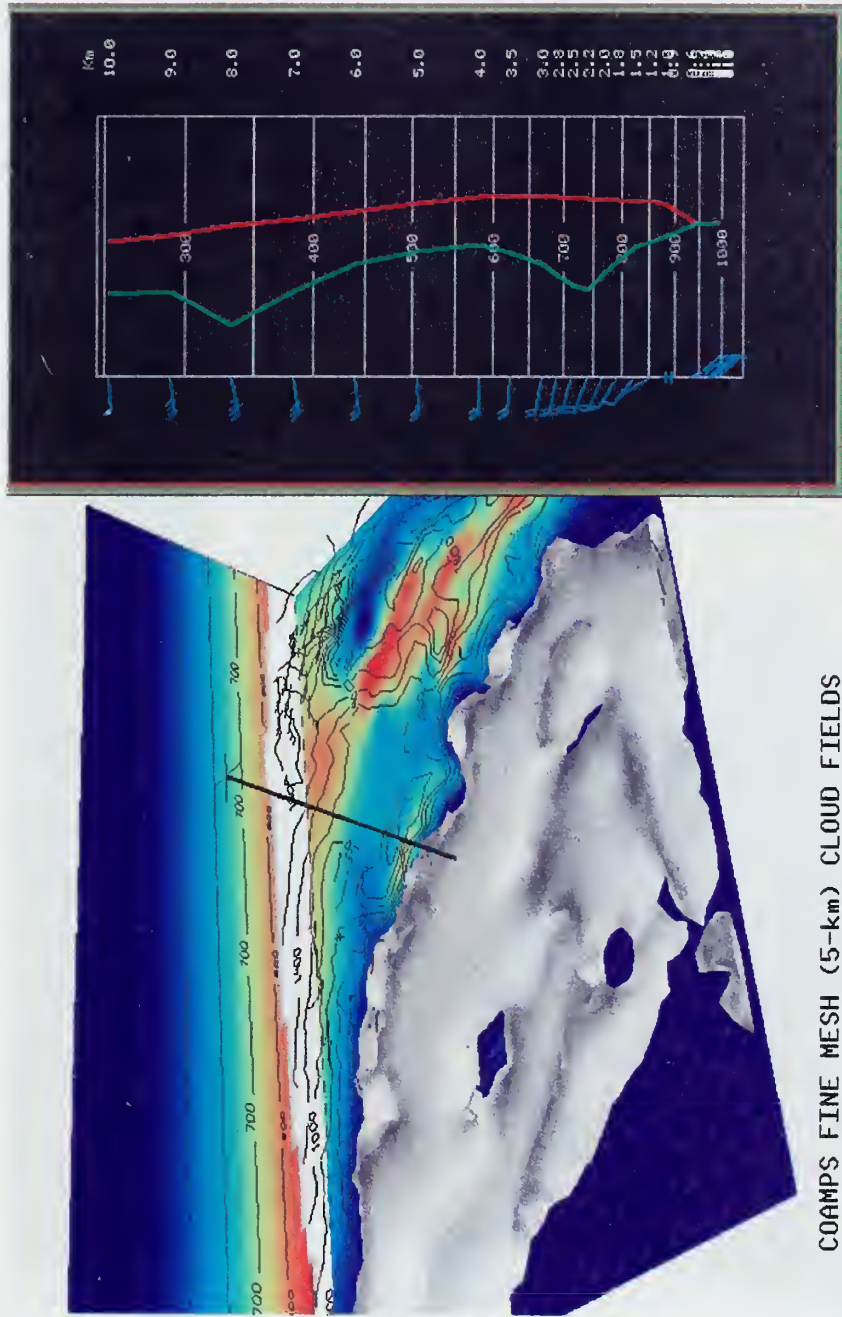


Figure 5-34. COAMPS cloud fields showing good agreement with the actual cloud conditions (Figure 5-34), especially in the depiction of the thicker cloud layer along the coast that spreads inland into the valleys and onto the western slopes of the coastal mountain range.



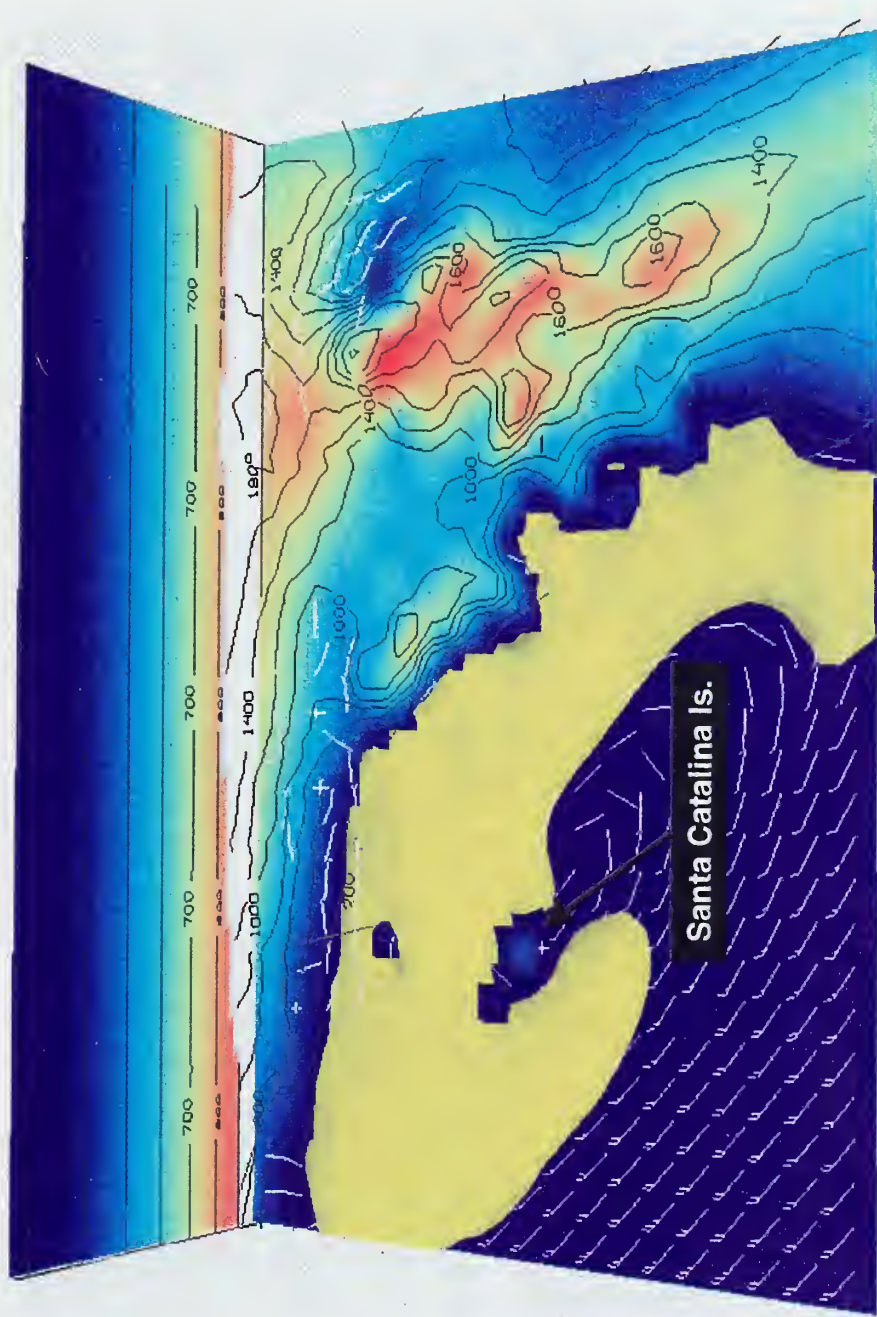


Figure 5-35. A potential temperature surface (285 K) which also clearly indicates the presence of this cold tongue along the coast and is in line with the Mass and Albright (1989) theory of development.



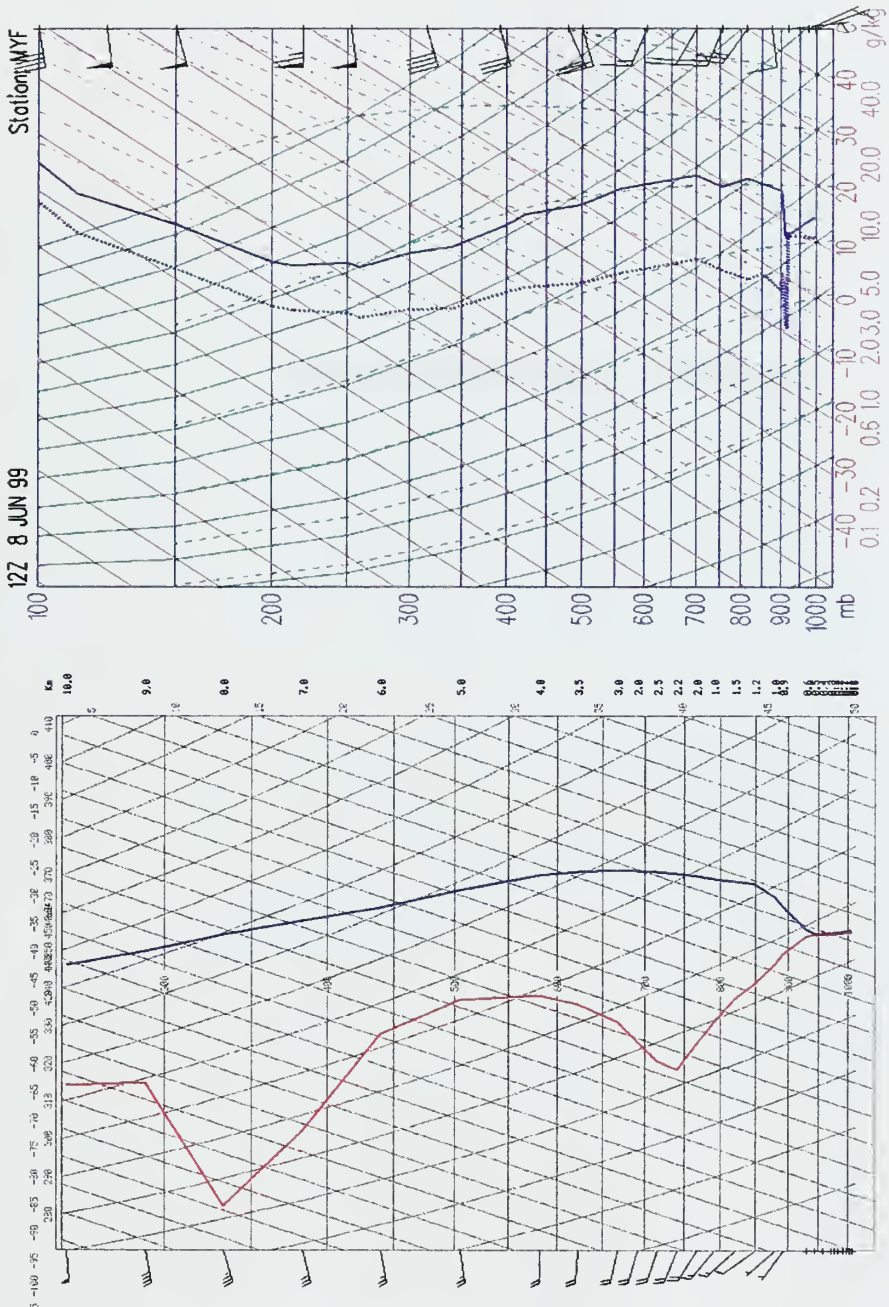


Figure 5-36. COAMPS forecast sounding (left) and the actual sounding for Montgomery Field (MYF) (right) valid at 1200 UTC on the 8<sup>th</sup>. COAMPS demonstrates skill in depicting the inversion base height, but lacks the resolution to capture both the inversion temperature and dew point gradients (as should be expected). Note that the marine boundary layer compares favorably even though COAMPS has errors in the flow and temperature profile aloft.



THIS PAGE INTENTIONALLY LEFT BLANK



## APPENDIX B. Vis5D SETTINGS

The following discussion is intended to serve as a quick-start guide for using Vis5D in the forecast process. The following notes are based upon NPMOC San Diego's TAMS-RT basic output parameters for Vis5D and are best viewed with a white background. Other output parameters are possible. Threshold values are based on the forecast area in the vicinity of NPMOC San Diego and will need to be adjusted accordingly for other geographic areas as well as synoptic regimes. An updated COAMPS output variable list is maintained by NRL Monterey, CA. Sections 6.2 through 6.14 of the Vis5D Readme File (available online at <http://www.ssec.wisc.edu/~billh/vis5d.html>) contain detailed information on Vis5D features and is a must read for eventual users of these methods.

### NOTES ON SETUP:

- 1) Create and save a template for optimum viewing of both the coarse and fine mesh fields:

- i) Start Vis5D
- ii) If they are not already selected, activate:

TOPO, BOX, CLOCK, CONT #'s, REVERSE, PERSPEC, and LEGENDS

**NOTE:** Vis5D records every mouse click and setting in a history file. This history file is what is used to create a template that you can RESTORE later. Thus, in order to RESTORE the template quickly, it is important to minimize the number of mouse clicks when completing following initial setup for the first time.

- iii) Set parameter thresholds, contour intervals, location and height, color, and opacity. Refer to Table B-1 below for abbreviated parameter descriptions, recommended initial settings, and the order in which to make the settings.

Table B-1.

SYMBOL <sup>1</sup>	NAME	UNITS	TYPE	VALUE	INTERVAL	LOC/HGT	COLOR	OPACITY
MAP	Geopolitical Map	-	Horiz/Contour	-	-	SFC <sup>2</sup>	Default	Default
PPPP	Pressure	mb	Isosurface	500/850 <sup>3</sup>	-	-	Default	Default
	-	-	Vert/Contour	-	100 <sup>4</sup>	North wall <sup>5</sup>	Black <sup>6</sup>	-
	-	-	Vert/Color	-	-	North wall <sup>5</sup>	Default	Default
	-	-	Horiz/Contour'	-	2	~500 mb	Black	-

**NOTE:** Leave MAP and pppp vertical slices on. These fields help the forecaster to orient themselves spatially within the 3-D field and serve as a reference for orienting future parameter slices. As you adjust the settings on each new parameter, you may want to toggle them "off" in order to unclutter the display.

Table B-1 cont'd.

SYMBOL	NAME	UNITS	TYPE	VALUE	INTERVAL	LOC/HGT	COLOR	OPACITY
Hwind1 <sup>8</sup>	Wind barbs	m/s	Horiz/Slice	-	-	SFC	Black	-
Hwind2 <sup>8</sup>	Wind barbs	m/s	Horiz/Slice	-	-	SFC	White	-
Hstream	Stream lines	-	Horiz/Slice	-	-	~500 mb	Yellow	-
wspd	Wind Speed	m/s	Isosurface	45	-	-	Purple	0.5 <sup>9</sup>
-	-	-	Horiz/Contour	-	3 (12,100) <sup>10</sup>	~300 mb/SFC	Black	-
-	-	-	Vert/Contour	-	5	Default	White	-
-	-	-	Horiz/Color	-	-	0.2 km	T/C 15 <sup>11</sup>	Default
-	-	-	Vert/Color	-	-	Default	0.6	0.5
rvor	Relative vorticity	units/s	Isosurface	10/14	-	-	Orange	0.5
-	-	-	Horiz/Contour	-	3 (12,100)	~500 mb	Default	-
-	-	-	Vert/Contour	-	3 (12,100)	Default	Default	-
avor	Absolute vorticity	units/s	Isosurface	20/22	-	-	Orange	0.3
-	-	-	Horiz/Contour	-	3 (22,100)	~500 mb	Default	-
-	-	-	Vert/Contour	-	3 (22,100)	Default	Default	-
W	Vertical velocity	m/s (+)=up (-)=down	Isosurface	0.05/0.2	-	-	Red	0.5
-	-	-	Vert/Contour	-	-0.02/-0.2	// flow <sup>12</sup>	Black	-
-	-	-	Vert/Color	-	// flow	T/C 0	0.6/0.8	0.6
pott	Potential Temperature	°K	Isosurface	285	-	-	Default	0.6
-	-	-	Vert/Contour	-	5	// flow	Black	-
-	-	-	Vert/Color	-	// flow	Default	0.8	0.8
ttt	Air Temperature	°C	Isosurface	0 (fzg pt)	-	-	Default	Default
-	-	-	Horiz/Contour	-1	~850 mb	Red	-	-
-	-	-	Vert/Contour	-5 (-15,15)	Default	Blue	-	-
-	-	-	Horiz/Color	-	~850 mb	T/C 0	Default	Default
dmdz	Refractivity gradient	units/m	Isosurface	0	-	-	Light Blue	0.6
relh	Relative humidity	%	Isosurface	95	-	10 (50,100)	2.5 km	Default
-	-	-	Horiz/Contour	-	10 (50,100)	2.5 km	Default	Default

Table B-1 cont'd.

SYMBOL	NAME	UNITS	TYPE	VALUE	INTERVAL	LOC/HGT	COLOR	OPACITY
qccc	Cloud droplet mixing ratio	g/Kg	Isosurface	0.01 <sup>13</sup>	-	-	White	0.5
qrrr	Rain drop mixing ratio	g/Kg	Isosurface	0.01	-	-	Green	0.3
qiii	Ice crystal mixing ratio	g/Kg	Isosurface	0.01	-	-	Default	0.6
qsss	Snow flake mng/ratio	g/Kg	Isosurface	0.1	-	-	White	0.6
blht	Boundary layer height	m	Horiz/Contour	-	200	SFC	White	-
-	-	-	Horiz/Color	-	-	0.3 km	T/C 300	-
topo <sup>14</sup>	Model topography	m	Horiz/Contour	-	200	SFC	Black	-
-	-	-	Horiz/Color	-	-	0.0 km (sfc)	Default	Default
s1p4	Mean sea-level pressure	mb	Horiz/Contour	-	1	SFC	White	-
-	-	-	Horiz/Color	-	-	0.1 km	T/C 1008	-
prcp	Tot. 12-hr accum Precip	mm	Horiz/Contour	-	3	SFC	Green	-
-	-	-	Horiz/Color	-	-	0.1 km	T/C 7	-
SFC_T <sup>15</sup>	Ground Temp	°C	Horiz/Contour	-	2	SFC	Red	-
-	-	-	Horiz/Color	-	-	0.0 km	Default	-
C_AIR <sup>15</sup>	Sea-Air Temp Difference	°C	Horiz/Contour	-	1	SFC	White	-
-	-	-	Horiz/Color	-	-	0.2 km	D/Center 0	-
T <sup>15</sup>	New Var = Air temp.	°C	-	-	-	-	-	-
TD <sup>15</sup>	New Var = Dew Pt temp.	°C	-	-	-	-	-	-
RELH <sup>15</sup>	New Var = Rel humid	%	-	-	-	-	-	-

Table B-1 cont'd.

## COMPARISON VARIABLES

NOTE: The following Comparison Variables will be set at a later time.

SYMBOL	NAME	UNITS	TYPE	VALUE	INTERVAL	LOC/HGT	COLOR	OPACITY
P_DIFF	Pres. Diff. Fields	mb	Horiz/Contour	-	1	5.9 km	Black	-
			Horiz/Color	-		5.8 km	T/C 0	0.75
T_DIFF	Temp. Diff. Fields	°C	Horiz/Contour	-	0.5	1.4 km	Black	-
			Horiz/Color	-		1.3 km	T/C 0	0.75
SLP_D	MSLP Diff. Fields	mb	Horiz/Contour	-	0.5	SFC	Black	-
			Horiz/Color	-		0.1 km	C 0	Default
WND_D	Wind Diff. Fields	m/s	Horiz/Contour	-	2	SFC	Black	-
			Horiz/Color	-		0.0 km	T/C 0	Default
W_DIFF	Vert. Veloc. Diff. Fields	m/s	Vert/Contour	-	5	Default	Black	-
			Vert/Color	-		Default	Default	0.6
			Isosurface	45 m/s	-	-	Orange	-
			Vert/Contour	-	0.05	// flow	Black	-
			Vert/Color	-	-	// flow	T/C 0	0.6

## FOOTNOTES

(1) Left mouse click on the parameter widget button toggles the graphic on and off and also opens a small pop-up control panel window to adjust the threshold values.

(2) Section 6.6. The position of horizontal slices can be changed using the height control panel that is automatically displayed when a horizontal slice is selected. Simply slide the diamond to the desired elevation when an elevation is given. This panel also contains a **SFC** button (version 5.1 or higher) that causes the horizontal slice data to be sampled from the topographic surface then displayed on top of the topographic surface (Note: The topography surface used is Vis5D's and not the model topography. The position of slices can also be changed interactively using the mouse. Use the vertical pressure contours on the north wall to help orient the horizontal slices in elevation referenced to millibars. To move the slices you must first be in **SLICE** mode by selecting the **SLICE** button. To move any slice, simply point at the slice's corner with the mouse, press the right mouse button and drag it to the suggested position. Vertical slices may also be moved in a perpendicular motion by "grabbing" with a right mouse click a "handlebar" found in the middle of the top or bottom edges and dragging it to the suggested location. (Note: you may have to rotate the view slightly, or select the **TOP** or **SOUTH** buttons for the handlebars to come into view).

(3) The first number applies to the coarse mesh and the second number applies to the fine mesh. Set the first value initially for the coarse mesh. Later you will go back to these parameters and reset it to the fine mesh value to save the fine mesh template. The two meshes require different threshold settings because some parameters (e.g., vertical velocity) increase in magnitude when computed on smaller and smaller scales. These are highlighted in yellow (or italicized) to quickly find them the second time through.

(4) Section 6.6.1. This is the interval to use between contour lines.

(5) "Nwall" means to place the vertical slice against the back wall. In cases where both contour and color vertical slices are viewed, ensure that the contour slice is slightly in front of the color slice so that you can see it.

(6) Section 6.6.2. Right mouse click on the parameter widget allows you to change the color of the graphic.

(7) The "pppp Horizontal Contour Slice field" is different from the geopotential height field. This is a constant height field and thus is most similar to a mean-sea level pressure chart, only at altitude. This field is useful for synoptic orientation as the forecaster shifts from another synoptic field graphic display system to the Vis5D display.

(8) Section 6.6.3. Set Hwind1 and Hwind2 scale and density to 2 (doubles the wind barbs length) and 0.5 (displays half of the number of wind bars) respectively.

(9) Decreasing the opacity allows the parameter slice to become transparent which helps to view multiple slices simultaneously.

(10) Section 6.6.1. The first number before the parentheses is the interval to use between contour lines. Entering a negative interval will display negative contour values as dashed lines and positive contour values and solid lines. The values inside the parentheses indicate the range of values to contour from the lowest to the highest.

(11) Section 6.6.2. "T/C #" means to "tighten" the color scale for that parameter and "center" it on the value suggested. This is accomplished by the following steps:

- Place your cursor within the Vis5D color control panel for that parameter.

- (b) Left click below the bottom scale bar within the color control panel window to display the scale values. Drag the arrow to the suggested centering value.
- (c) Using the left/right arrow to "center" the scale on the suggested parameter value.
- (d) Use the down arrow to "tighten" the color scale.

Notes:

- Tighten the color scale until you get a full range of colors for the parameter of interest.
- Type "r" within the color control panel to "reset" the colors and "h" for "help".
- (12)"// flow" refers to orienting the vertical slice so that it parallels the expected dominant flow (e.g., from upstream to downstream) in order to display meaningful cross-sections. Choose a desired orientation for your vertical slice. In the case of fronts, for example, a northwest to southeast or "alongcoast" orientation would be meaningful, whereas in the case of Catalina Eddies either an east-west orientation traversing the eddy in the bight or a north-south orientation across the mountains north of the bight would produce meaningful cross-sections. These orientations will need to be adjusted as the actual flow varies from the dominant climatological flow direction.
- (13) Low threshold settings to lower confidences for the actual occurrence of that parameter (e.g., setting qccc on its lowest threshold setting shows you everywhere (according to the model) a cloud may exist, whereas a higher threshold setting should give you more confidence that a cloud will in fact occur where the model has placed it). The above assumption is not validated and needs verification; however, we have qualitatively observed that mesoscale models have a tendency to over-forecast at higher resolutions.
- (14)"topo" refers to the model's rendition of the actual topography, whereas "TOPO" is the standard Vis5D world topographic database which has very coarse resolution relative to most COAMPS domains, especially the fine mesh domains.
- (15) Create new analysis parameters from existing variables for both normal view and for use in the vertical sounding mode (sounding mode requires proper scaling and CAPS):
  - (a) Select NEW VAR.../Make type-in expression...
  - (b) Enter "SFC\_T=ttgg-273
  - (c) Click "OK"
  - (d) Repeat for:
    - (i) C\_AIR=ttgg-(tttt+273)
    - (ii) T=tttt+273
    - (iii) TD=dwpf+273
    - (iv) RELH=relh"

2) After setting all of the parameters in accordance with Table B-1, select only the desired parameters and initial viewing angle for both the COARSE and FINE mesh domains. The following recommendations are based upon the suggested methods in this paper and are primarily focussed on rapidly obtaining both synoptic orientation on the coarse mesh and mesoscale orientation on the fine mesh.

- (1) Build the COARSE mesh template:
  - TOPO, MAP, BOX, CLOCK, CONT#'s, REVERSE, PERSPEC, LEGENDS
  - Hwind1, Hwind2

- wspd Isosurface, pppp contour horizontal slice, and pppp contour and color vertical slices.
- (2) Click on **TOP** view.
- (3) Click on the **SAVE...** button.
  - A suggested initial filename is **coarse.SAVE**. Future files can be saved to reflect each forecaster's preferences or specific grid domains or synoptic regimes.
- (4) Reset applicable parameter thresholds from their coarse mesh values to their fine mesh values. Refer to the yellow highlighted (or, italicized) text items in Table B-1
- (5) Build the **FINE** mesh template:
  - MAP, BOX, CLOCK, CONT#s, REVERSE, PERSPEC, LEGENDS
  - Hwind1, Hwind2
  - pppp contour and color vertical slices, topo contour and color horizontal slice, and slp4 contour and color horizontal slices.
- (6) Click on **TOP** view.
- (7) Click on the **SAVE...** button.
  - A suggested initial filename is **fine.SAVE**.

3) To restore these templates at a later time, simply run Vis5D from the same directory and click on **RESTORE** and enter the filename of the template you wish to restore.

- Note: You may need to activate or re-activate **MAP**, **REVERSE**, **LEGENDS**, and any parameters other than T or TD on the vertical sounding each time you restore a template

4) You are now ready to explore your model fields. Please refer to Section X for suggested methods.

THIS PAGE INTENTIONALLY LEFT BLANK

## APPENDIX C. Vis5D AMPLIFIED PROCEDURES FOR TOPOGRAPHY STUDIES

The following discussion provides a detailed procedure for making the figures as displayed in this thesis.

### TOPOGRAPHIC STUDY

**Purpose:** *To compare “modeled” versus “real” topography including the coastline resolution, especially in areas of critical topographic forcing (e.g., mountainous terrain, land/sea boundaries) that might result in the development of mesoscale features or structure.*

**Frequency:** *This study should be conducted on both the coarse and fine mesh each time the forecast domain is relocated.*

#### Vis5D Parameter:

- 1) topo

#### Procedure:

- 1) Select **topo** Horizontal Colored Slice on Vis5D control panel.
- 2) Access a high-resolution topographic map.
- 3) Note: If a high-resolution topographic background map is not already loaded in Vis5D, then you will need to first bring up one:
  - a) Open a web browser, go to <http://fermi.jhuapl.edu/states/> to select your region of interest
  - b) Open a second web browser, go to the same site and open up the “elevation key” map.
- 4) Select **TOP** view in Vis5D and examine the general character of the modeled topography and coastline resolution.  
Note: Toggle LEGENDS off (it interferes with the probe readouts)
- 5) Select **Probe** mode/**SOUTH** view/move probe to surface/rotate view to an angled top-down view (ensure probe is visible)/move probe by shift and arrow keys:  
Note: the probe must be on the ground surface to get a topographic readout value.
  - a) up arrow = due north at current level
  - b) down arrow = due south at current level
  - c) right/left arrow = due east/west at current level
  - d) shift + up arrow = straight up in the vertical
  - e) shift + down arrow = straight down in the vertical
- 6) Examine modeled topography and coastal resolution versus the high-resolution topographic map to note areas of significant deviation. Consider the potential impacts on the forecast.  
Note: Please refer to Section 4.c for discussion on possible impacts to model performance.

THIS PAGE INTENTIONALLY LEFT BLANK

## APPENDIX D. VIS-5D COMPARISON PROCEDURES

The following procedures provide detailed instructions for creating the comparison graphics as displayed in this thesis.

### PROCEDURES:

- 1) Import a previous COAMPS model run for comparison with the current model run.
  - a) With the current model run open in VIS-5D:
    - (1) Click on **IMPORT**→ **Read file...**
    - (2) Input file name (including directory path if the data is not in the current working directory that you are in) and click **OK** (e.g., /d/case1/sd/990315/v5d/)
    - (3) Select previous forecast file name and click **OK** (e.g., 1412v5d.g1.SanDiego\_3)
    - (4) Click on **Select by variable...**→ Highlight desired comparison variables and hit **CLOSE**
      - (a) Recommend selecting variables: W, wspd, pppp, tttt, slp4
    - (5) Enter filename-- **DO NOT OVERWRITE CURRENT COAMPS FILES!**
      - (a) e.g., use this format-- DDHHrun
    - (6) Enter context name-- **CURRENT FCST IS 0, DO NOT OVERWRITE!**
      - (a) Recommend entering 1 for first imported run, and subsequent numbers (2,3,etc.) if more than one file is imported)
    - (7) Click on **Make**
      - (a) Note: current model run (or first file open) parameter names are appended with the context number while the one just imported is appended with the new context number you assigned (e.g., pppp.0 is from the current run and pppp.1 is from the run you just imported).
  - b) Create new difference variables (refer back to the footnotes in Table B-1 for procedures) :
    - (1) MSLP Difference, SLP\_D=slp4.0-slp4.1
    - (2) Pressure Field Difference, P\_DIFF=pppp.0-pppp.1
    - (3) Temperature Field Difference, T\_DIFF=tttt.0-tttt.1
    - (4) Wind Speed Field Difference, WND\_D=wspd.0-wspd.1
    - (5) Vertical Velocity Field Difference, W\_DIFF=W.0-W.1
  - c) Set parameter thresholds, contour intervals, location and height, color, and opacity for the newly imported parameters and newly created difference variables. Refer to the Comparison Fields section in Table B-1 for abbreviated parameter descriptions, recommended initial settings, and the order in which to make the settings.
  - 2) Compare data from current forecast to previous forecast in one of two display formats:
    - a) Single map, simultaneous display of fields from each run on a single graphic.
    - b) Multi-display, simultaneous display of fields from each run on individual displays
  - 3) Refer to Section X of this paper for suggested graphics and techniques.

THIS PAGE INTENTIONALLY LEFT BLANK

## INITIAL DISTRIBUTION LIST

	No. Copies
1. Defense Technical Information Center.....	2
8725 John J. Kingman Road, STE 0944	
Ft. Belvoir, Virginia 22060-6218	
2. Dudley Knox Library.....	2
Naval Postgraduate School	
411 Dyer Rd.	
Monterey, California 93943-5101	
3. Chairman, Code MR/Wx.....	1
Department of Meteorology	
Naval Postgraduate School	
Monterey, California 93943-5101	
4. Chairman, Code OC/Ga.....	1
Department of Oceanography	
Naval Postgraduate School	
Monterey, California 93943-5101	
5. Professor Wendell A. Nuss, Code MR/Nu.....	1
Naval Postgraduate School	
Monterey, California 93943-5101	
6. Commander.....	1
Naval Meteorology and Oceanography Command	
1020 Bach Boulevard	
Stennis Space Center, Mississippi 39529-5005	
7. Commanding Officer.....	1
Naval Pacific Meteorology and Oceanography Center San Diego	
California	
P.O. Box 357076	
San Diego, CA 92135-7076	
8. Commanding Officer.....	1
Fleet Numerical Meteorology and Oceanography Center	
7 Grace Hopper Ave., Stop A	
Monterey, CA 93943	

9.	Commanding Officer.....	1
	Naval Atlantic Meteorology and Oceanography Center	
	McAdie Building (Bldg. U-117)	
	Naval Air Station Norfolk	
	9141 Third Ave.	
	Norfolk, VA 23511-2394	
10.	Commanding Officer.....	1
	Naval European Meteorology and Oceanography Center	
	PSC 819 Box 31	
	FPO AE 09645-3200	
11.	Commanding Officer.....	1
	Naval Pacific Meteorology and Oceanography Center	
	PSC 473 Box 68	
	FPO AP 96349-2902	
12.	Commanding Officer.....	1
	Naval Central Meteorology and Oceanography Center	
	PSC 451	
	FPO AE 09834-2800	
13.	Mr. John Cook, Code 7542.....	1
	Naval Research Laboratory Monterey California	
	7 Grace Hopper Ave., Stop 2	
	Bldg. 702, Rm. 113	
	Monterey, California 93943-5502	
14.	Dr. Ed Harrison.....	1
	Space and Naval Warfare Systems Command (PMW-185)	
	53560 Hull St.	
	San Diego, CA 92152	
15.	LCDR Arthur J. Reiss.....	3
	Naval Atlantic Meteorology and Oceanography Facility Jacksonville	
	Florida	
	PO Box 85, Bldg. 118	
	NAS Jacksonville	
	Jacksonville, FL 32212-0085	



69 290NPG  
6/02 TH 2675  
22527-200 NLB







DUDLEY KNOX LIBRARY



3 2768 00402656 7